

AMERICAN UNIVERSITY OF BEIRUT

EXPERIMENTAL INVESTIGATION OF CYCLIC P-Y CURVES
FOR RIGID WALLS SUPPORTING SANDS

by
JOSEPH ELIAS GHANEM

A thesis
submitted in partial fulfillment of the requirements
for the degree of Master of Engineering
to the Department of Civil and Environmental Engineering
of the Maroun Semaan Faculty of Engineering and Architecture
at the American University of Beirut

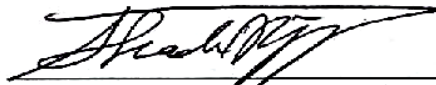
Beirut, Lebanon
January 2020

AMERICAN UNIVERSITY OF BEIRUT

EXPERIMENTAL INVESTIGATION OF CYCLIC P-Y CURVES
FOR RIGID WALLS SUPPORTING SANDS

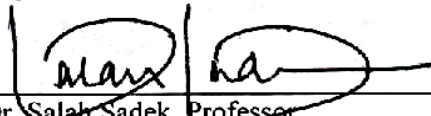
by
JOSEPH ELIAS GHANEM

Approved by:



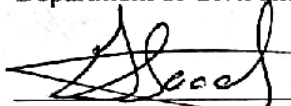
Dr. Shadi Najjar, Associate Professor
Department of Civil and Environmental Engineering

Advisor



Dr. Salah Sadek, Professor
Department of Civil and Environmental Engineering

Member of Committee



Dr. George Saad, Associate Professor
Department of Civil and Environmental Engineering

Member of Committee

Date of thesis defense: January 23, 2020

AMERICAN UNIVERSITY OF BEIRUT
THESIS, DISSERTATION, PROJECT RELEASE FORM

Student Name: Ghanem Joseph Elias
 Last First Middle

Master's Thesis Master's Project Doctoral Dissertation

I authorize the American University of Beirut to: (a) reproduce hard or electronic copies of my thesis, dissertation, or project; (b) include such copies in the archives and digital repositories of the University; and (c) make freely available such copies to third parties for research or educational purposes.

I authorize the American University of Beirut, to: (a) reproduce hard or electronic copies of it; (b) include such copies in the archives and digital repositories of the University; and (c) make freely available such copies to third parties for research or educational purposes after:

One --- year from the date of submission of my thesis, dissertation, or project.
Two --- years from the date of submission of my thesis, dissertation, or project.
Three --- years from the date of submission of my thesis, dissertation, or project.



Signature

February 5, 2020

Date

ACKNOWLEDGEMENTS

I would like to express my profound gratitude to my professor Dr. Shadi Najjar who has guided me throughout a worthwhile experience. Also, I would like to thank Dr. Salah Sadek and Dr. George Saad for their insightful remarks and engagement in my research.

A special thanks go to Imad El Chiti and Abed Al Mikati for their assistance, and a warm thanks to my friends and family for their continuous support and encouragement during the course of my master.

AN ABSTRACT OF THE THESIS OF

Joseph Elias Ghanem for Master of Engineering
Major: Geotechnical Engineering

Title: Experimental Investigation of Cyclic p-y Curves for Rigid Walls Supporting Sands

P-y curves have been widely used in the analysis of piles under lateral loads. However, the use of p-y curves for the analysis of rigid retaining walls supporting granular backfill is still in its early stages. There is a need for realistic and simplified models that could describe the p-y relationship for rigid retaining walls to be used as input in robust soil-structure-interaction problems in the context of performance-based design. These relationships will be of value if integrated in structural analysis software to describe the lateral earth pressures versus relative lateral displacements. The objective of this thesis is to investigate the cyclic p-y relationship for rigid walls supporting sands of different densities. This objective will be attained by designing and implementing an experimental testing program using a small-scale tank. One of the walls of the tank will be instrumented with pressure sensors that can record the lateral earth pressure on the wall under controlled cyclic movements. The experimental program builds on previous work that was done at the American University of Beirut on the p-y response under static loading conditions and extends it to cyclic loading. The main aim is to fill a void in the literature on the p-y response of rigid walls for applications involving soil structure interaction under seismic loading.

CONTENTS

ACKNOWLEDGEMENTS	v
ABSTRACT	vi
ILLUSTRATIONS	ix
TABLES	xi
Chapter	
1. INTRODUCTION	1
2. BACKGROUND REVIEW	3
2.1. Pile-related SSI studies	4
2.2. Wall-related SSI studies	9
2.3. Objectives and Scope	17
2.4. Experimental Program	18
3. EXPERIMENTAL SETUP	20
3.1. Backfill Material	20
3.2. Setup	21
3.2.1. Tank Configuration	21
3.2.2. Pluviator Configuration	25
3.3. Retained Backfill Preparation	29
3.3.1. Filling Procedure	29
3.3.2. Emptying Procedure	31
3.4. Testing Procedure	32

4. RESULTS AND DISCUSSION	34
4.1. Raw data for Loose and Dense Sand Cases.....	34
4.2. Effect of Previous Loading Cycles on the P-Y Response	41
4.3. P-Y Curves at Large Displacements	45
4.4. Sidewall interface friction angle	48
4.5. Discussion	52
4.5.1. Impact of relative density on p-y curves	52
4.5.2. Comparison with Medium Dense Behavior (El-Chiti et al. 2019).....	58
4.5.3. Effect of number of cycles (Medium Dense Sand with 22 cycles)	61
4.5.4. Representing the passive p-y response	67
4.5.5. Effect of “holding” time and temperature on the p-y response	73
5. CONCLUSIONS	84
REFERENCES	86
 Appendix	
EXPERIMENTAL RESULTS	90

ILLUSTRATIONS

Figure 1. Soil modeled as a series of uncoupled nonlinear springs	2
Figure 2. p-y curves	2
Figure 3. Elastic-plastic back-bone p-y curve (a), and stitched back-bone p-y curve (b)	3
Figure 4. Matlock's miniature pile (a), and clay resistance due to slow cyclic loading (b)....	4
Figure 5. Matlock's proposed p-y curves for piles in clay	5
Figure 6. (a) Reese et al.'s proposed p-y curves, (b) passive failure wedge, (c) factors proposed by Reese et al.	6
Figure 7. Proposed model by Wang et al. (1998)	7
Figure 8. Findings of Wilson et al. (1998) compared to previous studies	8
Figure 9. P-Y curves for soft clay and dense sand.....	9
Figure 10. Finite element model proposed by Wood (1975).....	10
Figure 11. Enhanced model proposed by Nadim and Whiteman (1983).....	11
Figure 12. Model proposed by Richard et al. (1999).....	12
Figure 13. Model proposed by Maleki et al. (2010)	12
Figure 14. Finite element model adopted by El Chiti et al. (2017)	13
Figure 15. Experimental program	13
Figure 16. Difference between the first and last passive p-y curves	14
Figure 17. p-y path during construction stages (Briaud and Kim, 1998)	15
Figure 18. p-y curves for the three components proposed by Briaud and Kim (1998)	15
Figure 19. Floor plan	16
Figure 20. Back-bone p-y curve for the side soil.....	17
Figure 21. Grain-size distribution of the soil.....	20
Figure 22. Tank to be used.....	23
Figure 23. Front end of tank	23
Figure 24. Sensors configuration on the inner face of the rotating wall.....	24
Figure 25. Low range force gauge and load cell mounted on opposites sides facing each other (a), load cell installed perpendicular to a block and flush with the inner face of the sidewall (b), force gauge parallel to a sliding block (c), sliding block flush with the inner face of the sidewall (d),.....	24
Figure 26. PLEXI-glass fitted on the inner faces (a), grease coating (b), plastic wrap covering all inner sides excluding the moving wall (c)	25
Figure 27. Pluviator setup.....	27
Figure 28. Density calibration	27
Figure 29. Variation of density with respect to drop height	29
Figure 30. Filling process	30
Figure 31. Horizontal sand bed during filling (a), Horizontal sand bed at the red mark at the end of filling (b).....	30

Figure 32. System placed on four jacks and ready for the emptying process (a), container under each valve (b), #4 sieves (c)	31
Figure 33. Raw data for test #1 on loose sand	37
Figure 34. Raw data for test # 2 on dense sand	38
Figure 35. Repeated against normal cycles for test # 1	43
Figure 36. Repeated against normal cycles for test # 2	44
Figure 37. Static push compared to previous cycles for test # 1	46
Figure 38. Static push compared to previous cycles for test # 2	47
Figure 39. Sidewall interface friction angle during test #1.....	50
Figure 40. Sidewall interface friction angle during test # 2.....	51
Figure 41. Consecutive peak passive pressures for all cycles during test # 1 and 2.....	53
Figure 42. Effect of density on the cyclic response	54
Figure 43. Effect of density on the static response	55
Figure 44. Rate of change for peak values for tests #1 and 2	57
Figure 45. Peak pressures for three different densities	60
Figure 46. Effect of numerous 5 mm cycles on soil response	62
Figure 47. Effect of numerous 20 mm cycles on soil response	63
Figure 48. Peak response in function of repeated cycles	65
Figure 49. Percent change in peak response with every cycle.....	66
Figure 50. Slope analysis for ± 5 mm cycles during test #3	68
Figure 51. Slope analysis for ± 20 mm cycles during test #3	69
Figure 52. First slope variation with number of cycles.....	71
Figure 53. Second slope variation with number of cycles.....	72
Figure 54. 1 st and 2 nd ± 5 mm cycles with waiting enforced at specific locations	75
Figure 55. 5 th and 8 th ± 5 mm cycles with waiting enforced at specific locations	76
Figure 56. Investigating temperature effect on wall movements.....	78
Figure 57. Interface angles during cycles 2, 5 and 8	80
Figure 58. Pressure change during the enforced time for ± 5 mm cycles.....	81
Figure 59. Pressure change during the enforced time for ± 5 mm cycles.....	82
Figure 60. Pressure change during the enforced time for ± 20 mm cycles.....	83

TABLES

Table 1. Testing Program.....	18
Table 2. Summary of soil properties from El-Chiti et al. (2019).....	21
Table 3. Summary of pluviation results.....	28
Table 4. Method for loading the bed in the passive direction.....	33
Table 5. Passive theories of Coulomb (1776) & Lancellota (2002)	41

CHAPTER I

INTRODUCTION

The interdependent relationship between structural motion and soil response is the foundation of soil-structure interaction (SSI) problems. Most structures include substructures (foundations or retaining walls) in direct contact with underlying soil. Studying the soil-structure-interaction mechanism between these structural elements and the soil has been of great interest for researchers to try to understand the effect of SSI on the performance-based seismic design of structures. The deformations produced by a cyclic motion in the soil can reach the limit of its linear-elastic behavior, thus the necessity to study its non-linear behavior in the dynamic soil-structure interaction problem (DSSI), especially for moderate to strong motions. The dynamic response of laterally loaded structures can be evaluated using several techniques, including (1) numerical methods such as finite element method (FEM) (Randolph, 1981), (2) boundary element method (BEM) (Sanchez, 1982), (3) beam on nonlinear Winkler foundation (BNWF) method which simulates the soil as a series of closely spaced uncoupled springs (Figure 1) and (4) p-y curve methods (Boulanger et al. 1999, Allotey 2007), which will be the main focus of the proposed research.

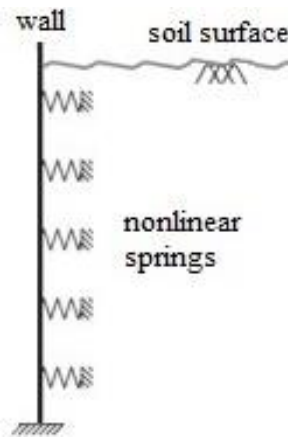


Figure 1. Soil modeled as a series of uncoupled nonlinear springs

The relationship between the lateral soil resistance (p) and relative soil displacement (y) can be visualized using p - y curves represented by a constant or varying stiffness “ k ” as shown in Figure 2. These curves are usually derived empirically from field or laboratory experiments then used in a computer program to analyze a system. P - y curves have been extensively used in the analysis of laterally loaded piles. Yet, this is not the case in analyzing retaining walls. Therefore, there is a lack in practical models capable of explaining the soil-rigid wall interaction that can be of value in design.

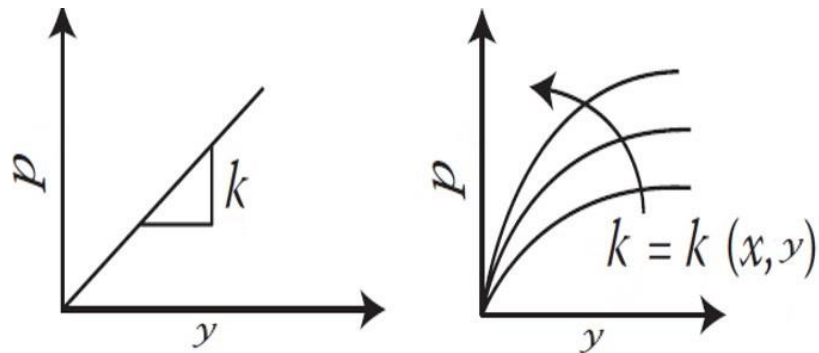


Figure 2. p - y curves

CHAPTER II

BACKGROUND REVIEW

The simplest representation of the effect of soil on the seismic response of a structure was suggested by E. Winkler in 1967 (Kerr, 1984). The idea is to transform the relationship between soil and foundation into a bed of independent vertical springs. The main drawback of this method is the difficulty in determining the stiffness of the springs (p - y elements) replacing the soil below the foundation (Dutta & Roy, 2002). Moreover, the literature is filled with back-bone p - y curves with varying complexities, from bilinear, polynomial, hyperbolic to stitched models of different curves/lines (Matlock & Ripperger, 1956) (Brown, Morrison, & Reese, 1988) (Dunnivant & O'Neill, 1989) (Reese, Cox, & Koop, 1974). Figure 3(a) shows a perfectly elastic-plastic back-bone p - y model while Figure 3(b) shows a stitched model.

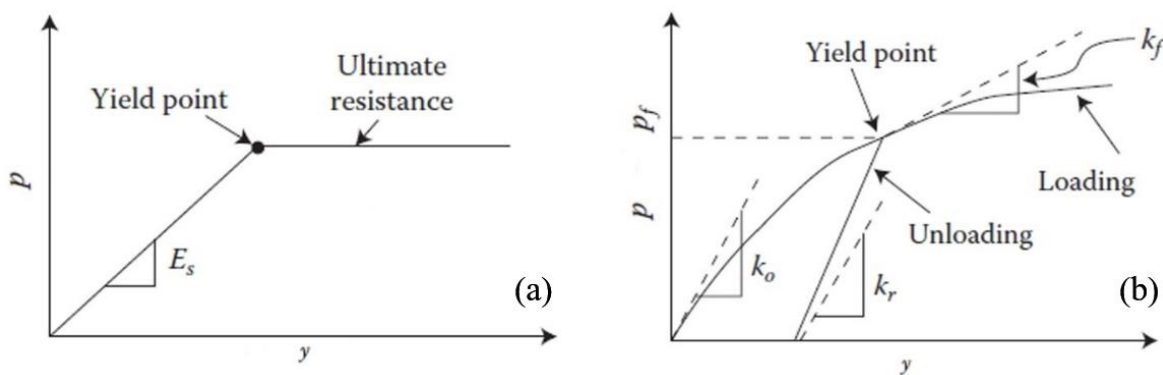


Figure 3. Elastic-plastic back-bone p - y curve (a), and stitched back-bone p - y curve (b)

2.1. Pile-related SSI studies

For laterally loaded piles, p-y material models were developed in the 1960s and 1970s for static and slow cyclic conditions. Oil companies financed research programs at the University of Texas at Austin to study the response and behavior of piles under lateral loading. Examples include the American Petroleum Institute (API) sand model [API RP 2 A-WSD (API 1993)].

Matlock (1970) came up with p-y models for clayey soil after a series of experiments using miniature piles cyclically pushed between two opposite pre-selected displacements as shown in Figure 4. Matlock discovered three back-bone p-y curves related to the type of lateral loading on a pile: static, slow cyclic, and loading after cyclic shown in Figure 5.

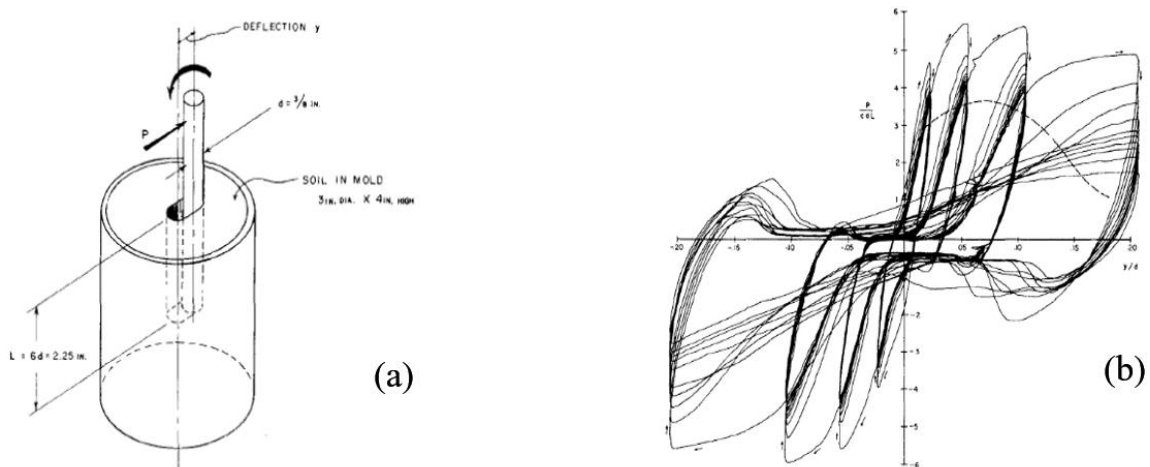


Figure 4. Matlock's miniature pile (a), and clay resistance due to slow cyclic loading (b)

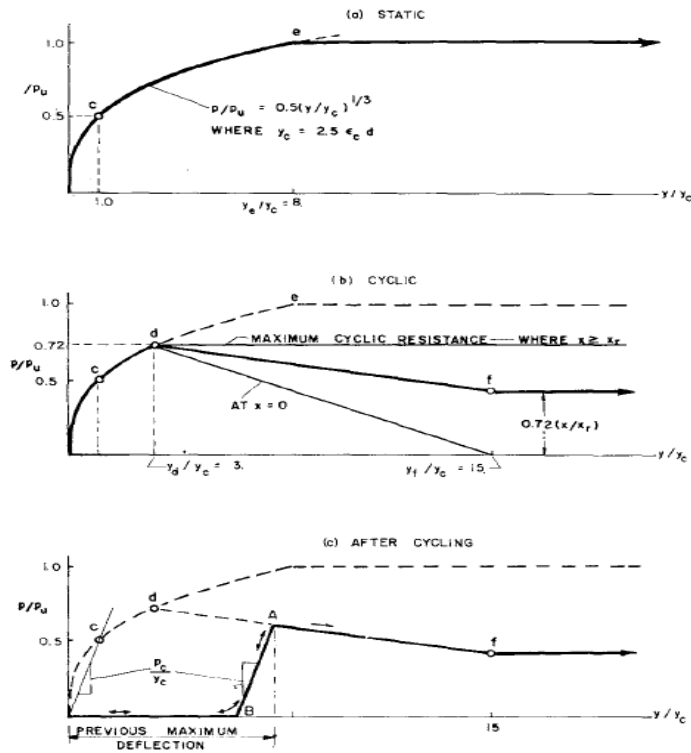


Figure 5. Matlock's proposed p-y curves for piles in clay

Reese et al. (1974) proposed a stitched p-y model for piles in cohesion-less soil consisting of a linear segment until point “k”, followed by a transitional segment where the soil gradually loses its stiffness until reaching a stable value “m”, another elastic segment, and lastly a perfectly plastic ultimate region that start at point “u” as shown in Figure 6(a). In this method, a theoretical three-dimensional passive wedge of soil shown in Figure 6(b) was developed in front of the deflected pile to calculate the ultimate soil resistance. The p-y model described above represents the backbone curve for a static lateral pile loading. In order to introduce the effect of cyclic loading, Reese et al. suggested that points ‘m’ and ‘u’ should be multiplied by the factors B-cyclic and A-cyclic instead of B-static and A-static,

respectively, as shown in the Figure 6(c). Note that the cyclic factors are remarkably smaller than the static factors, inducing degradation of soil resistance.

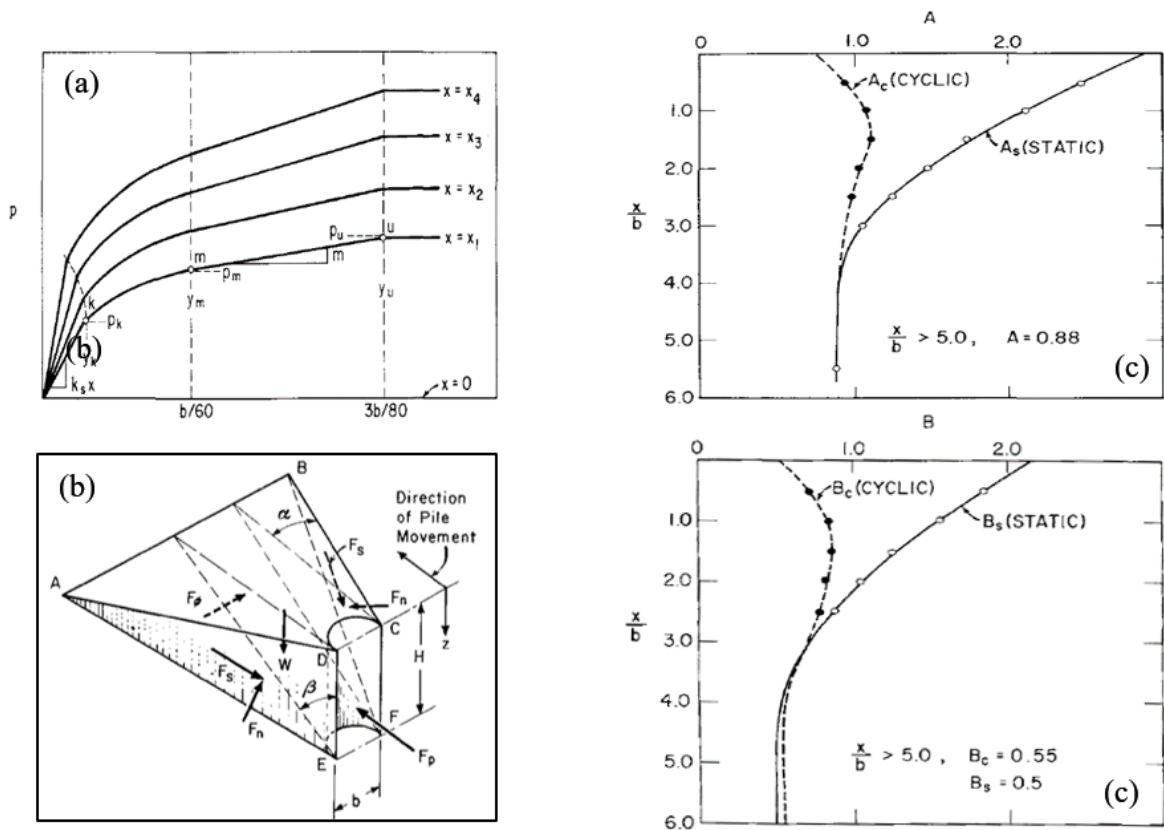


Figure 6. (a) Reese et al.'s proposed p-y curves, (b) passive failure wedge, (c) factors proposed by Reese et al.

Finn et al. (2005) argued that static and slow cyclic loadings will not accurately predict the dynamic behavior of a pile. El Naggar and Novak (1996) developed a model built on the Winkler proposition for assessing lateral response of piles and pile groups using a hyperbolic stress-strain relationship to account for nonlinearity, slippage and gapping at the pile-soil interface. El Naggar and Bentley (2000) further developed the model by proposing dynamic p-y curves equivalent to the two springs simulating both far-

field and near-field; far-field soil not affected by the structure, and near-field soil in direct contact and affected by the structure. Badoni and Badoni and Makris (1996) used the non-linear Bouc–Wen spring in parallel with dashpots to study the response of pile under dynamic loading. Wang et al. (1998) related several applications of non-linear springs based on p–y curves and dashpots to describe radiation damping in BNWF models for piles under seismic loading shown in Figure 7. Allotey and El Naggar (2008) proved the significant role of soil cave-in and recompression in the cyclic soil–pile response by developing a dynamic BNWF model with rules for loading, unloading, and reloading that accounts for cyclic degradation, slack zone formation and reduced radiation damping.

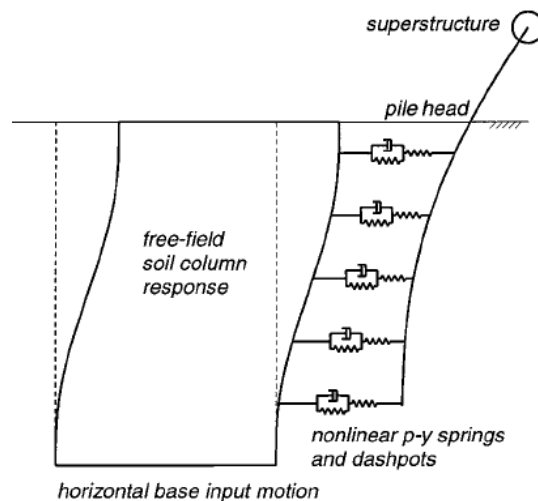


Figure 7. Proposed model by Wang et al. (1998)

Boulangier et al. (1999) developed a BNWF model to investigate a series of centrifuge tests conducted by Wilson et al. (1998) for piles under seismic loading. Figure 8

shows the results obtained from these tests, where it is clear how the presence of an inertial load had a great effect on the behavior of piles.

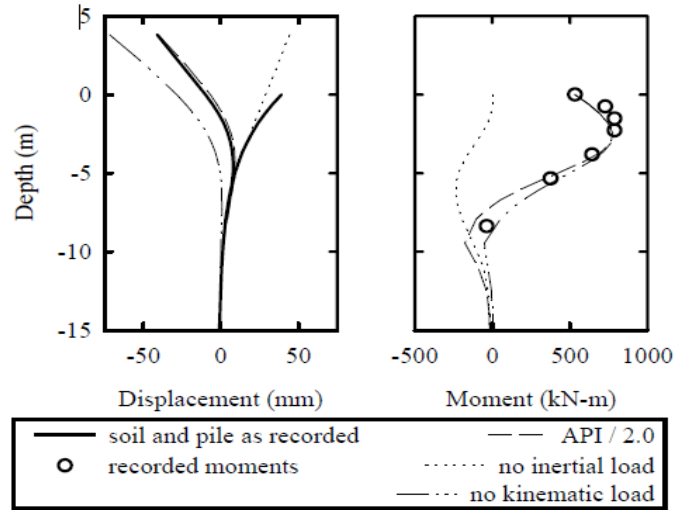


Figure 8. Findings of Wilson et al. (1998) compared to previous studies

Boulanger et al. (1999) performed a series of centrifuge tests on piles embedded in a double layer of soft clay and dense sand, over a wide range of earthquake shaking events. The clay layer was modeled using a non-linear p-y curve according to Matlock (1970), taking into consideration gapping zone, plastic zone, elastic zone and radiation damping. Alternatively, the sand was modeled using p-y back-bone curve recommended by API 1993 as shown in Figure 9.

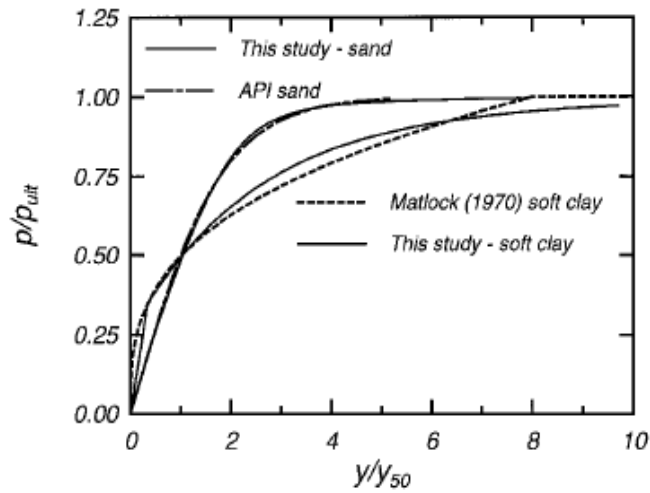


Figure 9. P-Y curves for soft clay and dense sand

2.2. Wall-related SSI studies

The earliest studies done in 1926 by Okabe and 1929 by Mononobe-Matsuo resulted in the formulation of the Mononobe-Okabe (M-O) method, a static force equilibrium method based on Coulomb's theory, for determining the dynamic active pressure behind yielding retaining walls under seismic conditions. Despite the simplicity of the method, its drawback is the assumption that the wall displacement during a seismic occurrence will cause the soil to reach a limit state. Seed and Whitman (1970) modified the M-O theory after conducting a parametric study and divided the dynamic pressure into a static component and a dynamic component.

Both the original and modified M-O methods require large wall displacement during a seismic event to create a sliding wedge behind it, thus altering the earth pressure from at-rest to active conditions, which is not always the case in all soil retaining systems or during low amplitude seismic events. Wood (1973) examined the reaction of a

homogeneous linear elastic soil, retained by a rigid non-yielding wall connected to a rigid base subjected to harmonic excitations. Wood proved that lateral pressures can be determined from a static solution for the case of a constant horizontal acceleration when the dynamic amplification was insignificant which is at low frequency input motions were most problems lie. Wood (1975) also proposed a plain-strain finite element model shown in Figure 10 to analyze lateral stresses exerted on a wall from a backfill soil assumed as an elastic continuum that is horizontally pushed with a static 1g force.

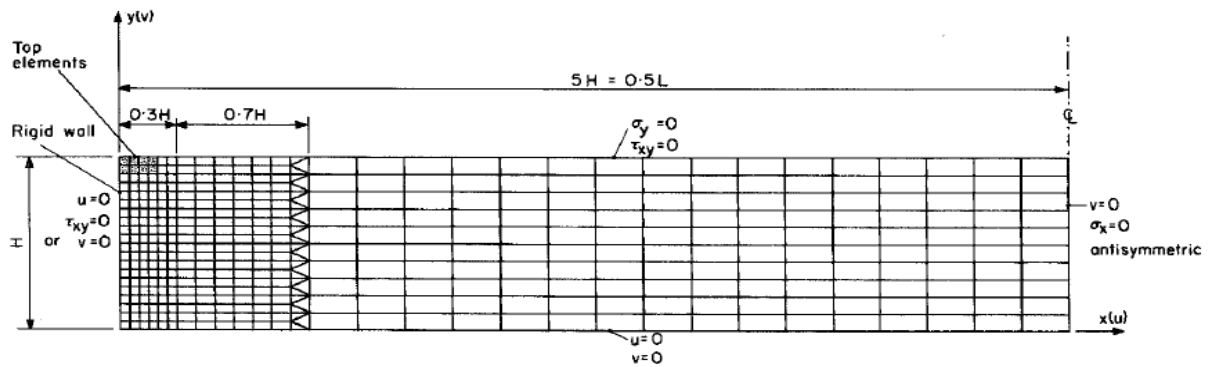


Figure 10. Finite element model proposed by Wood (1975)

Nadim and Whiteman (1983) introduced two predetermined slip planes on the proposed model, one along the wall-soil contact zone and another one inclined inside the retained soil, from the bottom of the wall to the surface as shown in Figure 11.

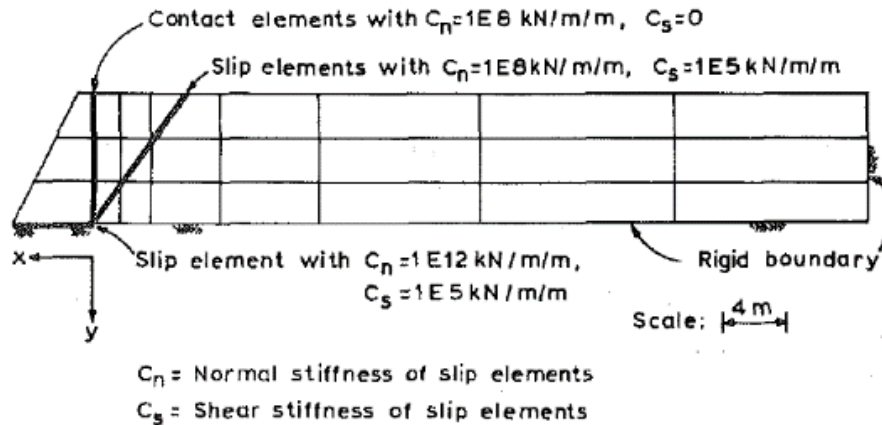


Figure 11. Enhanced model proposed by Nadim and Whiteman (1983)

A simpler method was proposed by Scott (1973), who modeled the soil as a shear beam coupled using elastic springs to a fixed boundary from one side, and a retaining wall from the other side. Although, the forces acting on the wall were found to be higher than those predicted by the M-O method. Richard et al. (1999) improved Scott's method by adding a free-field and a near-field region to the model as shown in Figure 12. The near-field soil was simulated by a series of springs having a bilinear p-y curve. Moreover, Maleki and Mahjoubi (2010) considered the effect of wall flexibility under dynamic loading on the soil resistance as shown in Figure 13. The model used a series of springs having a p-y curve similar to that proposed by Richard et al. (1999) for the near-field soil, and a discretized semi-infinite continuum of plain strain elements for the free-field soil was proposed.

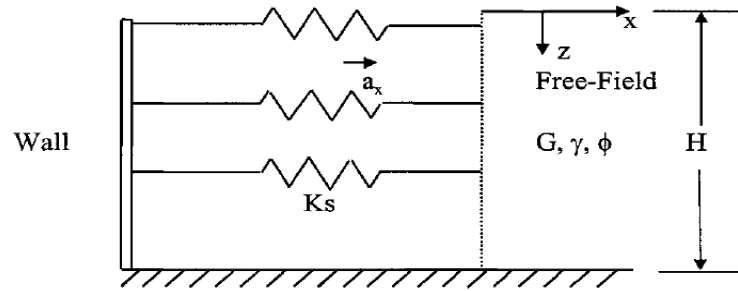


Figure 12. Model proposed by Richard et al. (1999)

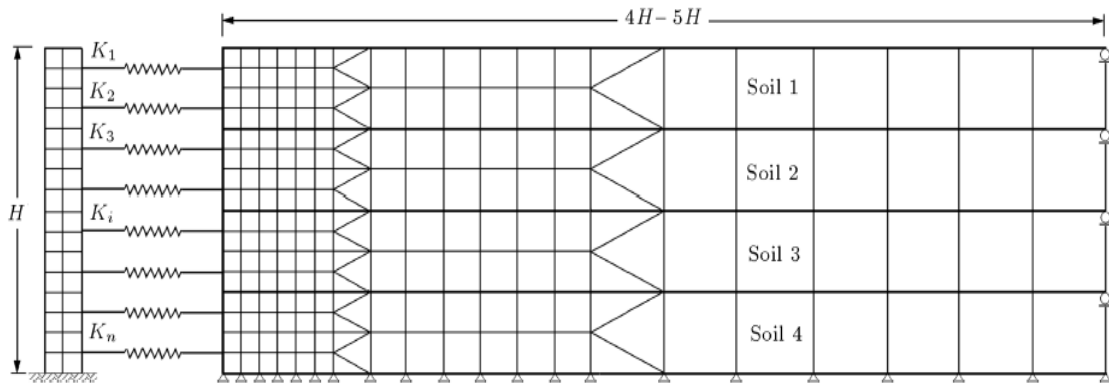


Figure 13. Model proposed by Maleki et al. (2010)

El Chiti et al. (2017 and 2018) used PLAXIS2D to analyze and investigate the change in the active earth pressures exerted on a rigid wall. Figure 14 shows the adopted model in which a 30 cm thick elastic concrete wall is used to retain a semi-infinite half space soil medium involving a medium to dense granular backfill. The wall was mobilized towards the active side by a prescribed displacement that prevented bending and ensured a bottom movement equal to 20% of that of the top. Simulation results showed that the p-y curves are non-linear, and sensitive to various parameters such as depth, interface friction angle, height of wall, and relative density.

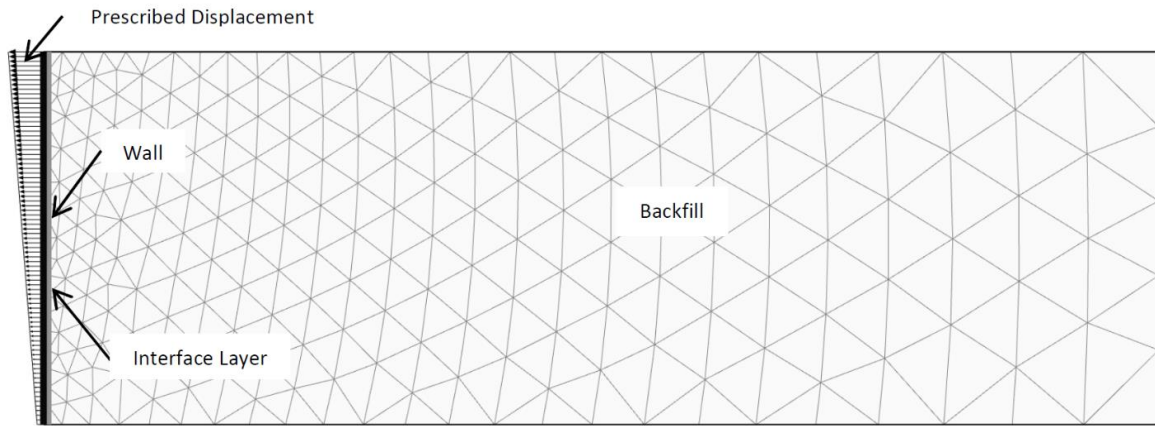


Figure 14. Finite element model adopted by El Chiti et al. (2017)

Furthermore, El Chiti et al. (2019) used a rigid steel wall supporting granular backfill to derive cyclic p-y curves by quantifying the complex relationship between lateral earth pressure and lateral wall displacements. Figure 15 shows the adopted cyclic testing program, in which four cycle amplitude (2, 5, 10 and 20 mm) were adopted, each repeated 10 times consecutively. Figure 16 shows the difference between the first and last passive p-y curves recorded from the sensor positioned at a depth of 50 cm, for each cycle amplitude.

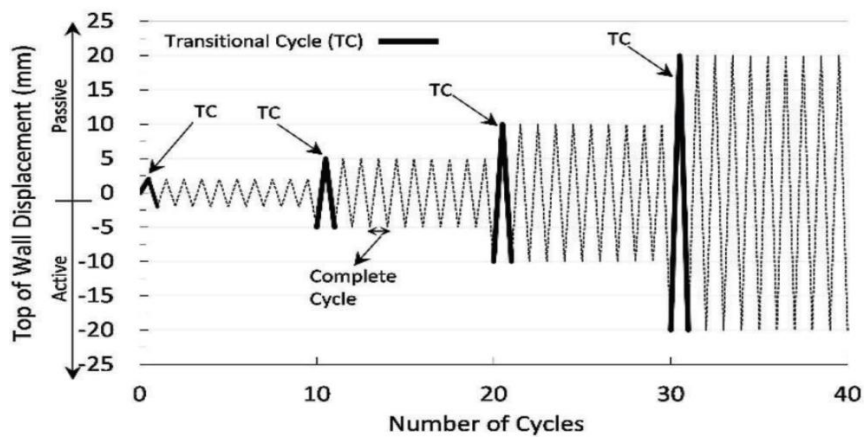


Figure 15. Experimental program

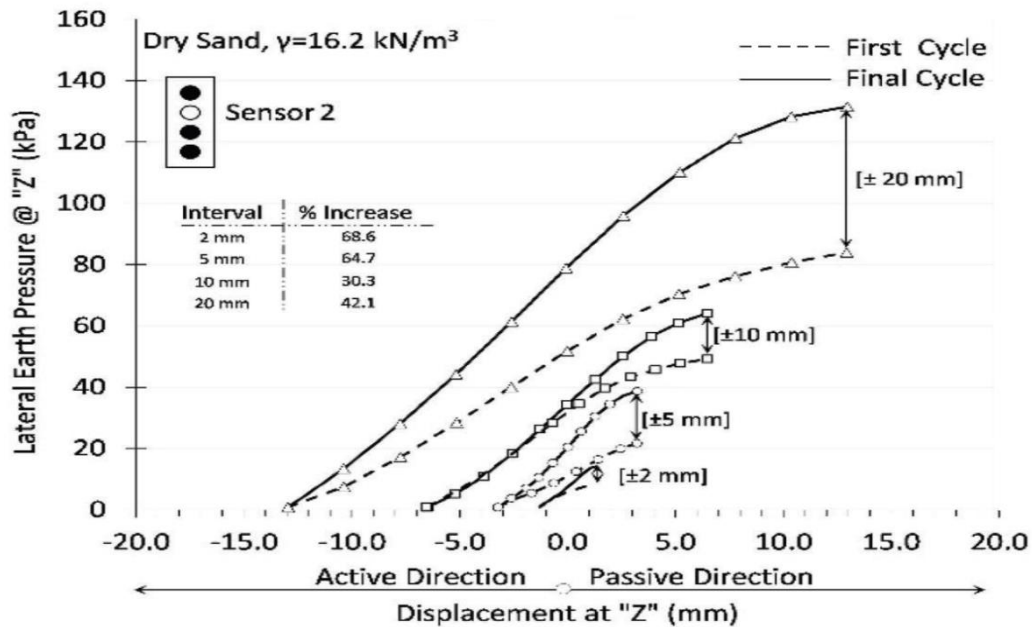


Figure 16. Difference between the first and last passive p-y curves

The beam-column method was investigated for the case of tie-back walls that were statically loaded as a result of construction stages as shown in Figure 17. Many p-y curves were implemented for this type of wall as shown in Figure 18. P-y curve for the retaining wall above the excavation (plain strain), the single-pile p-y curve below excavation, and the anchor p-y curve. Kim and Briaud (1994) back-calculated using cubic spline interpolation and bending moment profiles measurements that were taken from a full-scale test wall in sand. The recommended elastic limits for active (y_a), and passive displacements (y_p), were considered constant at 1.3 mm and 13 mm, respectively. This ensured the variation in the soil stiffness with respect to changes in P_{active} and $P_{passive}$ at different depths. El Ganainy and El Naggar (2009) and Saad et al. (2012 and 2016) implemented these recommendations in studying the response of buildings with underground stories.

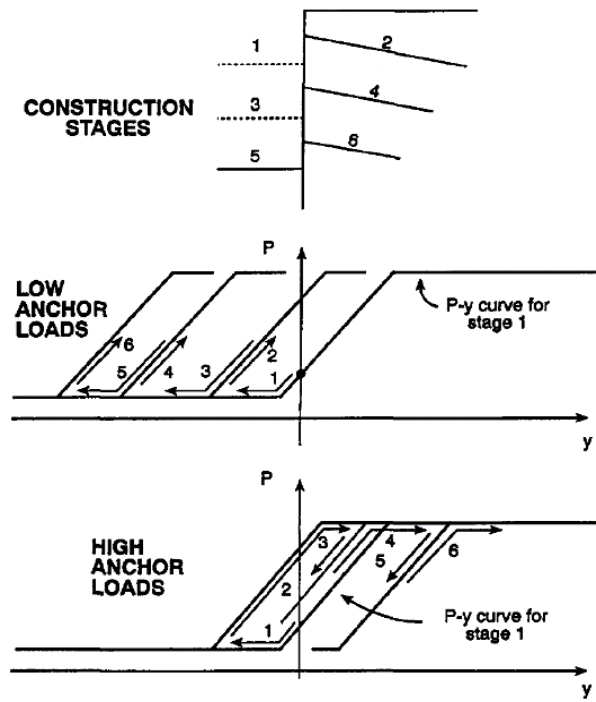


Figure 17. p-y path during construction stages (Briaud and Kim, 1998)

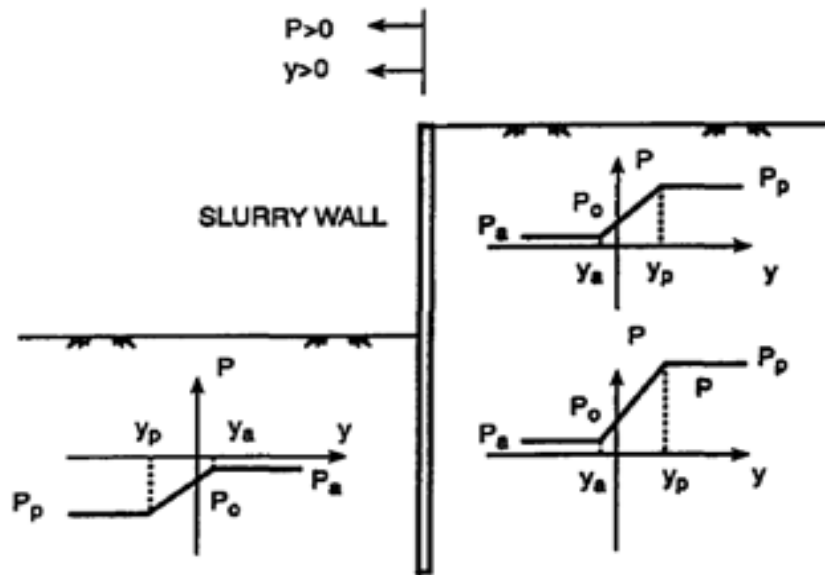


Figure 18. p-y curves for the three components proposed by Briaud and Kim (1998)

Saad et al. (2012) evaluated the seismic response of structures subjected to 1940 El Centro earthquake. The analysis was conducted using the software SAP2000 (CSI 2007), while varying the number of above and below ground stories, in addition to altering the soil conditions between class C and class D according to ASCE7-05. The analyzed structures were typical reinforced concrete shear wall buildings that are fixed at the ground level, with a constant floor height of 3 m, and a slab area of 550 m² shown in Figure 19. Lateral earth pressures were modeled as p-y curves acting on the basement walls. These simplified models were assumed to be bounded by a active pressure (P_a) and an passive pressure (P_p) as recommended by Briaud and Kim (1998) and shown in Figure 20.

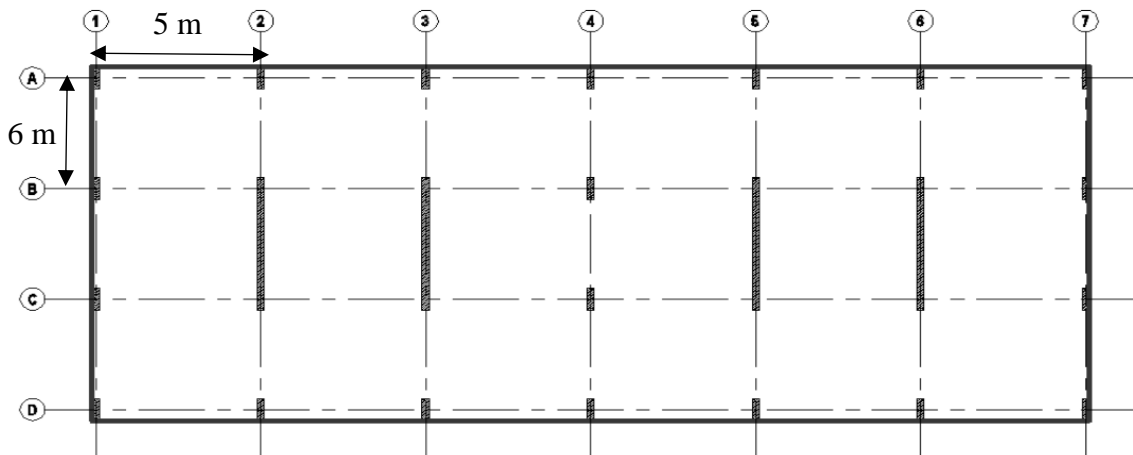


Figure 19. Floor plan

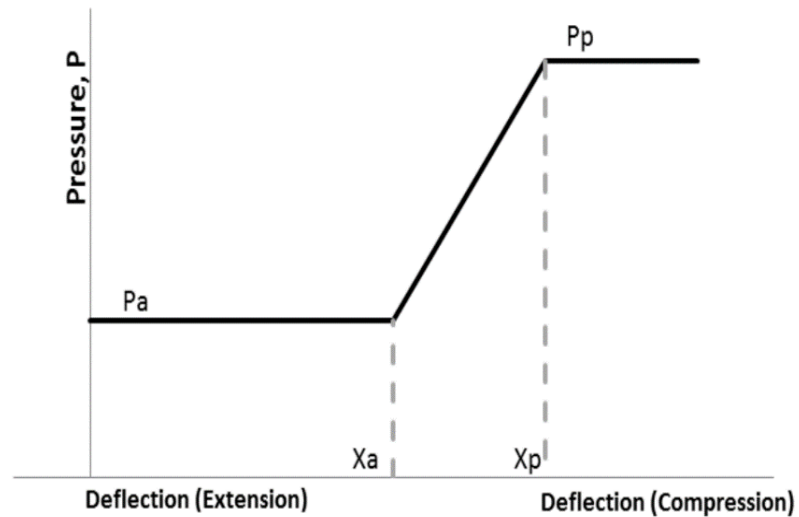


Figure 20. Back-bone p-y curve for the side soil

2.3. Objectives and Scope

The existing literature points to a need for experimental investigations of the cyclic p-y response of rigid walls that restrain granular soils. Such experimental investigations will shed light on the mechanism in which lateral earth pressures develop behind rigid walls that are cycled from active to passive states of loading. These experiments will be of value in the context of performance-based design since they will provide useful data on the relationship between lateral earth pressure and local wall displacements for sands of different density. This is close to the common concept used in modeling the reaction of the soil for laterally loaded piles.

The existing literature is limited to investigations of the static p-y response with no experimental investigations on the cyclic response of laterally loaded rigid walls.

Therefore, the main objective of this study is to examine the cyclic p-y response of a

system consisting of a rigid wall supporting granular backfill, over the full displacements range (active to passive). The methodology needed to achieve this objective is presented in the following chapter.

2.4. Experimental Program

The proposed testing program is summarized in Table 1. The program includes four tests that are aimed at studying the effect of relative density and cyclic loading on the p-y response of rigid walls supporting sands.

Table 1. Testing Program

Test #	Type	Backfill Density (kg/m ³)	Displacements from vertical position of wall	Number of Cycles
1	Cyclic	1550	2 mm or 0.17% drift (active and passive)	10
			5 mm or 0.41% drift (active and passive)	10
			10 mm or 0.83% drift (active and passive)	10
			20 mm or 1.67% drift (active and passive)	10
	Static push		120 mm or 10% drift (passive)	1
2	Cyclic	1750	2 mm or 0.17% drift (active and passive)	10
			5 mm or 0.41% drift (active and passive)	10
			10 mm or 0.83% drift (active and passive)	10
			20 mm or 1.67% drift (active and passive)	10
	Static push		120 mm or 10% drift (passive)	1
3	Cyclic	1650	5 mm or 0.41% drift (active and passive)	22
			20 mm or 1.67% drift (active and passive)	22
	Static push		*	1
4	Cyclic (holding time at specific locations)	1650	5 mm or 0.41% drift (active and passive)	8
			20 mm or 1.67% drift (active and passive)	8

* To avoid damaging the sensors that were already carrying their maximum capacity after completing the 20 mm cycles, the static push in test #3 could not be completed.

The first two tests are aimed at studying the effect of sand density on the cyclic p-y response. In these tests, the relative density of the sand is varied from loose sand (1550 kg/m³) in the first test to dense sand (1750 kg/m³) in the second test. These two tests complement the test that was done by El-Chiti et al. (2019) on medium dense sand. This allows for a thorough investigation on the effect of relative density on the resulting p-y response.

The third test involves experimenting with the number of cycles needed for the measured p-y response to become stable. In this test, cycles with displacement amplitudes of 5 mm and 20 mm are adopted. Rather than conducting 10 cycles only at each displacement amplitude, the objective in this test is to keep cycling until the p-y response exhibits signs of stability. This test is conducted using medium dense sand only. Since the 2 mm and 10 mm cycles are not included, the test will also reveal the impact of conducting previous displacement cycles on the response of any given cycle.

The fourth test will be targeted towards investigating the effect of the rate of loading on the resulting cyclic p-y curves. The test will also be conducted using the medium dense sand. However, the wall displacement sequence during select cycles will be chosen to enforce a waiting time / pausing time whereby the fluctuation in the earth pressure is monitored with time. This investigation is triggered by observations in previous tests showing that the earth pressure in the active side could increase with waiting time, while the pressures in the passive side could decrease with waiting time. These fluctuations could be due to the viscous nature of the wax/oil that is used to minimize friction on the sides of the wall. This will be investigated in the proposed test.

CHAPTER III

EXPERIEMNTAL SETUP

3.1. Backfill Material

The soil used throughout this study is dry sand that has a minimum density of 1460 kg/m³ with a void ratio of 0.809, and a maximum density of 1800 kg/m³ with a void ratio of 0.467. Figure 21 shows three grain-size distribution curves obtained from three sieve analysis tests conducted on three soil samples. These results indicate a low percent of fines, uniformity coefficient (Cu) of 2.2 which is less than 6 for sands, and a coefficient of gradation (Cc) of 0.89 that is not between 1 and 3. Hence the soil is classified as poorly graded.

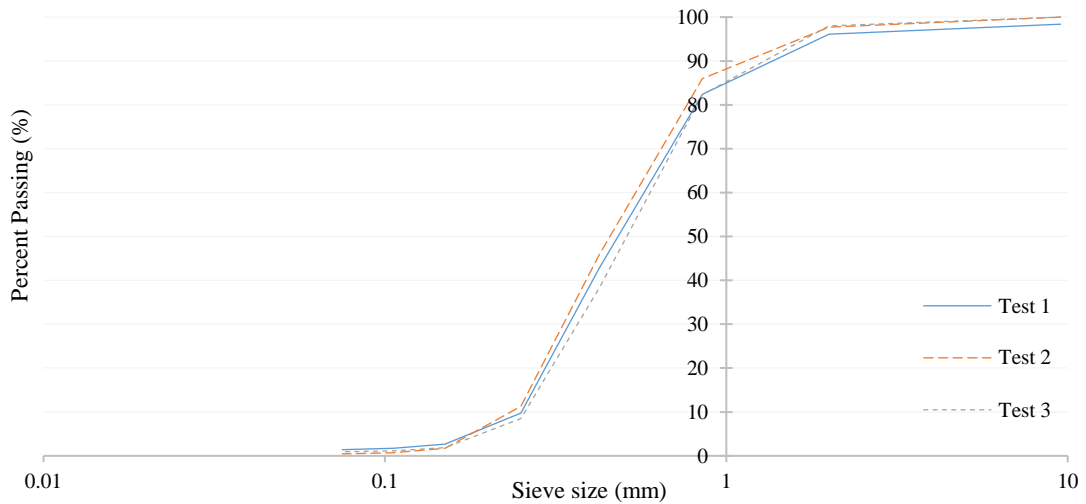


Figure 21. Grain-size distribution of the soil

Additionally, Table 2 summarizes the different properties determined from conducted pycnometer, direct shear, and triaxial experiments.

Table 2. Summary of soil properties from El-Chiti et al. (2019)

Density (kg/m³)	1550			1650			1750		
Relative density	0.31			0.61			0.88		
Specific gravity	2.64			2.64			2.64		
Triaxial Tests									
Confinement (kPa)	10	20	50	10	20	50	10	20	50
E₅₀ ref (MPa)	5000	6000	8000	12000	18000	25000	12500	17000	40000
E_{oed} ref (MPa)	5000	6000	8000	11700	18000	25000	10000	16000	40000
Φ_{sec} (sand-sand) (°)	42.1	37.6	35.3	47.9	44	41	52.3	48.3	44.6
Direct Shear Tests									
Confinement (kPa)	30	80	130	30	80	130	30	80	130
Φ (sand-sand) (°)	35.8			37.2			41.1		
Φ (sand-PLEXI) (°)	12.2			9.8			11.1		

3.2. Setup

3.2.1. Tank Configuration

In order to achieve the primary objective, a rigid tank having a width of 0.5 m, a height of 1.25 m and a length of 2.55 m shown in Figure 22 is used. The tank, which has been designed and constructed by El-Chiti et al. (2019) to study the cyclic p-y response of a rigid wall supporting medium dense sand, can hold 1.47 m³ of backfill, and is made of 4 mm thick steel plates, stiffened by a frame of hollow steel members, such that its maximum deflection is below 2 mm. The tank has one side that is hinged at the bottom and forced into rotation by fractions of a millimeters at its top, and all other sides fixed. A 30-ton

displacement controlled hydraulic piston of 0.01 mm accuracy is placed at the top of the free side to induce movement, and a linear variable differential transformer (LVDT) is placed next to it to track the displacements as shown in Figure 23. Two load cells in addition to four Geokon 4800 vibrating wire sensors are installed in a flush manner as shown in Figure 24, in order to extract horizontal lateral stresses at several depths. Finally, Figure 25(a) shows a low range force gauge and a load cell installed on opposite sidewalls to back-calculate the interface friction angle. The low range force gauge is mounted parallel to a custom-made sliding block as shown in Figure 25(b) that is installed flush with the inner face of the sidewall as shown in Figure 25(c). The load cell is mounted perpendicular to a fixed block installed in the same manner as shown in Figure 25(d).

To reduce frictional forces, 4 mm PLEXI-glass plates are fitted on all inner faces of the tank as shown in Figure 26(a). Before each test, a thin coat of grease is applied over the PLEXI-glass as shown in Figure 26(b), and a thin plastic sheet is overlain over the grease as shown in Figure 26(c).

The two weights shown in Figure 23 are present to avoid having a gap between the wall and the hydraulic piston during testing.



Figure 22. Tank to be used

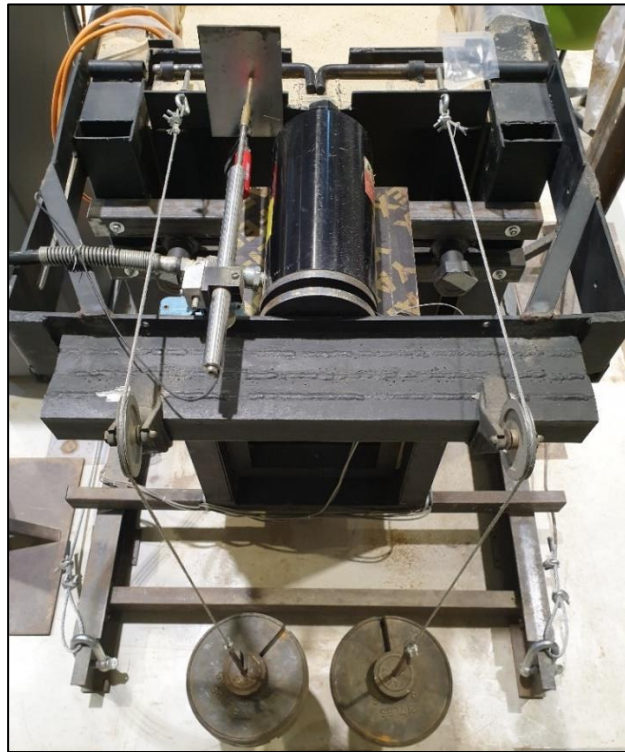


Figure 23. Front end of tank

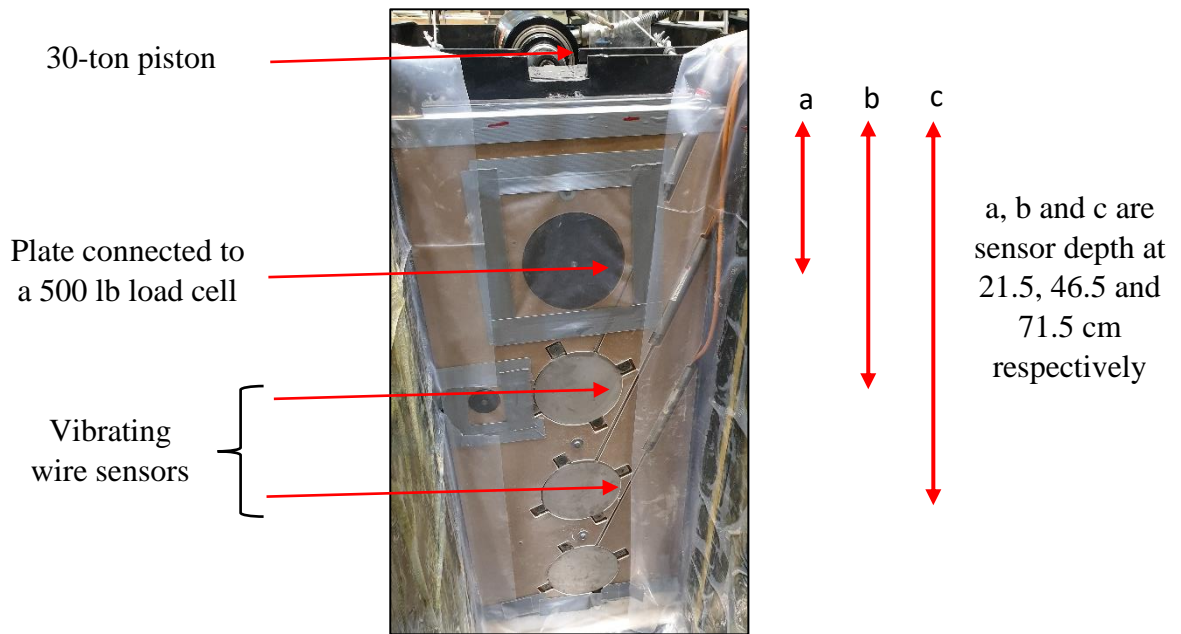


Figure 24. Sensors configuration on the inner face of the rotating wall



Figure 25. Low range force gauge and load cell mounted on opposite sides facing each other (a), load cell installed perpendicular to a block and flush with the inner face of the sidewall (b), force gauge parallel to a sliding block (c), sliding block flush with the inner face of the sidewall (d),

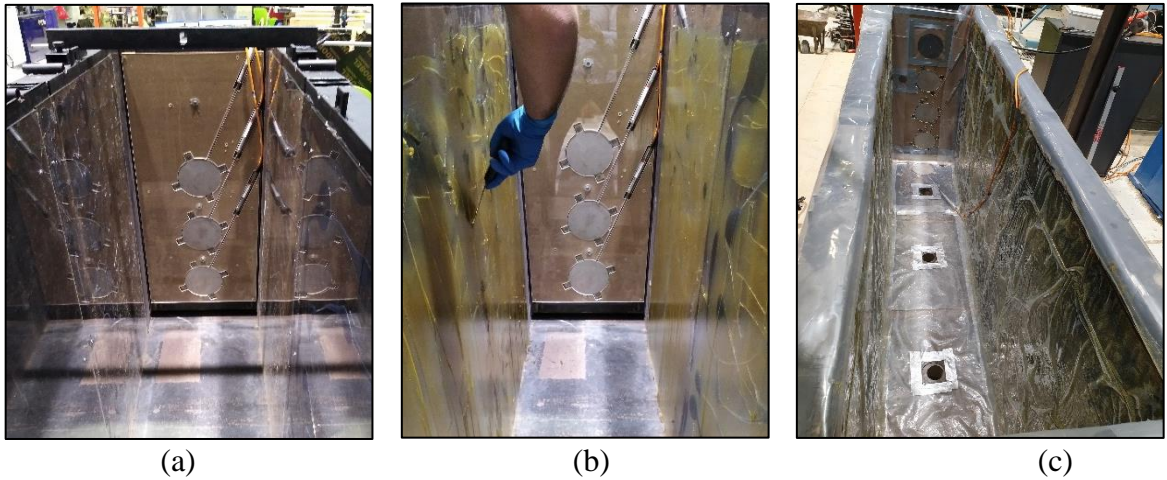


Figure 26. PLEXI-glass fitted on the inner faces (a), grease coating (b), plastic wrap covering all inner sides excluding the moving wall (c)

3.2.2. *Pluviator Configuration*

A key variable in the development of lateral earth pressure is soil density. In order to achieve a constant pre-set density for such large scale experiment, El-Chiti et al. (2019) experimented with the use of a pluviator technique (Dave, 2012; Gade, 2016; Tabaroei, 2017). Figure 27 shows a pluviator consisting of a sand storage container, an orifice at the bottom of the container that discharges sand at a specific rate, a flexible transporting tube, a funnel system to ensure vertical drop orientation at all times, and a 10 cm rigid tube with a sieve diffuser at its end to provoke the raining down of sand particles at a specific discharge rate.

Various experiments were conducted on a small-scale box as shown in Figure 28, in order to determine the configuration of the pluviator that can generate a uniform pre-set density. The procedure involved setting a final target density at first, then installing one of the three types of orifices shown in Figure 27 at the bottom of the container, using one of the three 10 cm rigid tubes shown in Figure 27 at the end, and finally alternating between

different drop heights until reaching the pre-set density. Both the configuration and the drop height corresponding to the pre-set density will be chosen to prepare the sand bed in the tank. A summary of results is shown in Table 3 and Figure 29.

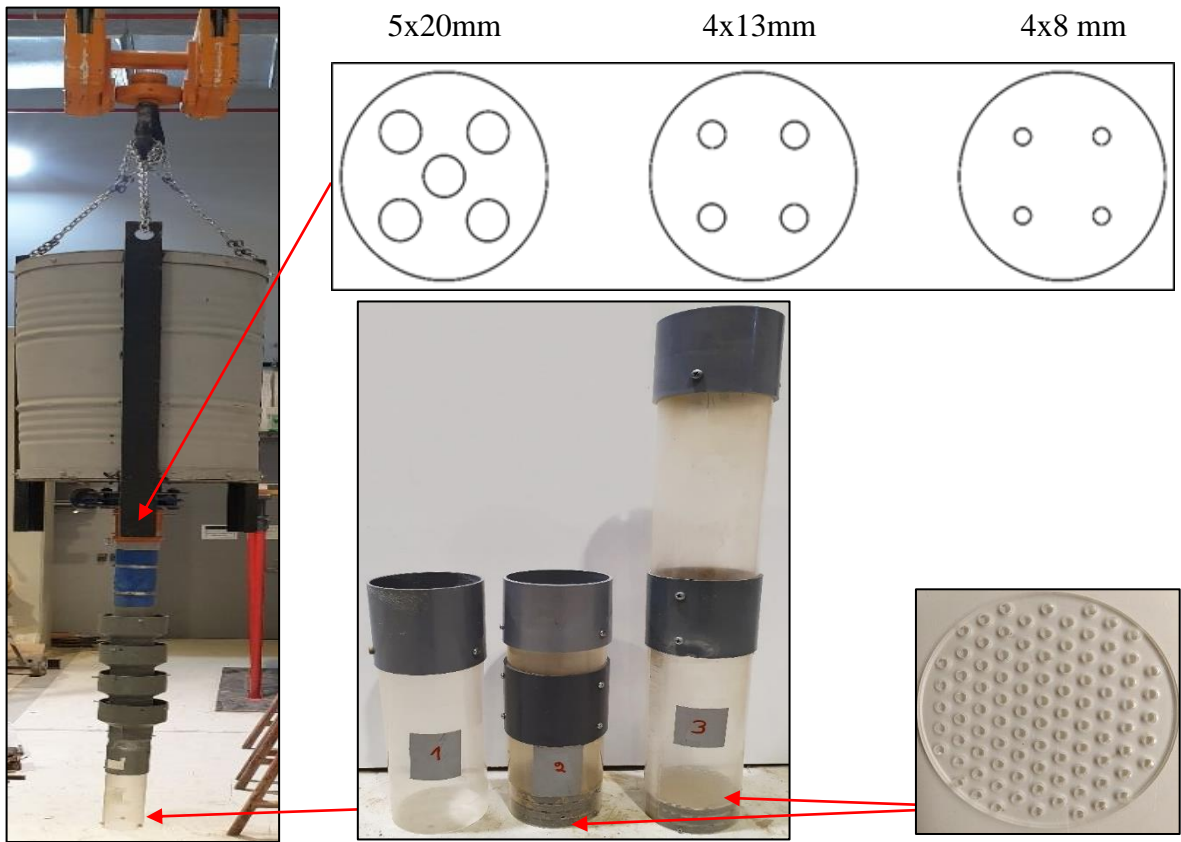


Table 3. Summary of pluviation results

Target density (kg/m ³)	Orifice	10 cm rigid tube (#)		Test #			Chosen drop height (cm)	Discharge rate (kg/min)
				1	2	3		
1550	5 x 20 mm	1	Drop height (cm)	10	20	30	20	39.7
			Weight tank (kg)	3.92	3.92	3.92		
			Weight sand + tank (kg)	24.45	24.28	24.69		
			Volume tank (m ³)	0.013	0.013	0.013		
			Density (kN/m ³)	15.41	15.28	15.59		
			Density (kg/m ³)	1571	1558	1589		
1650	4 x 13 mm	2 or 3	Drop height (cm)	40	45	55	45	11.04
			Weight tank (kg)	3.92	3.92	3.92		
			Weight sand + tank (kg)	25.27	25.51	25.35		
			Volume tank (m ³)	0.013	0.013	0.013		
			Density (kN/m ³)	16.03	16.21	16.08		
			Density (kg/m ³)	1634	1652	1639		
1750	4 x 8 mm	2 or 3	Drop height (cm)	50	60	70	60	2.76
			Weight tank (kg)	3.92	3.92	3.92		
			Weight sand + tank (kg)	26.61	26.78	26.58		
			Volume tank (m ³)	0.013	0.013	0.013		
			Density (kN/m ³)	17.03	17.16	17.01		
			Density (kg/m ³)	1736	1749	1734		

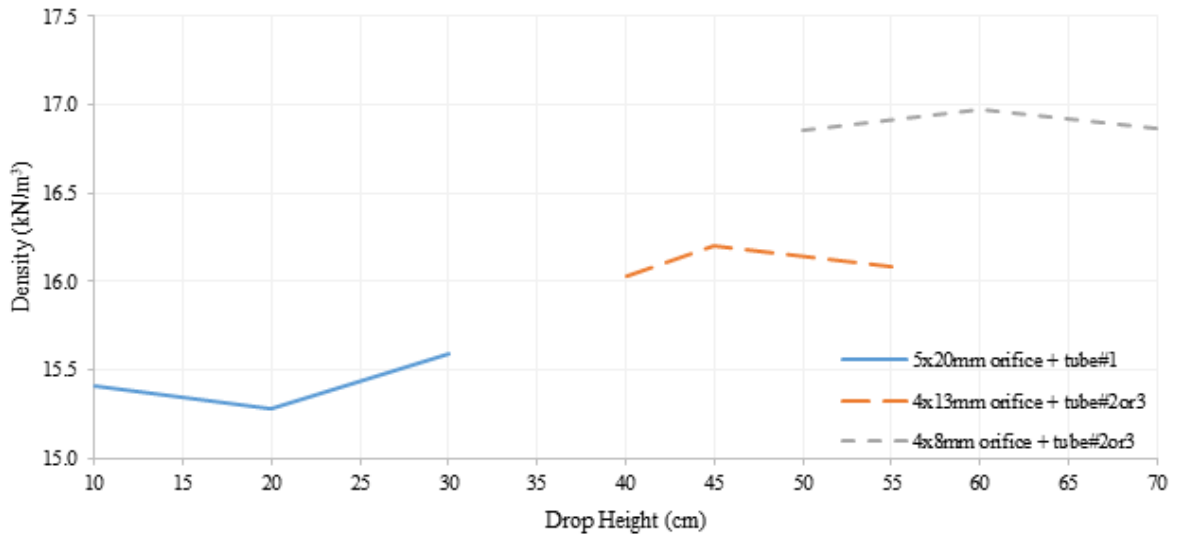


Figure 29. Variation of density with respect to drop height

3.3. Retained Backfill Preparation

3.3.1. Filling Procedure

After assembling the pluviator according to the chosen density, a container is filled with sand and raised using a crane above the tank as shown in Figure 30. At that position, sand particles are always pluviated while maintaining a horizontal sand bed as shown in Figure 31. The container is weighed before and after emptying it to track the total mass of sand dropped in the large tank. This procedure is repeated until reaching the 1.2 m mark present in Figure 31(a), which indicates that a 1.47 m³ sand bed is prepared as shown in Figure 31(b). At that moment it is possible to back-calculate the resulting average density. The wooden planks present in Figure 30 are used as supports during the handling of the pluviator.



Figure 30. Filling process



Figure 31. Horizontal sand bed during filling (a), Horizontal sand bed at the red mark at the end of filling (b)

3.3.2. Emptying Procedure

To empty the tank, three gate valves are installed at the bottom, each placed at one-third of the tank's length to facilitate the emptying process. Figure 32(a) shows the tank raised by a crane and placed on four jacks. Figure 32(b) shows three containers, each placed under a valve, and Figure 32(c) shows #4 sieves positioned directly under the valves to ensure that no large particles will clog the pluviator during the future succeeding test. After successfully emptying the tank, the inner sides are prepared again. Plastic wraps are removed, grease is re-applied, and new wraps placed over it.



(a)



(b)



(c)

Figure 32. System placed on four jacks and ready for the emptying process (a), container under each valve (b), #4 sieves (c)

3.4. Testing Procedure

In the first two tests, the tank is prepared according to the pre-selected density (loose or dense). The procedure that is followed involves initiating a 2 mm displacement cycle where the wall is moved from the at-rest position towards the active portion until reaching -2 mm, and then pushed in the passive direction by 4 mm to reach +2 mm. This cycle is repeated 10 times. Once the set is completed, cycles with the other displacement amplitudes are initiated (5 mm, 10 mm, and 20 mm) in a chronological order, and at the end of the 20 mm set, a static push of 120 mm is executed towards the passive side.

In the third test, the tank is filled with a medium dense sand and directly subjected to the 5 mm displacement cycle that is done according to the method mentioned for the first two tests. The cycle is repeated until a stable response is achieved, and then the cycle displacement amplitude is increased to 20 mm which is conducted in a similar manner.

The last test is similar in procedure to the third one, in terms of bed preparation and test initiation. However, instead of repeating the cycles until reaching a stable response, 8 cycles are performed while enforcing a waiting time between readings at specific wall positions, in both the active and passive sides.

Throughout the passive wall movement, both displacement and lateral earth pressures on the wall are recorded in the manner shown in Table 4. The average rate of loading was chosen to ensure that most of the inertial frictional resistance that could result from fast loading rates is dissipated. The side friction sensor is monitored to ensure that the frictional stresses have stabilized in each loading increment. The wall is then released towards the active portion in a continuous manner while recording the lateral pressures. The release velocity is initially in the order of 1/100 mm/sec, and later increased with the

decrease in lateral pressures to reach the order of 1/10 mm/sec. This scheme of loading allowed for the completion of two displacement cycles per day.

Table 4. Method for loading the bed in the passive direction

Type of loading	Average loading rates (mm/min)	Loading intervals (mm)	Duration between end of loading intervals and data capture (min)
2 mm cycles	0.07	0.4	Until dissipation of built-up frictional stresses on the sidewalls, hence a stable reading is attained
5 mm cycles	0.20	1	
10 mm cycles	0.60	2	
20 mm cycles	1.60	4	
Static push	0.40	10	

CHAPTER IV

RESULTS AND DISCUSSION

4.1. Raw data for Loose and Dense Sand Cases

The raw data that was collected in each displacement cycle consists of pressure readings from the pressure sensors that were located along the wall height and a horizontal displacement reading that is measured by the LVDT located at the top of the wall. Given that the rotating wall was designed and constructed to be rigid, the top wall displacement was used to predict the displacement at every sensor location using linear interpolation. This allowed for constructing p-y curves at each sensor location. Figures 33 and 34 represent the p-y response captured by three sensors, when the wall was cycled 10 times at each displacement interval for a loose and dense bed, respectively. Each column represents data from sensors located at increasing depths (21.5, 46.5 and 71.5 cm) from the top soil surface and each row consists of a specific cycle amplitude (± 2 , ± 5 , ± 10 and ± 20 mm). Since the displacements are applied and measured at the top of the wall, each sensor will move a fraction of the displacement measured by the LVDT.

Results on Figures 33 and 34 lead to several observations. First, the observed p-y curves that describe the response of the soil as the wall is moved in the passive and active directions are highly nonlinear for all densities, magnitudes of displacement intervals, and depths of sensor. This observation is in line with finite element results presented in Elchiti et al. (2017, 2018) for the active response. This indicates that simple elastic-perfectly

plastic p-y models may not be representative of the actual lateral earth pressure response of sands during cyclic loading.

More importantly, the results point to the importance of cyclic loading on the overall p-y response. At any given wall displacement in the passive direction, the lateral stress behind the wall is found to increase incrementally following each displacement cycle. Results indicate a significant increase in the maximum pressure at the passive side after 10 loading cycles. The largest increases are noted for the cases of small displacement intervals ($\pm 2\text{mm}$ and $\pm 5\text{mm}$) which seem to have benefited the most from cycled loading. The increased p-y response as a result of cyclic loading is likely to be associated with a process of densification of the sand with repeated loading cycles.

Second, an examination of the p-y response in the unloading portion of the p-y curves (passive side to active side) indicates that the lateral stress drops at a very fast rate as the direction of wall movement is reversed from passive to active. The rate of decrease in the lateral stress seems to be insensitive to the number of loading cycles, with the unloading sections of the p-y curves showing remarkable consistency between cycles. The shape of the active section of the p-y curve is “hyperbolic” and consistent with numerically derived curves as reported in Elchiti et al. (2018). The transition from the “passive” to the “active” side is characterized by an initial sharp decrease in lateral stress followed by a gradual reduction in stiffness leading eventually to the mobilization of full active conditions behind the wall. It is interesting to note that the wall displacement required for the lateral stress to reach active conditions increases as the range of the displacement interval increases. The wall displacement needed to reduce the maximum stress to the fully mobilized active stress increases from about 1mm for the 2mm displacement cycles to around 5mm for the 20mm

displacement cycles. Additionally, cyclic loading seems to have a marked effect on the active stresses measured by the sensors, whereby the active pressure is observed to reduce with cycles, possibly due to densification of the sand between cycles.

The impact of density and sensor location on the p-y curves will be discussed in detail in the following sections. In general, results indicate that the p-y curves are clearly a function of density with measured lateral stresses at any given displacement being always higher in the dense sand beds compared to the loose sand cases.

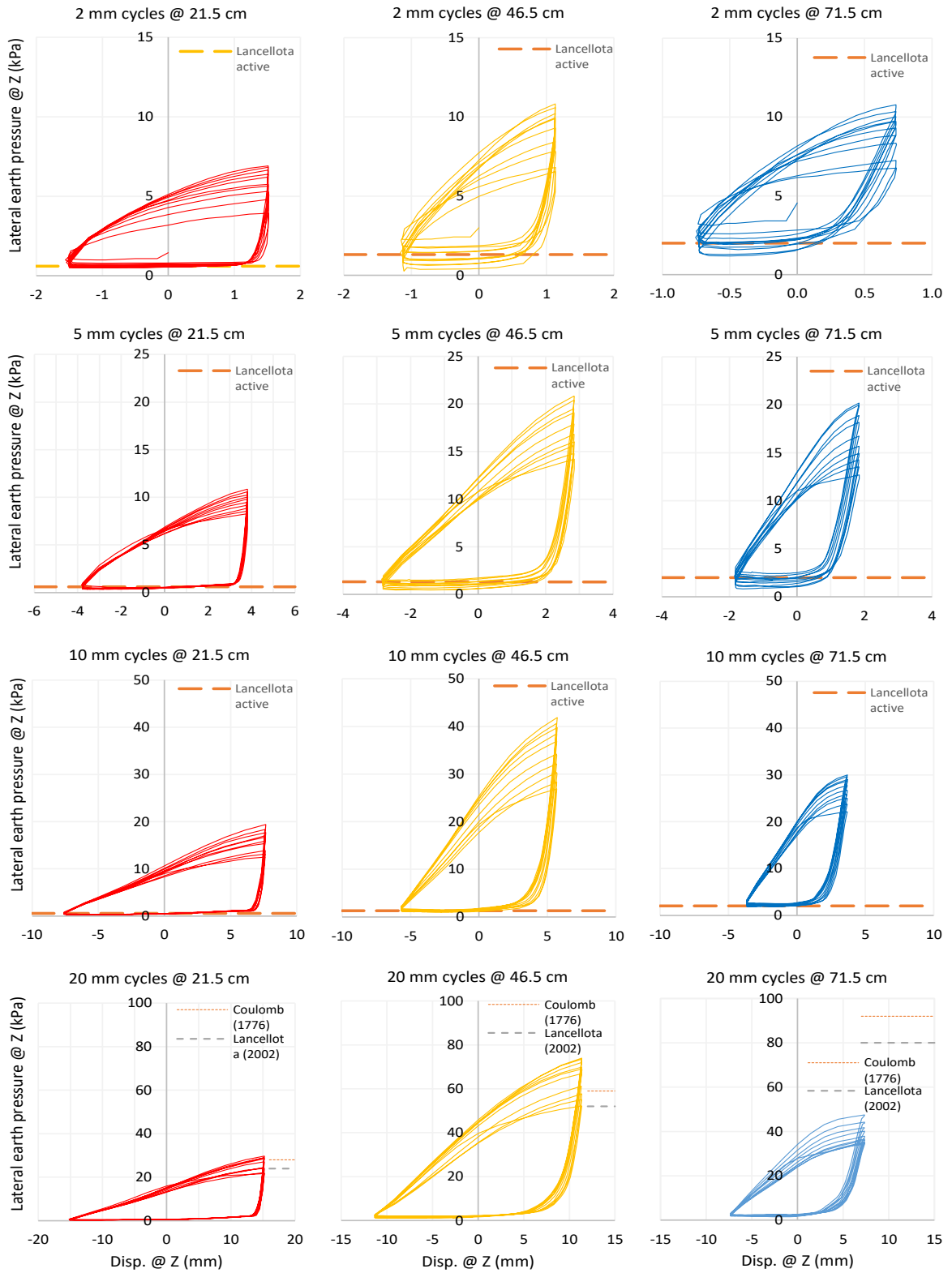


Figure 33. Raw data for test #1 on loose sand

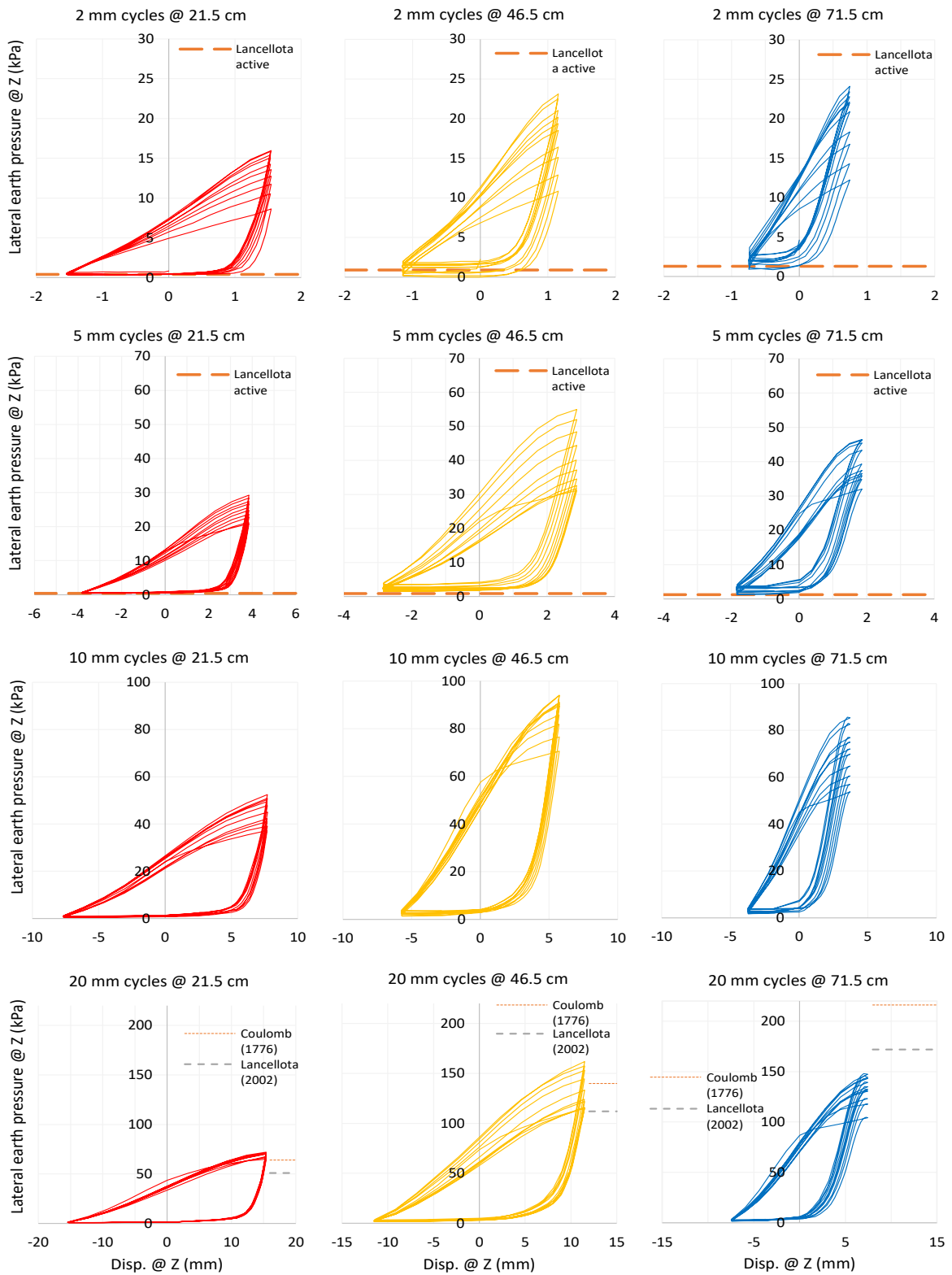


Figure 34. Raw data for test # 2 on dense sand

To put the results into perspective, the theoretical active and passive lateral stresses as computed from the theories of Coulomb (1776) and Lancellota (2002) were calculated for each sensor location and presented in Table 5. In computing these theoretical values, the friction angle of the sand as determined from triaxial tests that were conducted at the lowest confining pressure of 10 kPa were adopted (see Table 2). In the computations, the interface friction angle between the wall and the sand was determined from the sand/Plexiglas friction angle as obtained from interface direct shear tests. This interface friction angle varied between 10 and 12 degrees and was relatively insensitive to the density of the sand. As a result, an average interface friction angle of 11 degrees was adopted in computing the theoretical active and passive pressures at each sensor location.

The theoretical active and passive pressures are plotted on Figures 33 and 34. Comparison with the active experimental response is only shown at the lower cyclic amplitudes (2mm and 5mm) while comparison with the passive response is only shown at the highest cyclic amplitudes (20mm). The active pressures recorded during the two tests indicate an acceptable level of agreement with Lancellota's and Coulomb's methods which yielded similar predictions for the active pressure. For the loose sand case, the predicted active pressures overestimated the measured values with increased number of cycles and increased amplitude of cyclic displacement. This is expected given the densification that is expected to occur in the loose sand with number and displacement magnitude of repeated cycles. For the dense sand case, the measured active pressures showed a lower sensitivity to the number of cycles and magnitude of cyclic displacement.

The passive pressures at limit state as predicted by Coulomb and Lancellota methods are plotted on the measured p-y curves determined for the 20mm displacement

cycle in Figures 33 and 34. At this relatively large displacement amplitude, results show that the lateral stresses measured by the two shallower sensors (at 21.5cm and 46.5cm depth) approached the ultimate passive pressure predicted by the two methods, with the pressures predicted using Coulomb's theory being consistently larger than those predicted using Lancelotta's theory. For these two shallower sensors, the method by Lancelotta seems to yield closer predictions when compared to the maximum pressure measured in the first cycle at the largest applied displacement. With additional cycles, the effect of densification resulted in an increase in the measured maximum lateral stresses. This increase cannot be captured in Lancelotta and Coulomb's methods without an increase in the friction angle of the sand and/or the interface friction angle between the sand and the Plexiglass.

For the sensor placed at 71.5cm in the loose sand case, the maximum passive pressures that were reached in the experimental p-y curves were much smaller than the ultimate values predicted by the theoretical methods. The difference between the measured and predicted values decreased in the dense sand case. This difference between the predicted and measured passive pressures could be attributed to three factors: (1) the displacements reached at this relatively deep sensor (~ 7mm) were not enough to approach the passive limit state, (2) the assumed friction angle that was used in the Coulomb and Lancelotta models could have been larger than the actual friction angle in the sand bed at this confinement level, and (3) a possible boundary effect due to the proximity of this sensor to the bottom of the tank.

Table 5. Passive theories of Coulomb (1776) & Lancellota (2002)

Density (kg/m ³)	Sensor depth (m)	Vertical confinement (kPa)	Friction angles (δ)		Coulomb (1776) (kPa)		Lancellota (2002) (kPa)	
			Sand- Sand	Sand- PLEXI	Pa	Pp	Pa	Pp
1550	0.21	3	42	11	0.6	27.1	0.6	23.7
	0.46	7			1.3	59.3	1.3	51.9
	0.71	11			2.0	91.5	2.0	80.2
1650	0.21	3	48	11	0.5	43.6	0.5	36.5
	0.46	7			1.0	95.4	1.0	79.9
	0.71	11			1.6	147.2	1.6	123.3
1750	0.21	4	52	11	0.4	63.8	0.4	51.0
	0.46	8			0.9	139.7	0.9	111.6
	0.71	12			1.3	215.6	1.4	172.3

4.2. Effect of Previous Loading Cycles on the P-Y Response

After completing the 10th cycle at ± 20 mm displacement, 6 additional cycles were performed at ± 5 mm and ± 20 mm. The objective of this series of tests was to quantify the impact of previous cycles of loading on the p-y response. Figures 35 and 36 show a comparison between repeated p-y curves and the original p-y curves for the cases of loose and dense sands, respectively.

Results on Figures 35 and 36 point to two main observations in relation to the difference between the repeated and original p-y curves. First, a comparison between the p-y responses in the passive to active loading direction indicates no effect of previous cycles of loading on the repeated p-y response. Second, for the passive loading direction, it is clear that the p-y curves in the repeated tests show a significant increase in stiffness compared to the original tests. This increase in stiffness is mostly exhibited in the repeated ± 5 mm cycles, where the greatest percent increase between the 10th cycle of the original tests and

the last cycle of the repeated tests was recorded. The increase in the maximum passive pressure that was measured at the highest displacement reached values ranging between 90-100% for the loose sand and 45-55% for the dense sand. This indicates that loading the bed with ten ± 10 and ± 20 mm cycles in the original test significantly increased the density of the sand.

The effect of densification due to previous cycles on the p-y curves for the repeated ± 20 mm cycles is also evident in Figures 35 and 36, particularly for the loose sand case where the effect of densification is expected to be more dominant. In the dense sand case, the effect of previous loading cycles on the repeated ± 20 mm cycles was relatively modest. This is expected for the dense sand case at ± 20 mm displacement cycles given that the bed was not subjected in the previous loading cycles to any displacement that was larger than ± 20 mm.

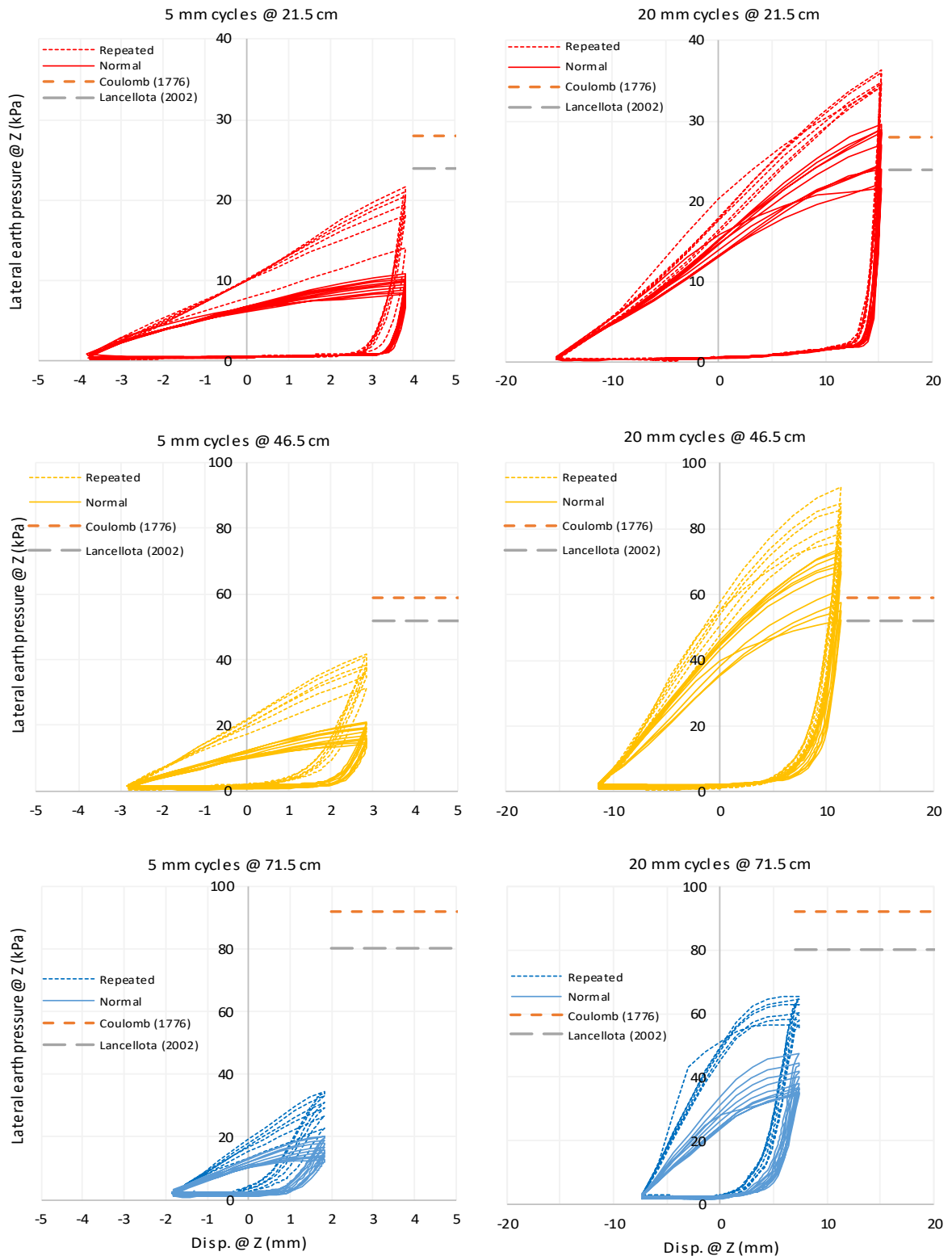


Figure 35. Repeated against normal cycles for test # 1

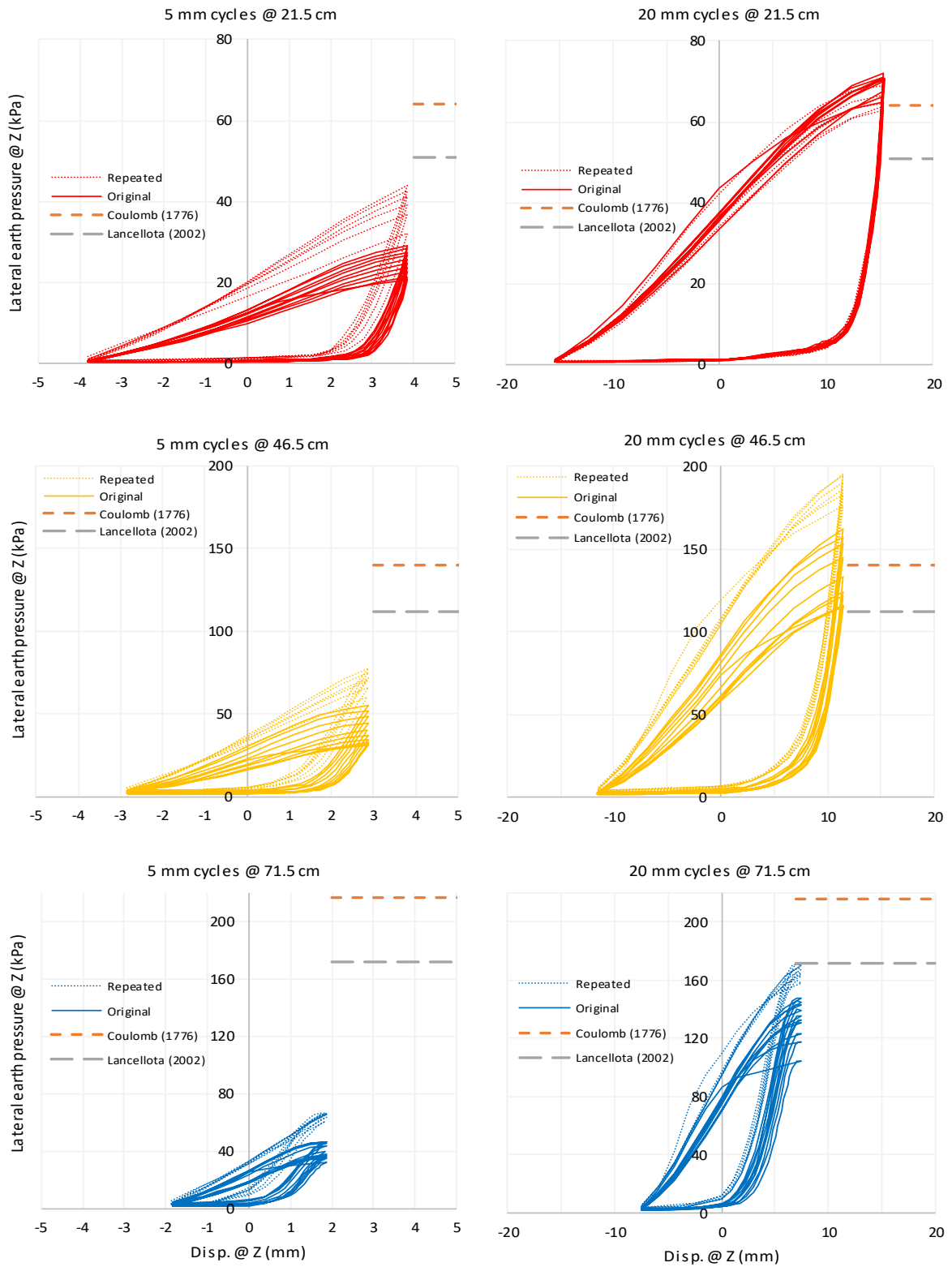


Figure 36. Repeated against normal cycles for test # 2

4.3. P-Y Curves at Large Displacements

At the end of each test, the wall was displaced from the active side to the passive side (from -20 to +120 mm) using the full stroke of the loading piston. The resulting p-y curves are plotted in Figures 37 and 38 with the cyclic p-y curves in the original and repeated ± 20 mm cycle.

An investigation of the measured large displacement p-y curves at each sensor location indicates several interesting observations. First, the two shallow sensors (21.5 and 46.5 cm) portrayed p-y relationships that exhibited clear peaks at a top wall displacement of about 30mm (10-mm after the maximum displacement reached in the cyclic test), irrespective of the sand density. The mobilization of a clear peak, followed by a strain softening response in the p-y curves, is an indication of densification that occurred in both the loose and dense sand beds during the previous loading cycles. Interestingly, the strain softening response was interrupted in the loose sand case at a top wall displacement of 50mm and was replaced by a strain hardening p-y response that could only be explained by the formation of a new failure plane. For the dense sand case, the p-y curves continued to strain soften as the wall was pushed towards critical state conditions at large deformations.

For the case of the third sensor (at a depth of 71.5cm), the confinement was large enough to switch the p-y behavior from a strain softening to strain hardening, whereby the lateral stresses increased continuously until reaching critical state.

It should finally be reiterated that the maximum passive pressures that were predicted by Lancellota's theory seem to provide a good estimate of the experimentally passive pressures, but only for the first cycle of loading due to changes in density as the number of cycles increases.

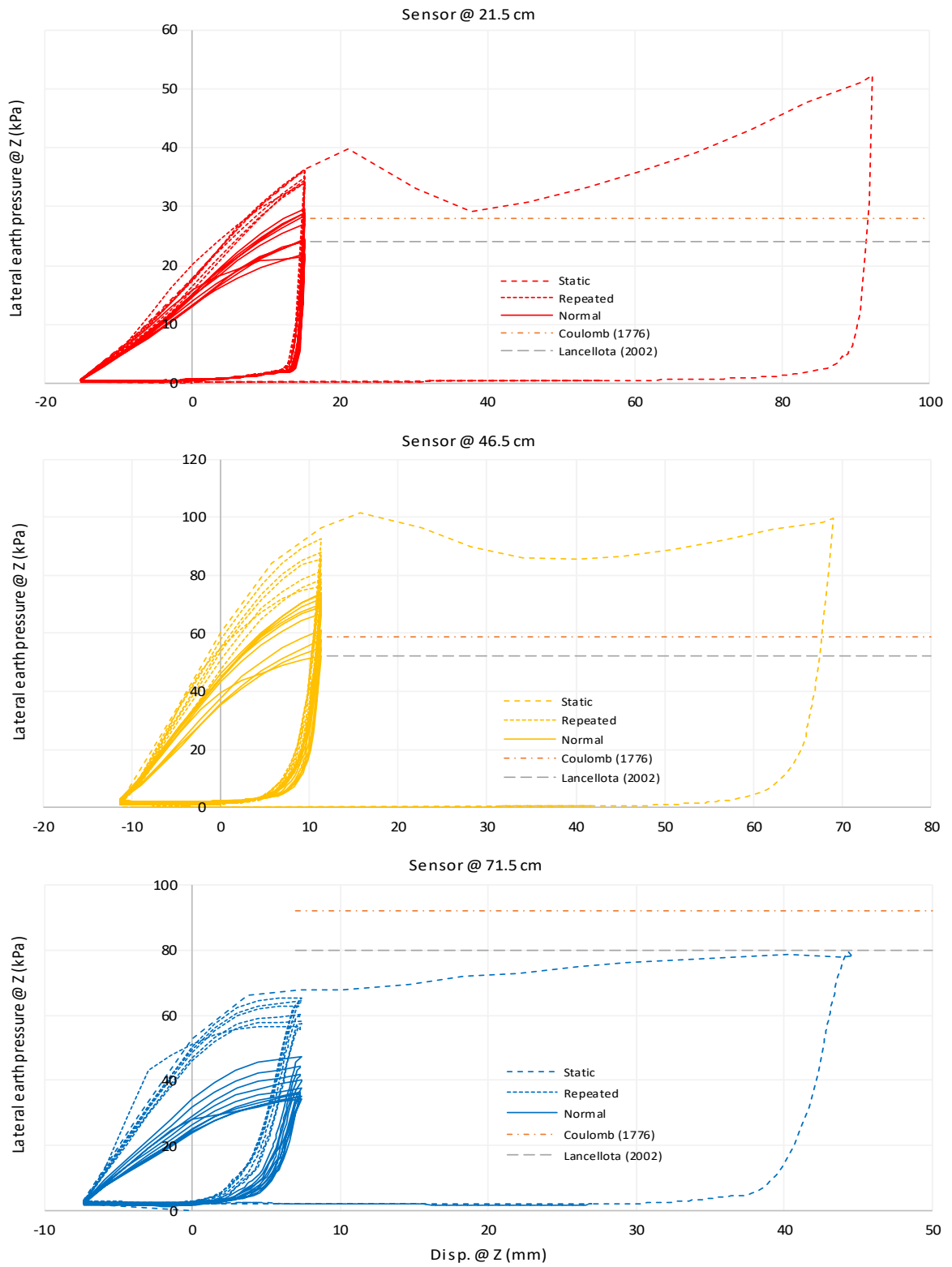


Figure 37. Static push compared to previous cycles for test # 1

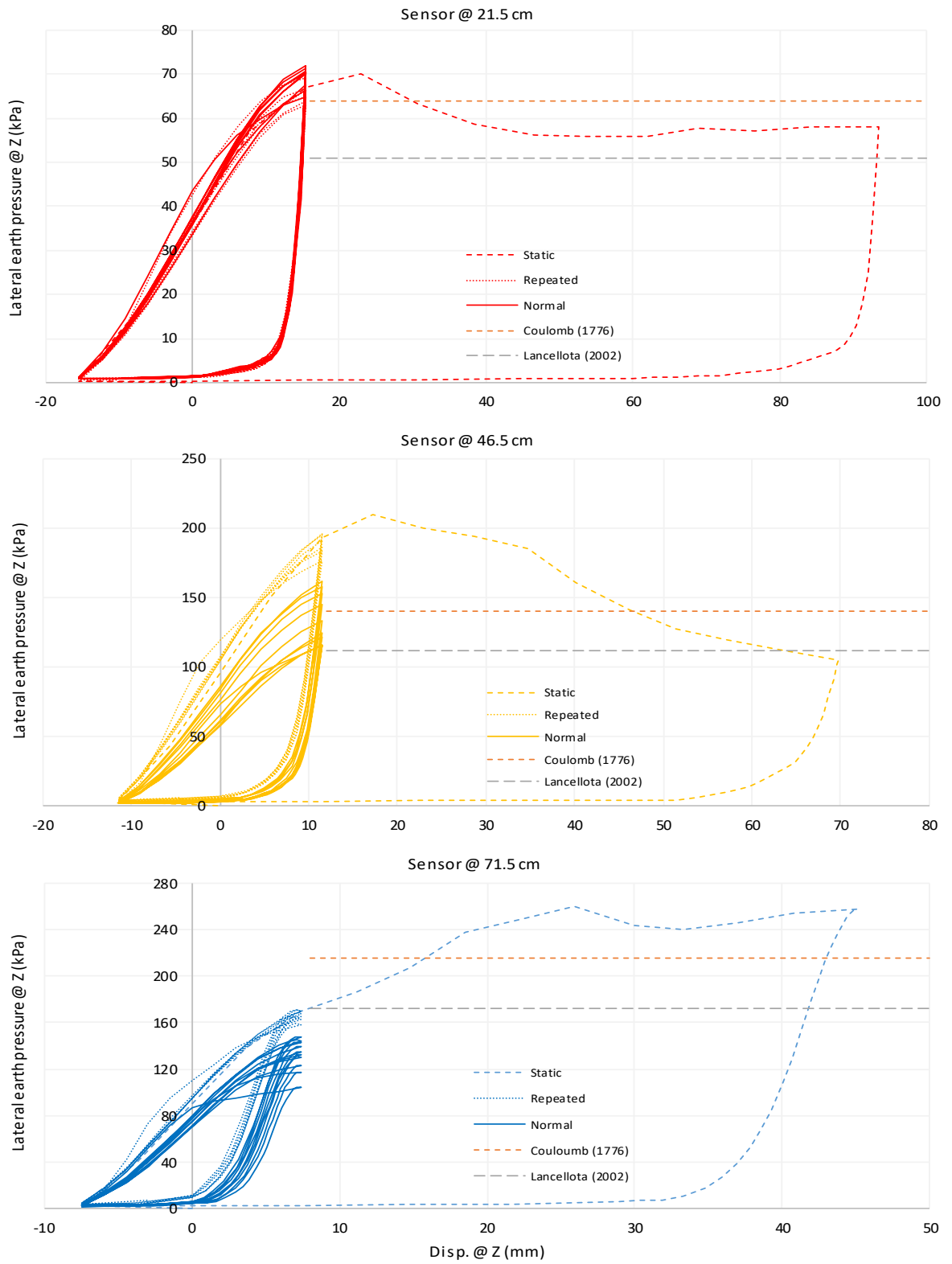


Figure 38. Static push compared to previous cycles for test # 2

4.4. Sidewall interface friction angle

The inner side walls of the tank were covered with grease coating and a plastic wrap to minimize the interface friction between the inner faces of the side walls and the sand. As the wall is displaced, the friction stresses that are mobilized between the side wall and the sand can be measured with the friction sensor that was custom-fabricated for this purpose. The measured side wall frictional stress is then divided by the lateral normal stress that is measured using a sensor that is placed on the wall opposite to the friction sensor at the same elevation to compute the interface friction coefficient and the interface friction angle between the wall and the soil. Figures 39 and 40 show the back-calculated interface friction angles that were measured during the active to passive loading as a function of applied top wall displacement for the loose and dense cases, respectively.

Results indicate that the mobilized friction angle increases as the wall is pushed from the active side towards the passive side, attaining maximum values that are as high as 6° in the loose sand case and about 3° for the dense sand case. These values are relatively small, indicating that wrapping the sidewalls with a plastic sheet and coating them with grease minimized the interface friction during the displacement of the wall. Reducing the interface friction on the side walls minimizes the impact of the boundary conditions on the lateral earth pressures that are measured by the pressure sensors in the middle of the wall at different depths. Minimal side friction will ensure that the measured lateral earth pressures are more or less indicative of the plain strain conditions that are typically encountered in practical basement/retaining walls.

A more detailed investigation of the interface friction angle data on Figures 39 and 40 indicates that, apart from the cases involving ± 2 mm cycles where significant scatter in

the friction angles was encountered with cyclic loading, all other cases (± 5 to ± 20 mm cycles) showed a trend whereby the interface friction angle at any given wall displacement decreases slightly with increasing number of cycles. Moreover, for the cases involving dense soils, the interface friction angles were found to be smaller than those observed in the equivalent loose sand case. This result is reasonable since the Poisson ratio for dense sands is relatively smaller than that of loose sand, resulting in proportionally smaller normal stresses on the sidewalls as the wall is displaced towards the passive direction. Lastly, during the large amplitude active to passive push where very high movements were induced, the interface angle remained relatively constant at around 3° and 2° , for loose and dense sand, respectively.

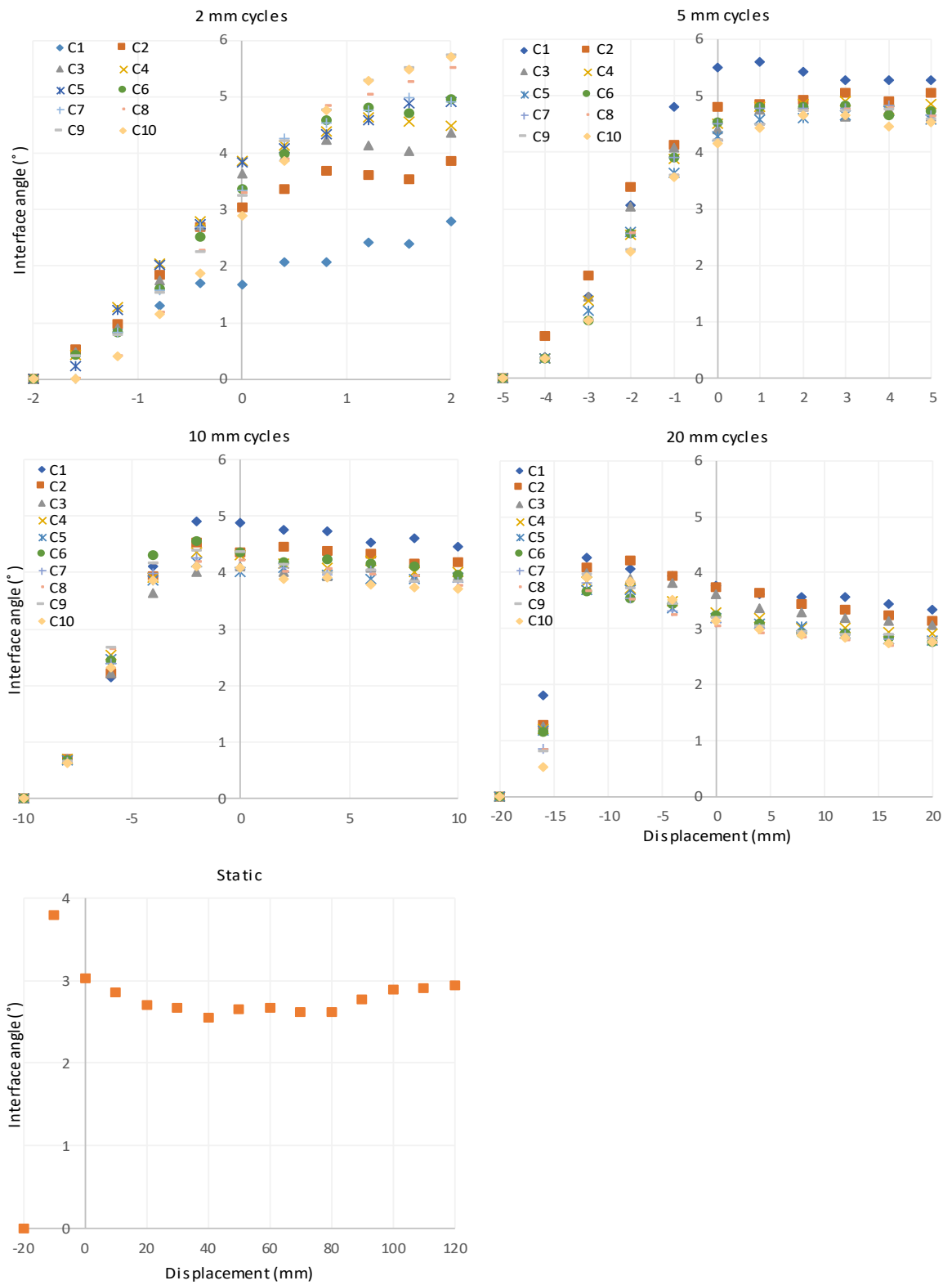


Figure 39. Sidewall interface friction angle during test #1

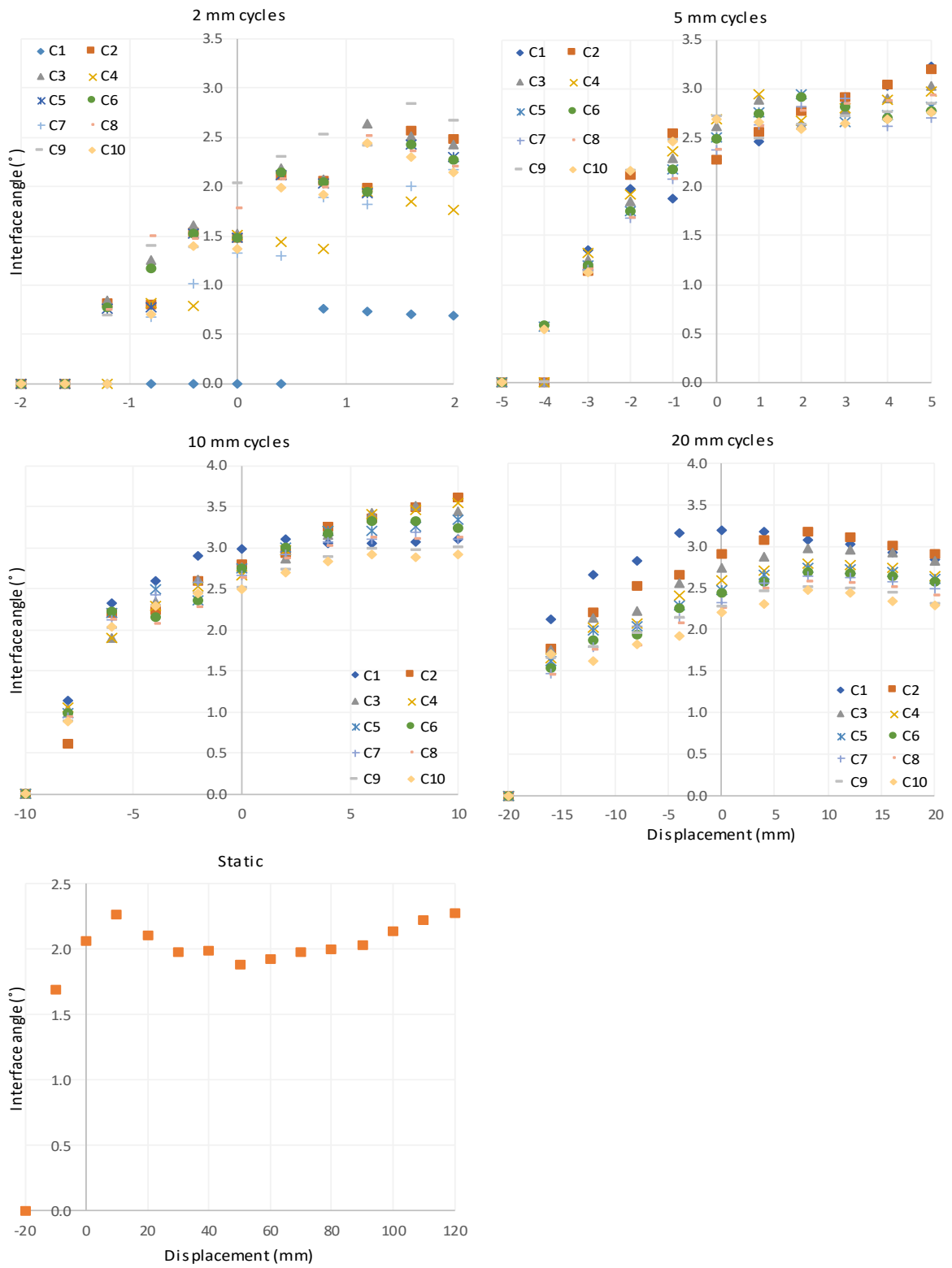


Figure 40. Sidewall interface friction angle during test # 2

4.5. Discussion

4.5.1. *Impact of relative density on p-y curves*

The density of the backfill was shown to have a clear effect on the measured p-y curves. For the same number of displacement cycles, and for the same magnitude of wall displacement, cases with higher densities induce higher maximum passive lateral stresses. Figure 41 shows a plot of the variation of the maximum passive pressure that was mobilized at the end of each cycle for all magnitudes of cyclic wall displacement. Aside from the clear observation that the maximum passive pressure increases with the number of cycles, the slope showing the increase in the maximum passive pressure with number of cycles is higher for cases with higher wall amplitudes (ex. rate of increase in case of $\pm 20\text{mm} > \pm 10\text{mm} > \pm 5\text{ mm} > \pm 2\text{ mm}$ cycles). This is particularly evident for the case of dense sands and less evident for the case of loose sands. Moreover, in any given displacement cycle, the maximum passive stress increases with the number of cycles at a decreasing rate without reaching a clear asymptote even after 10 cycles.

In Figure 42, the p-y curves for loose and dense sands are plotted on the same scale for comparison. The effect of backfill relative density is clearly exhibited whereby p-y curves in the dense sand cases portrayed higher stiffnesses at low levels of wall displacement and higher maximum passive pressures at the maximum wall displacements applied. At any given wall displacement, the lateral stresses mobilized behind the wall in the dense sand cases could be more than 2.0 to 3.0 times larger than those for the loose sand cases.

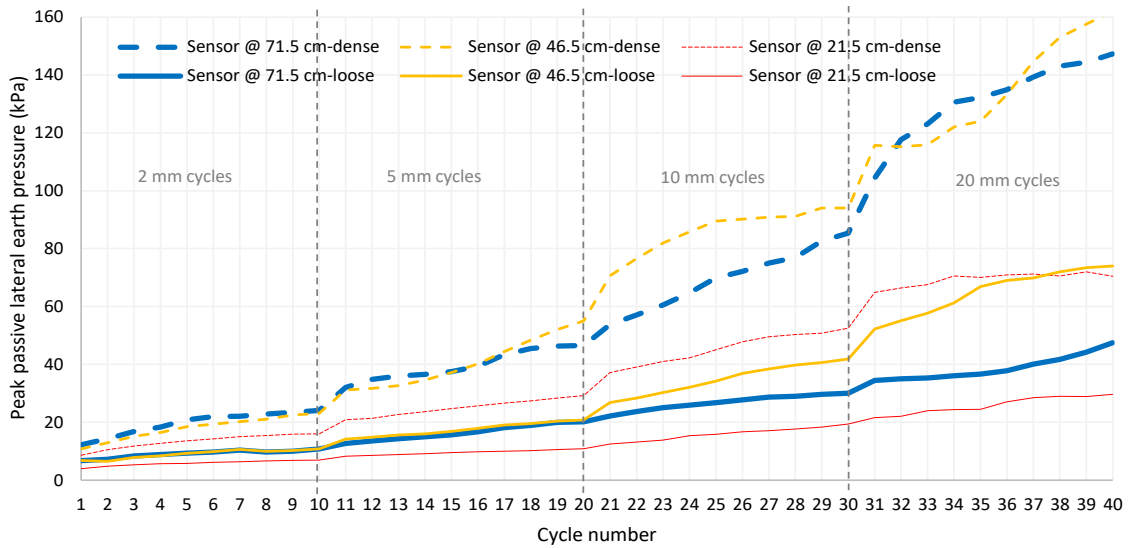


Figure 41. Consecutive peak passive pressures for all cycles during test # 1 and 2

Figure 43 shows a comparison between the p-y curves that were measured in the last active to passive large displacement push that was conducted at the end of each experiment. The figures illustrate the clear difference in the p-y responses as a result of the changes in density. The initial stiffness of the p-y curve is consistently larger in the cases involving dense sand, irrespective of the sensor location. The same applies to the maximum passive pressure mobilized during the static push. It is interesting to note that the local wall displacement required to mobilize the maximum passive pressure seems to be governed by the confining pressure (depth of sensor) and not on the relative density. For example, the maximum passive pressure is mobilized at a local wall displacement of about 21mm for the upper sensor, irrespective of the sand density. For the second sensor, the maximum passive pressure was mobilized at a local wall displacement (at the level of the sensor) of about 16mm (irrespective of density). For the deepest sensor, the p-y response was closer to a strain hardening response that did not exhibit early peaks.

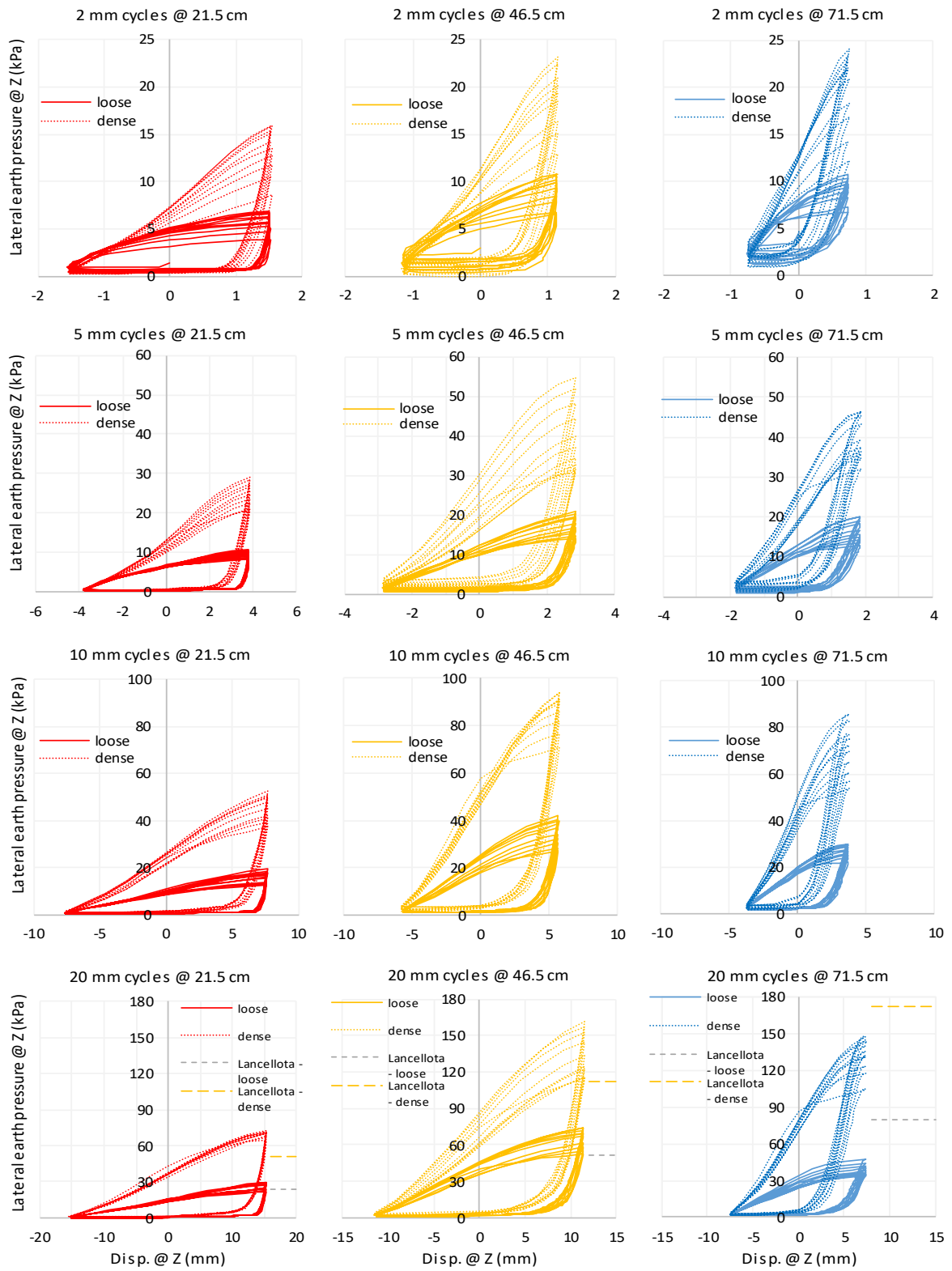


Figure 42. Effect of density on the cyclic response

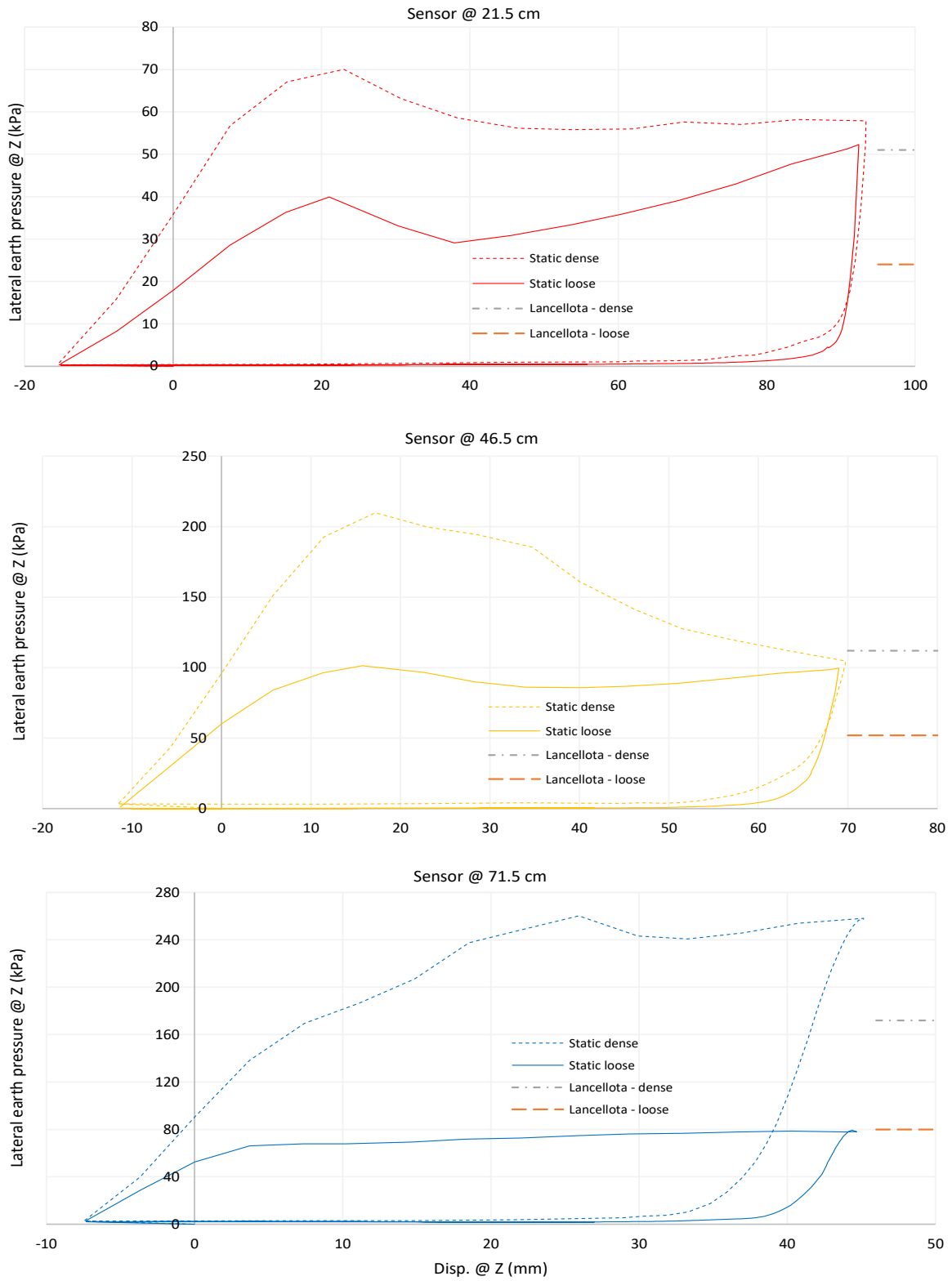


Figure 43. Effect of density on the static response

To shed light on the impact of densification due to cyclic loading on the p-y response, the percent increase in the maximum passive stresses between the first and last (10th) loading cycle in each wall displacement range was computed and plotted in Figure 44 as a function of the number of cycles. The percent increase in the passive stress with number of cycles is plotted on the same figure for the loose and dense sand cases for comparison.

Results on Figure 44 indicate that (1) the maximum passive pressure increases with the number of cycles at a decreasing rate, which is clearly reflected in the more-or-less hyperbolic variation of the percent increase in the stress with the number of cycles, (2) the maximum percent increase in passive pressure is observed in the last cycle (10th cycle) and varies depending on the wall displacement amplitude range, with the case involving the smallest cyclic amplitude (2mm) showing increases of up to 110% in passive pressure while cases involving the largest cyclic amplitude (20mm) showing maximum increases that are as low as 30% to 40%, and (3) the effect of relative density on the maximum percent increase in passive stress is affected by the wall displacement amplitude in the sense that cases of dense sands showed larger percent increases in passive pressure in the low displacement ranges (2mm and 5mm), while cases involving loose sands showed larger percent increases in passive pressure in the higher displacement range (10mm and 20mm). The observations in point (3) above are particularly applicable to the upper two sensors which exhibited higher local wall displacements compared to the deepest sensor which may have been affected by boundary effects due to its proximity to the bottom of the wall.

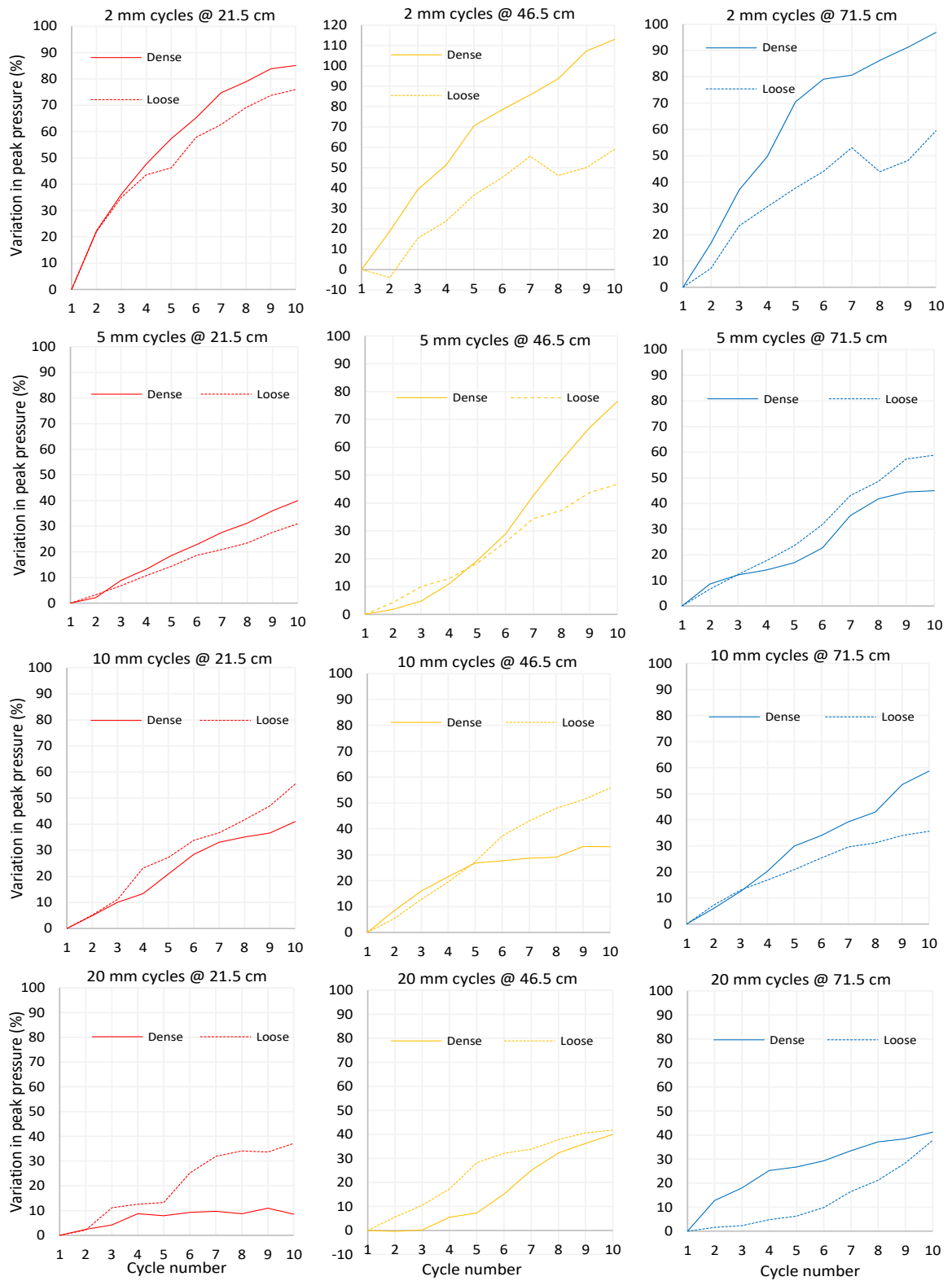


Figure 44. Rate of change for peak values for tests #1 and 2

4.5.2. Comparison with Medium Dense Behavior (El-Chiti et al. 2019)

El-Chiti et al. (2019) measured cyclic p-y curves using the same test setup that was used in this study, except that the backfill material was prepared at a density of 1650 kg/m^3 which is intermediate between the two densities of 1550 and 1750 kg/m^3 used in this research study. A comparison between the maximum passive pressures that were measured at the end of each loading cycle for beds with different relative densities is presented in Figure 55. All responses follow the same increasing trend of passive pressure with cyclic loading. As expected, the passive lateral stresses that were measured in the medium dense sand bed (El-Chiti et al. 2019) fell between the passive pressures measured for the loose and dense sand cases tested in this study.

Interestingly, the maximum lateral stresses that were measured in the loose and medium dense sand cases were closer to each other in the shallowest sensor situated at 21.5cm from the surface. For the deeper sensors, the maximum passive pressures were more systematically affected by increasing the sand density from 1550 to 1750 kg/m^3 . This difference in the response between the shallowest sensor and the other two sensors may be related to slight differences in the testing procedure between the work of El-Chiti et al. (2019) for the medium dense sand case, and this work (loose and dense cases). In the tests conducted by El-Chiti et al. (2019) on medium dense sands, observation of the surface of the bed during cycled loading pointed to reductions in the surface level of the bed near the moving wall due to densification of the soil. El-Chiti et al. (2019) did not add any sand to re-level the surface of the bed during the cyclic loading. The drop in the surface level of the bed due to densification in the medium dense test may have resulted in slightly lower passive earth pressures due to a slight decrease in the vertical stresses at the level of the

sensor. Such a potential decrease in vertical stresses may have affected the lateral stresses measured by the top sensor during passive loading, without imparting any markable impact on the lateral stresses measured in the lower two sensors.

In the tests conducted in this study on loose and dense sands, a decision was made to re-level the sand bed to 1.2m after the end of the 10 cycles in each cyclic displacement interval. This may explain the similarity between the lateral stresses measured in the loose and medium dense tests in the top pressure sensor, particularly for the large displacement cycles (± 10 and ± 20 mm), where densification was more pronounced leading to significant drops in the bed surface. Since the sand bed was re-leveled (by adding sand) in the case of loose sand but not in the case of medium dense sand, this could explain why the response measured by the sensor at 21.5 cm during the ± 10 and ± 20 mm cycles contradicts the increasing trend in passive pressure with additional cycles and the similarity between the loose and medium dense results for this sensor.

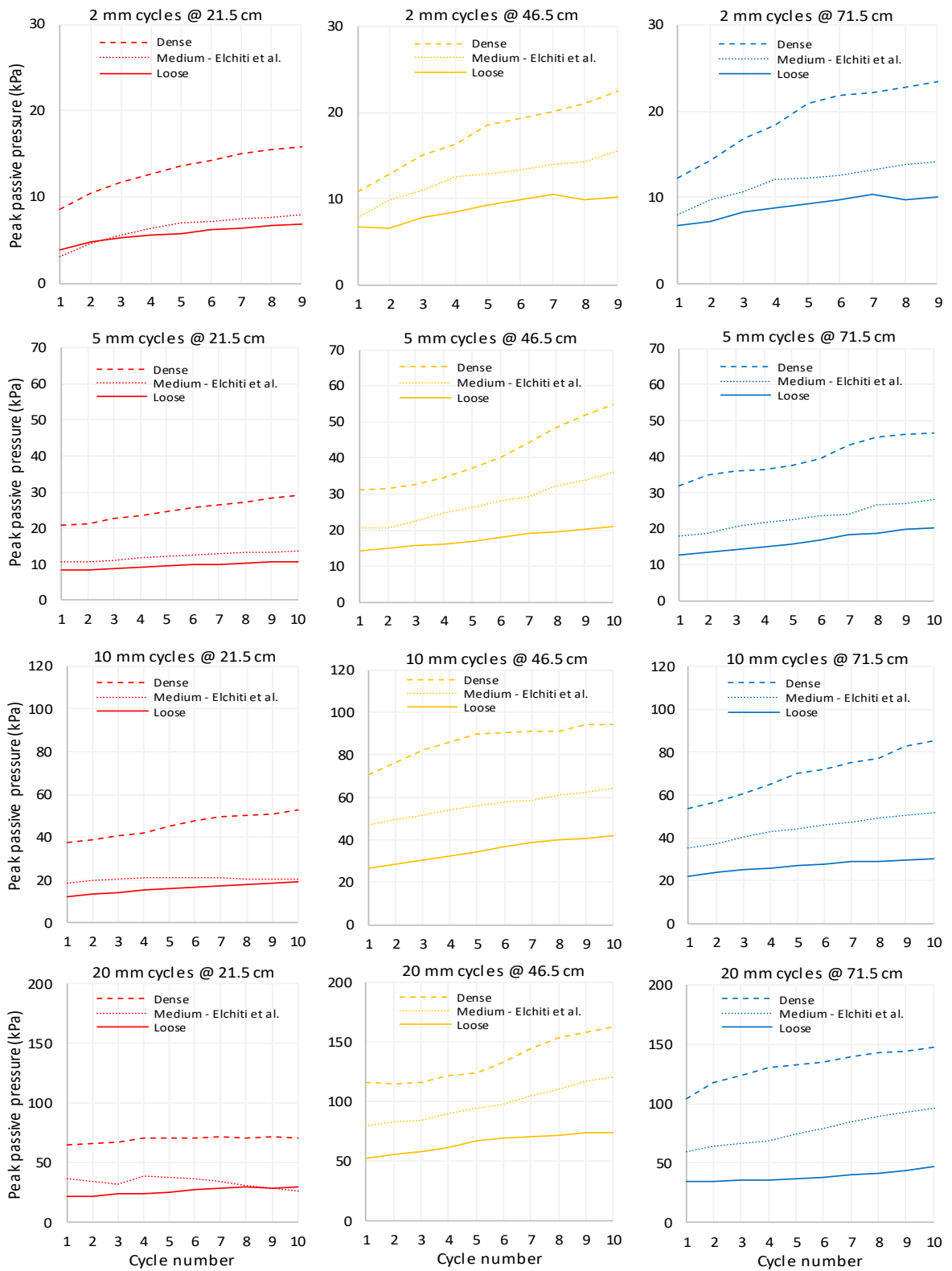


Figure 45. Peak pressures for three different densities

4.5.3. Effect of number of cycles (Medium Dense Sand with 22 cycles)

The results of the tests conducted using 10 cycles on sand beds with varying relative densities indicated an increase in the stiffness and maximum passive pressure with increasing number of cycles. The rate of increase in the maximum passive pressure decreased with the number of cycles but did not show signs of stability even after 10 cycles. A decision was made to conduct an additional test whereby the number of cycles would be increased beyond 10 to investigate whether a stable p-y response would eventually be reached. The test was conducted on a medium dense sand backfill with a cyclic testing program that is comprised of ± 5 and ± 20 mm cycles only (to reduce the time of the experiment) while doubling the number of cycles to 20. Eventually, the test was conducted with a maximum number of cycles of 22 for each cyclic displacement amplitude.

The measured p-y curves as obtained from 22 cycles are presented in Figures 46 and 47 for the ± 5 and ± 20 mm amplitudes, respectively. Also plotted on the same figures are the corresponding 10 cycles that were conducted in the test by El-Chiti et al. (2019). While analyzing the results of the ± 5 mm cycles in Figure 46, an important factor has to be taken into consideration. The ± 5 mm p-y cycles from El-Chiti et al. (2019) have been preceded by ten ± 2 mm cycles. This is not the case in the twenty-two cycles conducted in this study. The effect of the ten ± 2 mm cycles on the ± 5 mm cycles are clearly exhibited in Figure 47 by comparing the first p-y curve from the current study to the first p-y curve in the study by El-Chiti et al. (2019). It is clear that the initial p-y curves in this study are lower than the initial p-y curves by El-Chiti et al. (2019) for the three sensors analyzed. This is directly correlated to the effect of densification that has probably occurred in the tests by El-Chiti et al. (2019) due to the preceding ten ± 2 mm cycles.

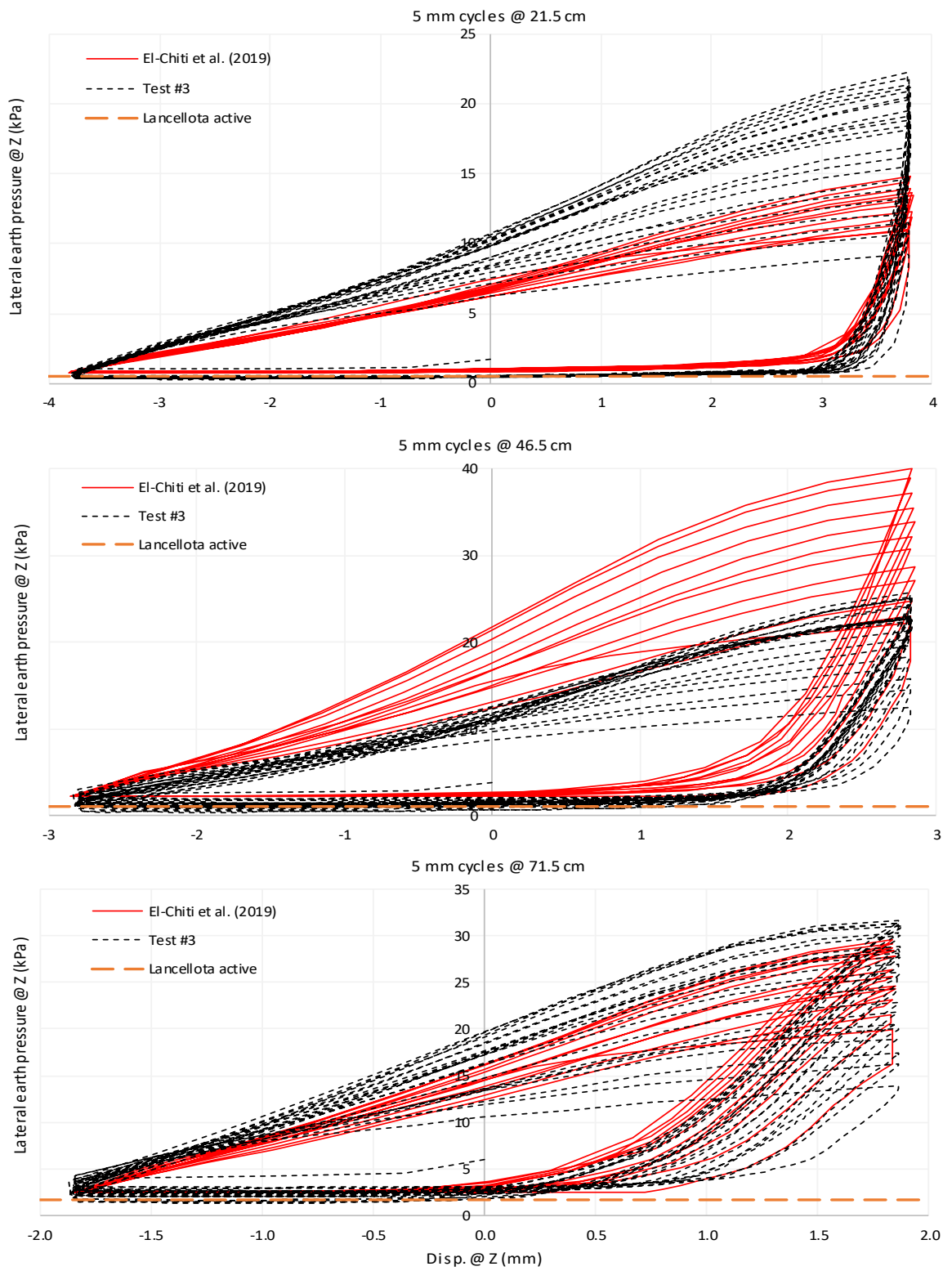


Figure 46. Effect of numerous 5 mm cycles on soil response

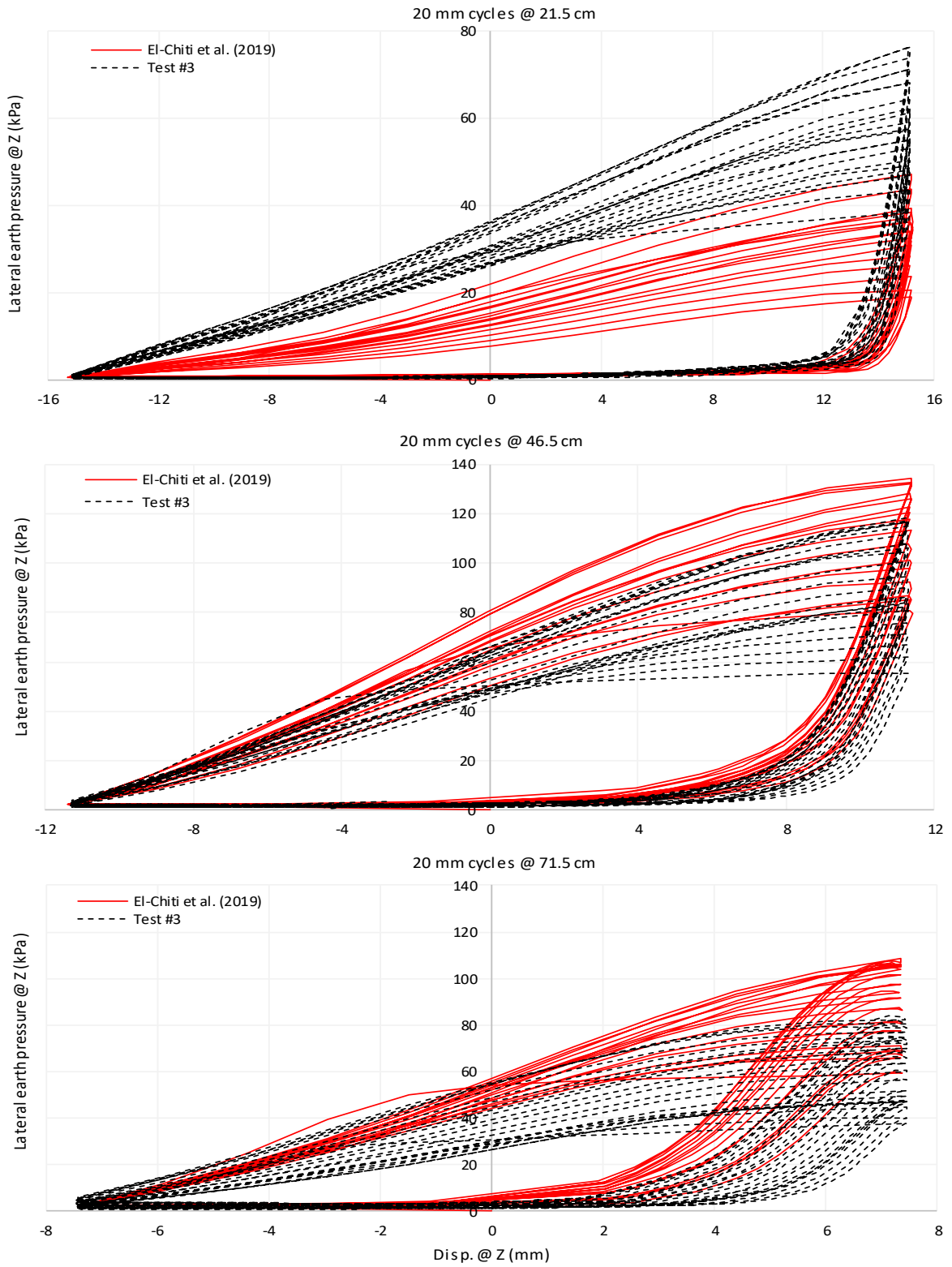


Figure 47. Effect of numerous 20 mm cycles on soil response

Upon repeated cycles, the p-y curves show increases in stiffness and maximum passive pressure. This observation is valid in the two tests (this study and the test by El-Chiti et al. 2019). For the shallowest sensor, results in this study indicate that the p-y curves continued to significantly benefit from cyclic loading even at cycles exceeding 10, although at a slower rate. For this sensor, the increase in the passive p-y curves with repeated cycles was more significant than that observed in the test conducted by El-Chiti et al. (2019). As mentioned previously, the p-y curves for the shallower sensor in El-Chiti et al. (2019) have been affected by the fact that no sand was added to re-level the sand bed between displacement intervals. For the middle and lower sensors which were not affected by re-leveling of the surface, the p-y curves show a similar rate of increase in the passive stresses with number of cycles in the first 10 cycles of the two tests. As the cycles were increased beyond 10 to a maximum of 22, additional increases in the passive p-y response were observed but at a clearly reduced rate.

For the ± 20 mm amplitude cycles, the first p-y curves (cycle 1) in the test conducted in El-Chiti et al. (2019) also showed higher stiffness and maximum passive pressure compared to the test conducted in this study, particularly for the middle and lower sensors that were not affected by the sand bed leveling. This is possibly due to the preceding ± 10 mm cycles that were implemented prior to the ± 20 mm cycles in the test by El-Chiti et al. (2019). With an increase in the number of cycles, densification occurred leading to higher passive p-y response in both tests. The rate of increase in the passive response in the first 10 cycles was relatively similar in the two tests, and as the number of cycles increased from 10 to 22, the pressures increased without reaching complete stability at the maximum number of cycles applied.

The variation of the maximum passive pressures with the number of cycles is plotted on Figure 48 for the ± 5 and ± 20 mm displacement cycles. The percent increase in the maximum passive pressure in any given cycle in reference to the first cycle was computed and plotted versus the number of cycles in Figure 49 for the ± 5 and ± 20 mm displacement cycles. Results indicate that the maximum passive pressures in the ± 5 mm cycles kept increasing with the number of cycles reaching percent increases as high as 105 to 140% in the 22nd cycle, compared to a percent increase of 80% at 10 cycles. These results indicate that the rate of increase in the passive pressure decreased slightly after 10 cycles. For the ± 20 mm cycles similar results were obtained with maximum increase in the order of 100% to 120% in the passive pressures at 22 cycles. Unlike the ± 5 mm, the rate of increase in passive pressure does not seem to reduce at larger cycles. In fact, the variation in the passive pressures with number of cycles increased from an average of 55% at 10 cycles to about 110% at 22 cycles.

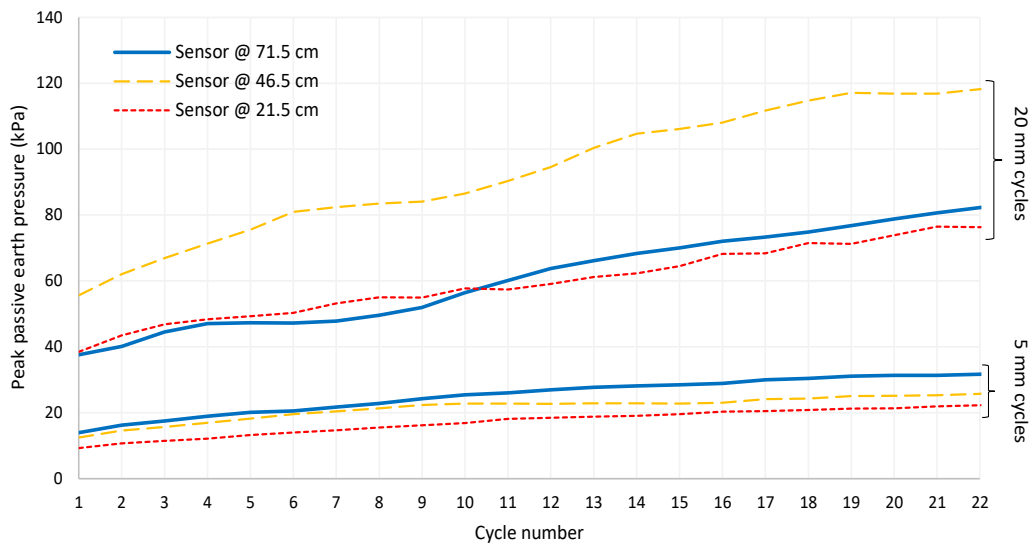


Figure 48. Peak response in function of repeated cycles

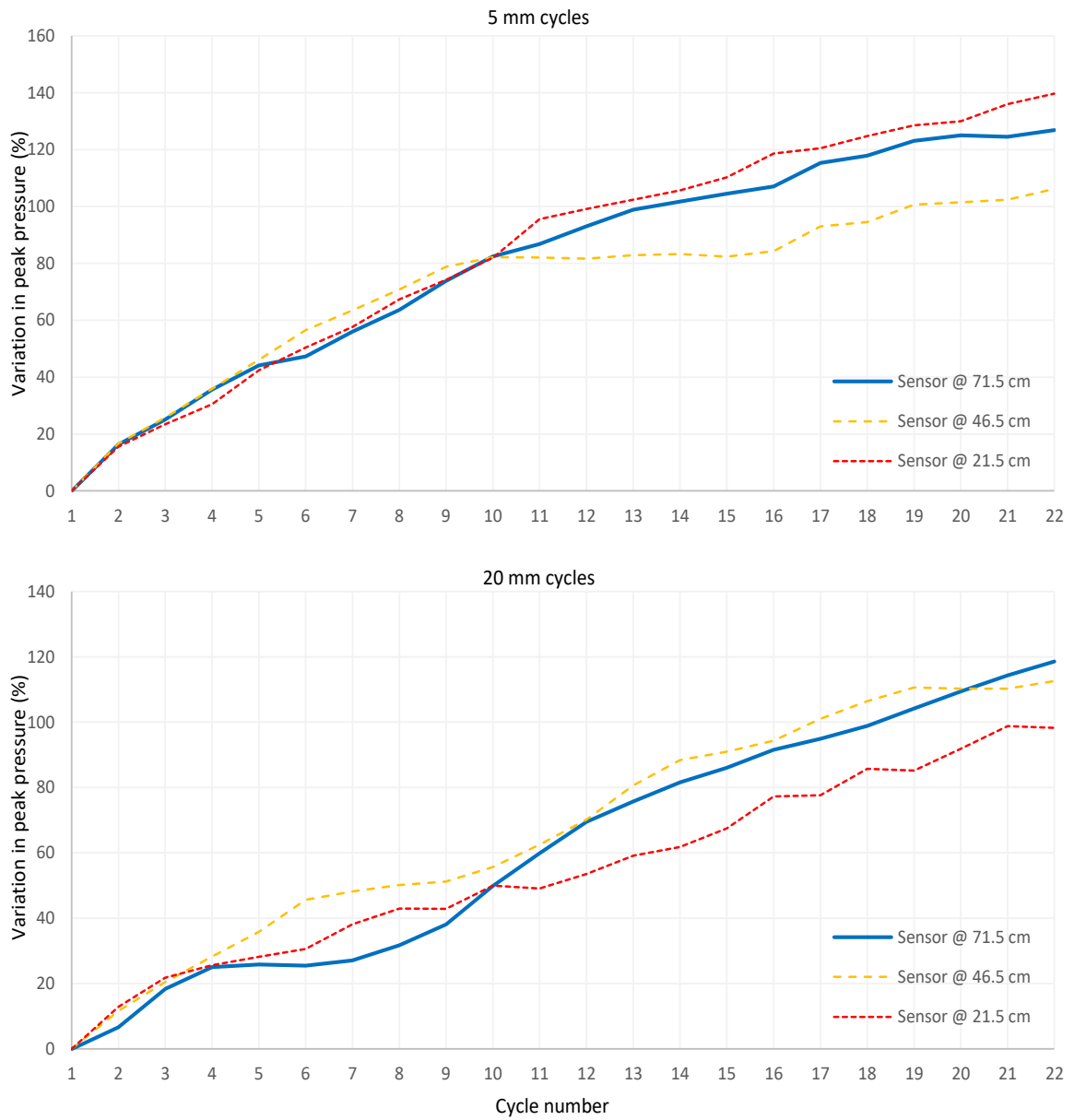


Figure 49. Percent change in peak response with every cycle

4.5.4. Representing the passive p-y response

For the limited cyclic displacement magnitudes (maximum 20 mm displacements) that were applied to the wall in this study, the passive p-y curves could be described by a simple bi-linear representation, with an initial steep slope that starts from the active stress state and ends at specific wall displacements, whereby the slopes of the p-y curves reduces dramatically. This reduced slope describes the second portion of the bi-linear response, which is expected to end at the ultimate passive pressure, after which the p-y response should either remain constant or strain soften with additional wall displacement. Since the ultimate passive pressure was not encountered in any of the cyclic tests, the focus in this section will be on describing the variation of the two slopes describing the observed cyclic p-y responses up to maximum top wall displacements of 20mm.

For illustration, the p-y curves for the medium dense test that was conducted in this study are presented in Figures 50 (for ± 5 mm cycles) and 51 (for ± 20 mm cycles). Also plotted on these curves are bi-linear representations of the observed p-y response. Similar graphs are presented in the Appendix for the other tests conducted in this study. The bi-linear representations of the p-y curves were used to back-calculate the slope of the initial segment of the p-y response (Slope 1) and the slope of the second segment of the p-y response (Slope 2). While analyzing the results, it was clear that Slope 1 is significantly affected by the number of cycles, whereas slope 2 seems to be more-or-less insensitive to the number of cycles. As a result, a decision was made to adopt a constant value for Slope 2 for any given sensor.

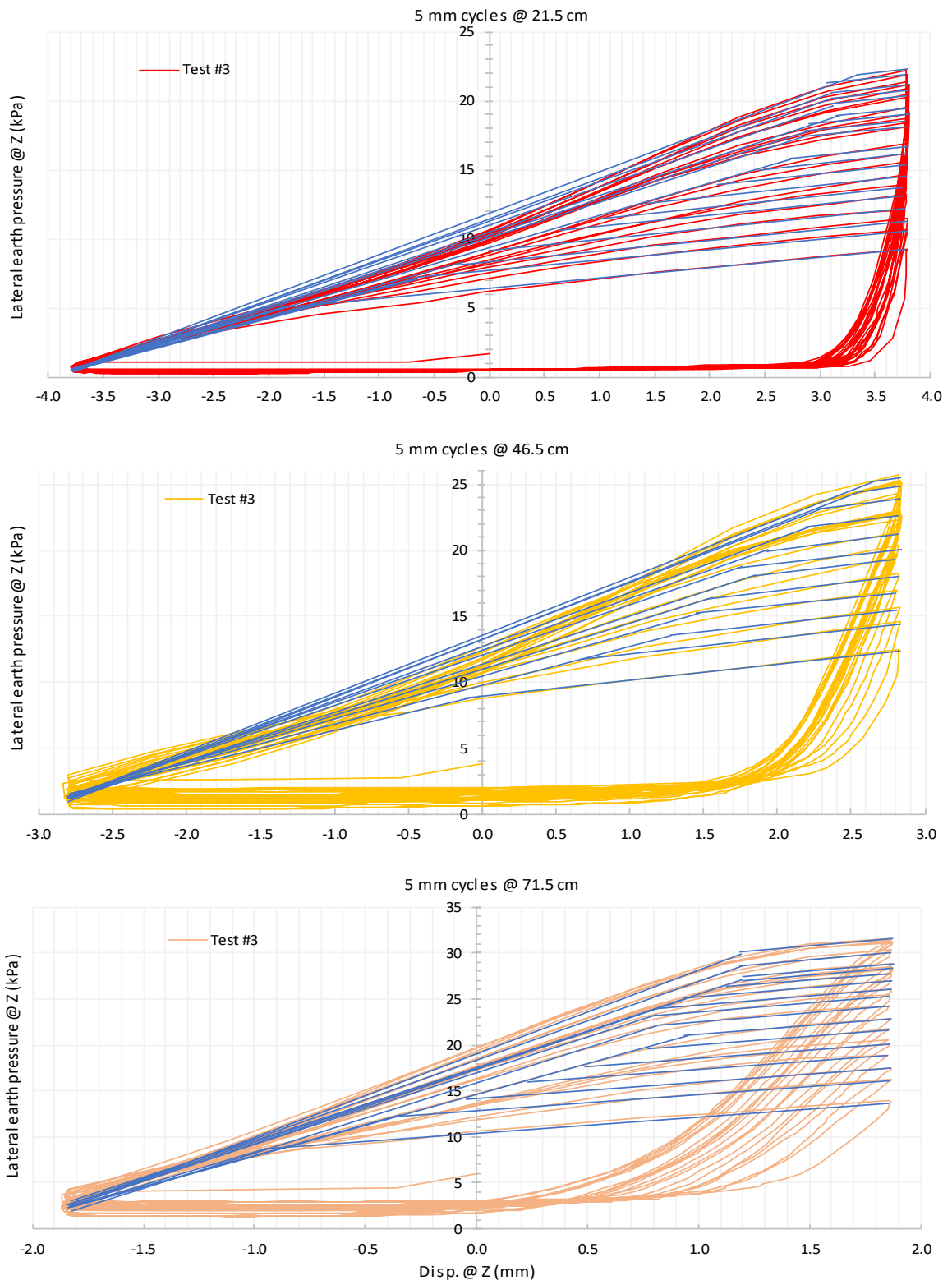


Figure 50. Slope analysis for ± 5 mm cycles during test #3

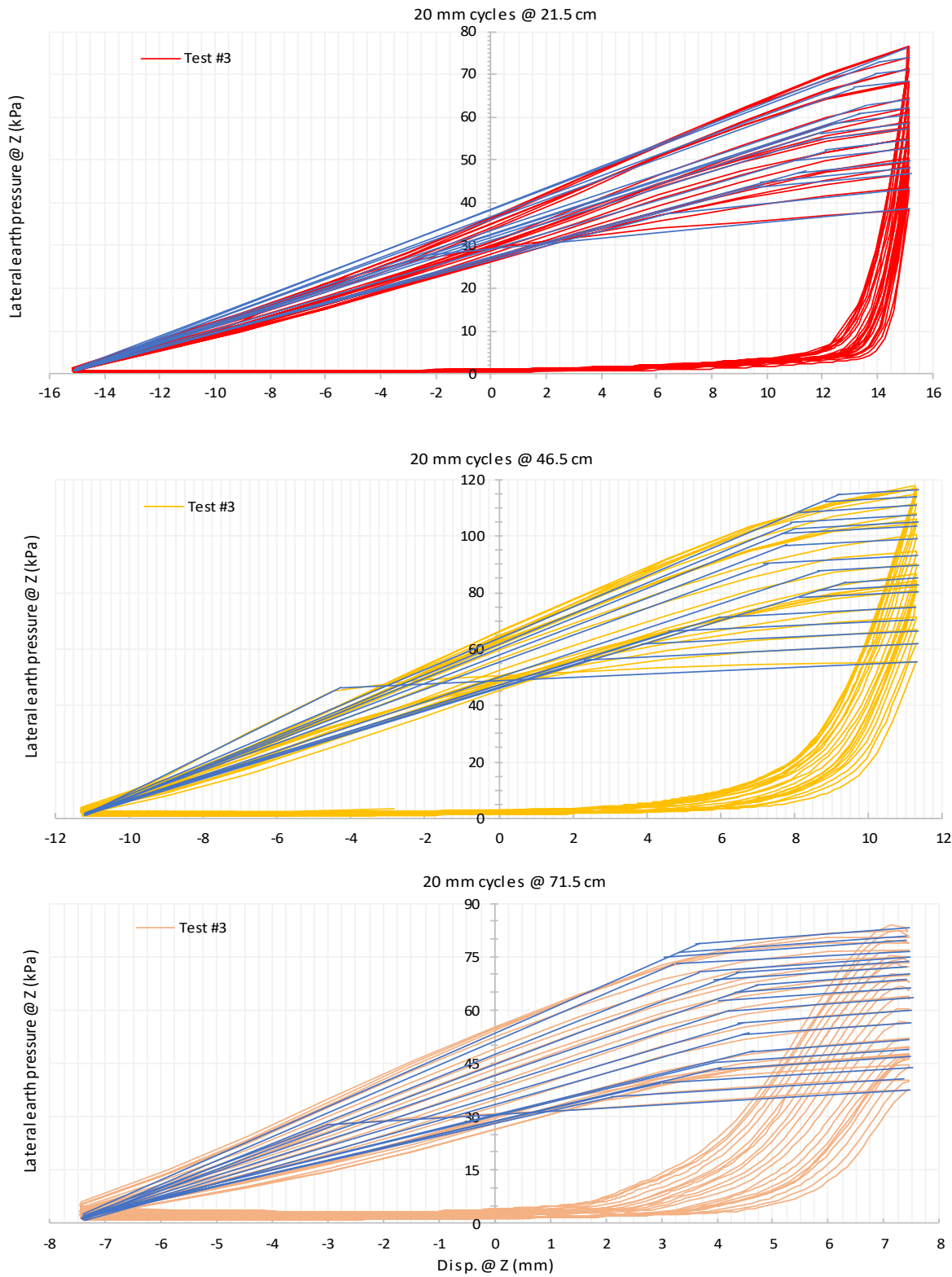


Figure 51. Slope analysis for ± 20 mm cycles during test #3

The variation of the initial p-y stiffness (Slope 1) with number of cycles is presented in Figure 52. Results indicate that Slope 1 is affected by the confining depth of the sensor, the cyclic displacement range, the relative density of the soil, and the number of cycles. An investigation of the data on Figure 52 leads to the following observations. First, Slope 1 increases as the confining depth increases, with slopes describing the p-y response at the deepest sensor being larger than those at shallower depths, irrespective of the cyclic displacement range and density of the soil. Second, the variation of Slope 1 with the cyclic displacement amplitude is counterintuitive in the sense that the slope seems to slightly decrease as the cyclic displacement amplitude increases. This reduction in the initial p-y stiffness for larger displacement cycles is attributed to the fact that Slope 1 is affected negatively by larger active displacements, which precede passive loading. Active displacements are larger for ± 20 mm cycles compared to ± 2 mm cycles, resulting in a reduction in passive stiffness with cycle amplitude. Third, Slope 1 shows a consistent increase with the relative density. This is expected given that the passive response is expected to be directly correlated to the friction angle of the sand bed. The final observation in Figure 51 is that Slope 1 generally increases with the number of cycles. This increase is evidently more consistent in cases involving dense sands and deeper sensors.

The variation of Slope 2 with the number of cycles is presented in Figure 52. It is clear from the figure that the magnitude of Slope 2 is much smaller than that of Slope 1 indicating significant reductions in stiffness as the soil approaches the ultimate passive condition. It is clear that Slope 2 increases with sand relative density, with no obvious trends related to changes in sensor position and cyclic amplitude that could be deduced from the data.

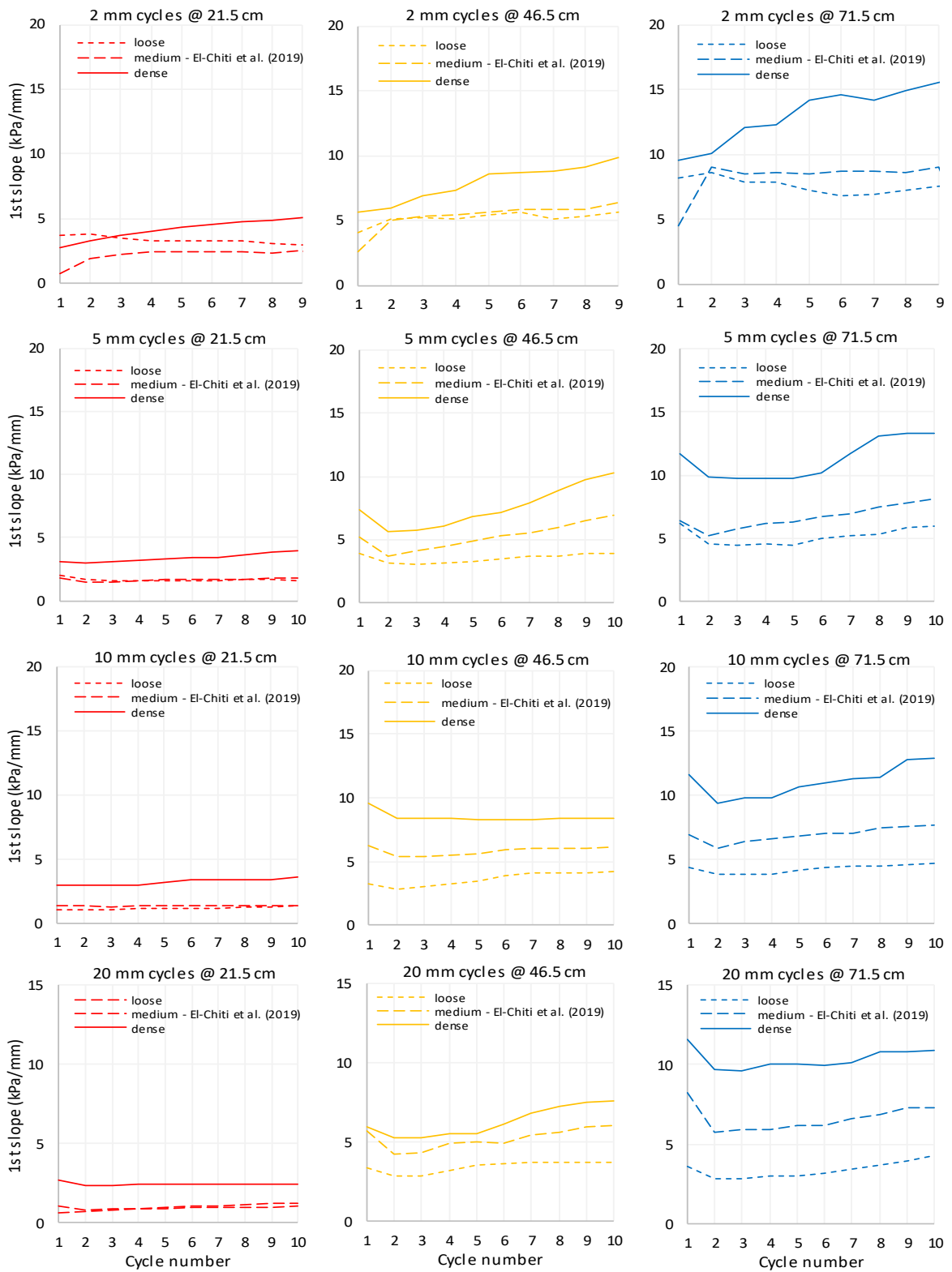


Figure 52. Fist slope variation with number of cycles

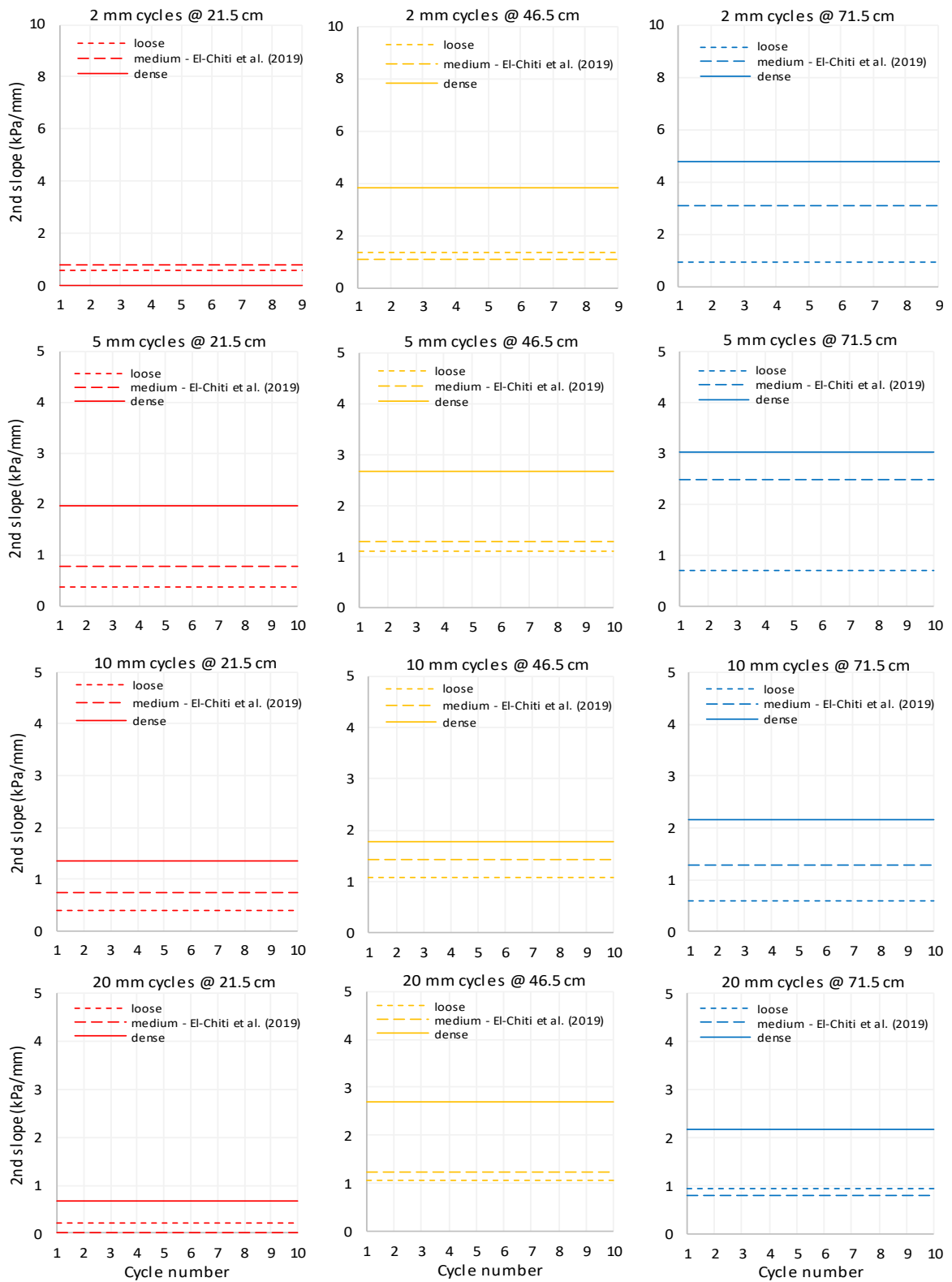


Figure 53. Second slope variation with number of cycles

4.5.5. Effect of “holding” time and temperature on the p-y response

In all previous tests, the test procedure involved applying the displacement increments at a rate that would allow for completing 2 to 3 cycles per day. During testing, it was noticed that the the rate of loading, as reflected in the waiting or holding time between displacement increments, seems to have a slight effect on the measured lateral stresses. For example, observations indicated that holding the wall at a given displacement for a long time may lead to slight reductions in the passive pressures (if the wall is being pushed towards the passive side) or to slight increases in the active pressures (as the wall is displaced backwards towards the active side). These changes in the lateral stresses with waiting time were correlated to measured reductions in the interface friction angle on the side walls with time, indicating that the time factor could be related to the viscous nature of the grease that was applied to the side walls to minimize side wall friction. Any additional resistance on the side walls due to the viscosity of the grease will reduce with “holding” time explaining the observed reductions in passive pressure and the observed increases in active pressure with waiting time.

To investigate the effect of “holding” time on the results, a fourth test was designed and implemented whereby the wall was held in a given position for a long period of time (generally 2 to 3 days) while monitoring the variation of lateral stresses with time at all sensors. The test was conducted using medium dense sands while enforcing waiting intervals at several wall positions in intermediate cycles.

Initial observations of the effect of “holding time” on mobilized active and passive pressures indicated that changes in temperature may have also played a role in the measured response. As a result, a decision was made to continuously monitor temperature

throughout the experiment. Temperature readings were collected starting from Cycle 2 onward. Although the initial intent was to monitor changes in lateral stresses, interface friction angle, and temperature for periods ranging between 2 and 3, days, several constraints that were beyond the control of the investigator necessitated longer waiting times in some instances.

The positions at which the wall was held fixed while monitoring the variation in temperature, lateral stresses, and displacements with time are presented in Figure 54 (for Cycles 1 and 2) and Figure 55 (for Cycles 5 and 8). These results pertain to 5mm wall displacement cycles. The effect of holding time on the measured lateral stresses is clearly illustrated in the figures which show changes in the lateral stresses at different displacement/stress levels along the p-y response. In the first cycle where no temperature readings were collected, results indicated that passive pressures could be reduced by as much as 30% as holding times in the order of 4 days, while active pressures could increase by as much as 20% for holding times in the order of 1 day. Similar trends were observed in all other cycles.

A detailed investigation of the effect of holding time on the results indicated that changes in temperature could have contributed to the measured response. Results indicated that reductions in temperature that approached or exceeded 2 degrees centigrade resulted in reductions in passive pressure coupled with a slight unloading of the wall towards the active side. This is clearly seen in Figure 55 during passive loading at a displacement increment of zero. A backward movement in the wall could only be the result of unloading in the hydraulic piston used to displace the wall. Such a displacement could be due to the effect of temperature on the viscosity of the oil in the hydraulic piston.

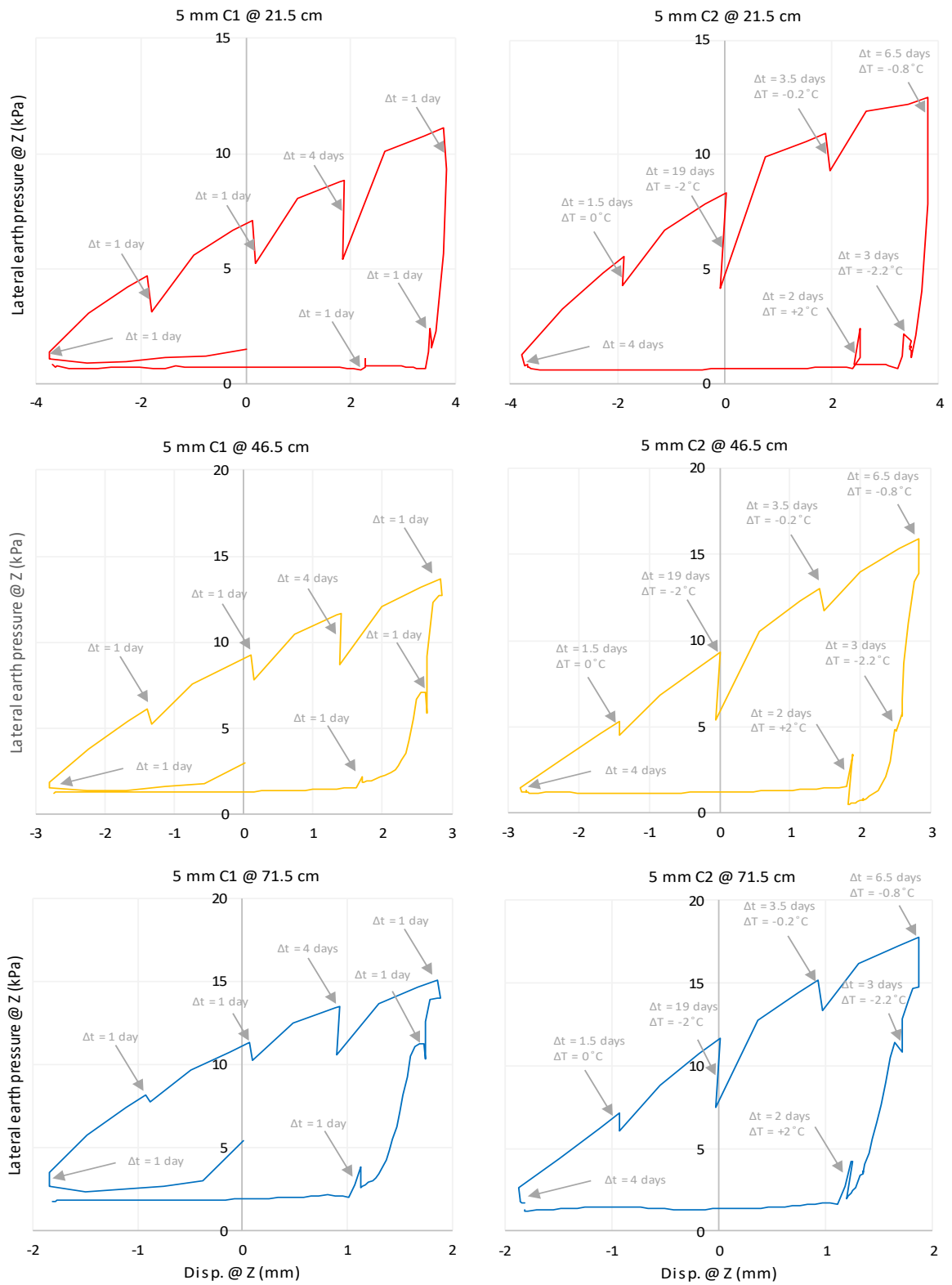


Figure 54. 1st and 2nd ± 5 mm cycles with waiting enforced at specific locations

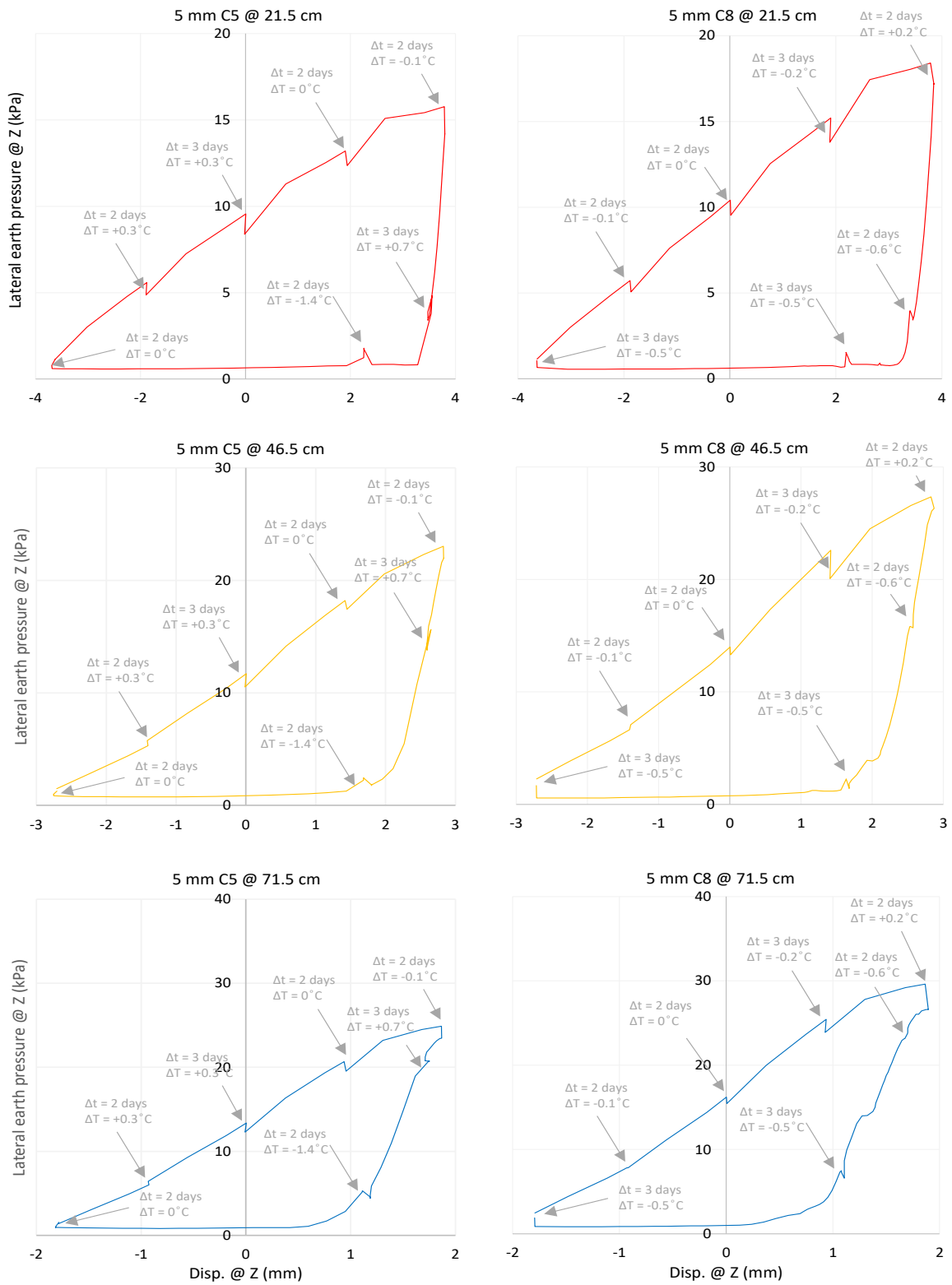


Figure 55. 5th and 8th ± 5 mm cycles with waiting enforced at specific locations

The effect of temperature was also witnessed while holding the wall during unloading increments. As an example, results in Cycle 2 at wall displacements in the order of 1.5 to 2.5 mm (at the level of the sensors) indicated that an increase in 2 degrees in temperature resulted in an increase in the active pressures with waiting time in all sensors. The increase in active lateral stress with waiting time at this displacement increment was associated with a slight wall movement towards the passive direction. Again, such a displacement in the wall could only be due to changes in oil viscosity as a result of the change in temperature.

In cycles 5 and 8, an effort was made to control the temperature in the laboratory to minimize changes in temperature. The effect of holding time on the stresses and displacements in these cycles can be observed to reduce dramatically compared to cycles 1 and 2 where larger changes in temperature occurred. In cycles 5 and 8, changes in temperature were reduced to less than 1 degree, and this has reduced the changes in lateral active and passive pressures to a maximum of 10 percent for all cases analyzed.

To ensure that the wall movements that were measured during holding time were not related to the effect of temperature on the LVDT itself, a second LVDT that is identical to that used in measuring wall displacement was fixed next to the latter without any contact with the wall. This allowed for the possibility to study the impact of temperature on the readings of an LVDT that is not connected to the wall and is thus not affected by what is happening in the hydraulic piston. The variation of the deformations measured by the two LVDTs in one of the holding times is presented in Figure 56. In addition to the LVDT readings, the variation in temperature was recorded and plotted on the same figure for comparison.

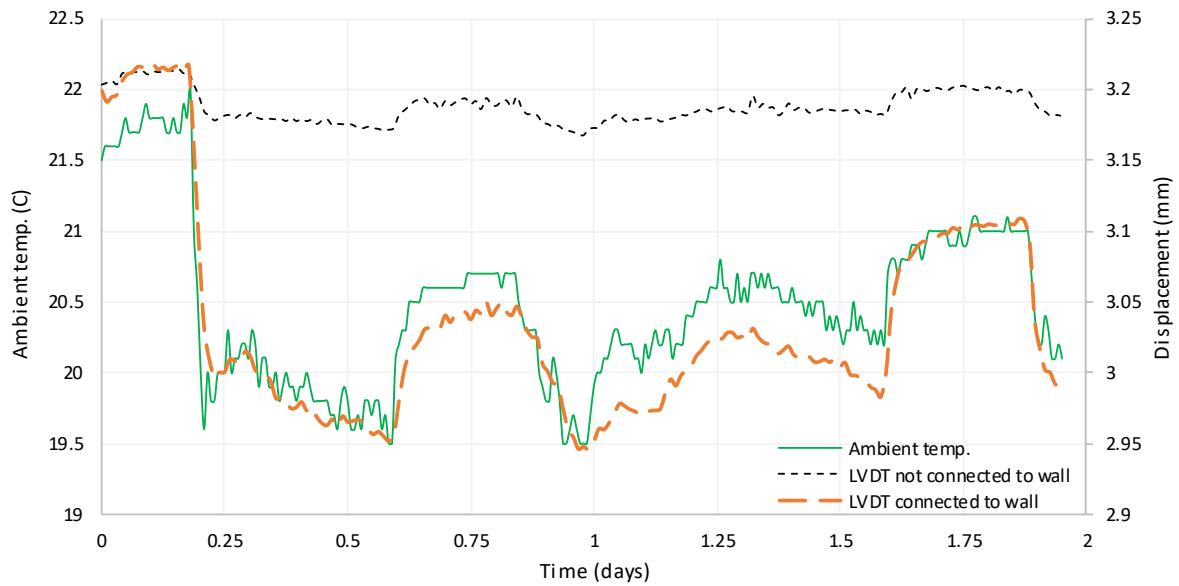


Figure 56. Investigating temperature effect on wall movements

Results on Figure 56 lead to two interesting and relevant observations. First, it is clear that there is a one to one correlation between the deformations recorded by the LVDT connected to the wall and changes in temperature. This clear association between the LVDT reading and the changes in temperature show without any doubt that changes in temperature could result in corresponding movements in the wall, explaining a significant portion of the changes that were observed in the lateral earth pressures with holding time. The second observation is that the second LVDT that was not connected to the wall also showed some variations in deformations with temperature. However, these movements were an order of magnitude smaller than those observed in the LVDT connected to the wall. This observation provides additional evidence that additional displacements that were observed during holding time are not related to errors in the LVDT due to changes in temperature but to a more complicated physical phenomenon that is related to the piston

and its sensitivity to changes in temperature. It should be noted that a drop of 2° C induced a 0.2 mm reduction in deformations measured by the LVDT connected to the wall in the active state while an increase of 1° C lead to an increase of 0.1 mm in the passive direction. In comparison, the second LVDT did not experience major variations throughout the recording period, with a maximum recorded change of 0.02 mm.

As mentioned previously, an effort was made to control the changes in temperature in the laboratory in cycles 5 and 8. The minimal changes in temperature in these cycles allowed for studying the effect of rate of loading on the lateral stresses during holding time. In the absence of changes in temperature, any observed decrease in passive pressure and increase in active pressure during holding time could be linked to the effect of the rate of loading on the mobilization of interface frictional stresses on the side walls.

The effect of holding time on the mobilized frictional stresses on the side walls is studied in Figure 57, which shows the difference in the mobilized interface friction angle at the beginning and end of the holding period at several wall displacements and different cycles. It is clear that the interface friction reduced with holding time due reduction in the viscous effects of the wax used to minimize side wall friction. Reductions of about 0.5 to 1° were measured, with maximum-recorded drops in the interface friction angle reaching values as high as 1.3° in cycle #8.

To get a clearer picture of the effect of holding time on the measured lateral earth pressures, the variations of lateral earth pressure, wall displacement, and temperature with time were recorded and plotted on Figures 58 (5th cycle with 5mm amplitude) and 60 (3rd cycle with 20mm amplitude). For the 5mm cycle, results on Figure 58a show that holding the wall at a displacement of 5mm toward the passive side results in a slight reduction in

the passive pressure with time. This reduction is relatively small (less than 7%) and stabilizes at about 12 hours. On the other hand, holding the wall during unloading at a wall displacement of 3mm results in a slight increase in the active pressure with holding time, particularly in the first 12 hours. For example, the deepest sensor exhibits an increase in lateral stresses from around 6.2 kPa to about 7.8 kPa after 12 hours of holding time. For the 20mm cycle (Figures 59 and 60), results show a smaller effect of holding time on both active and passive stresses, respectively.

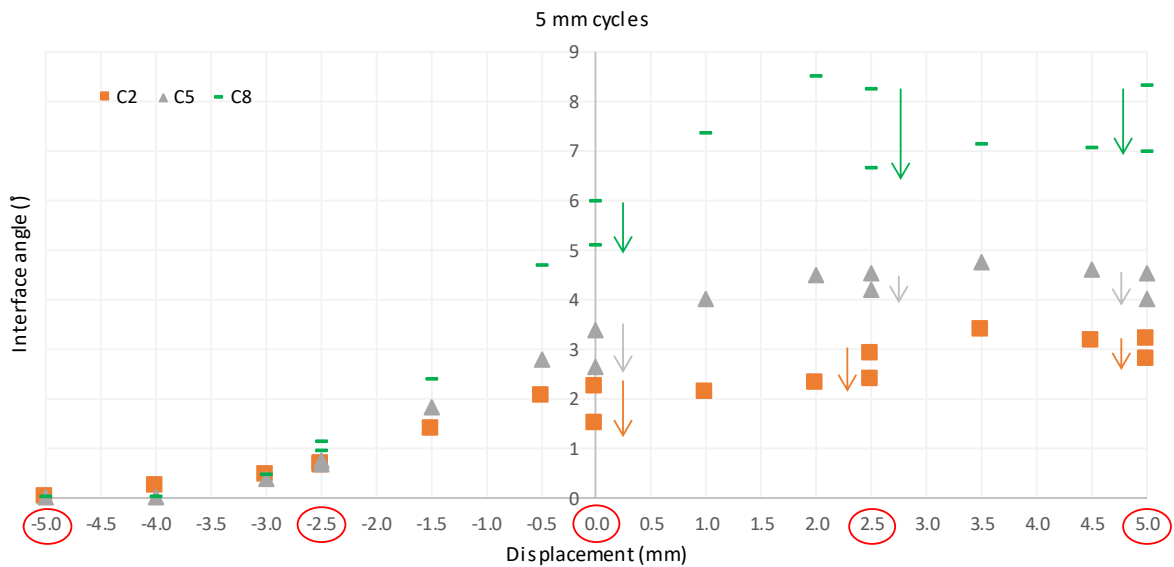


Figure 57. Interface angles during cycles 2, 5 and 8

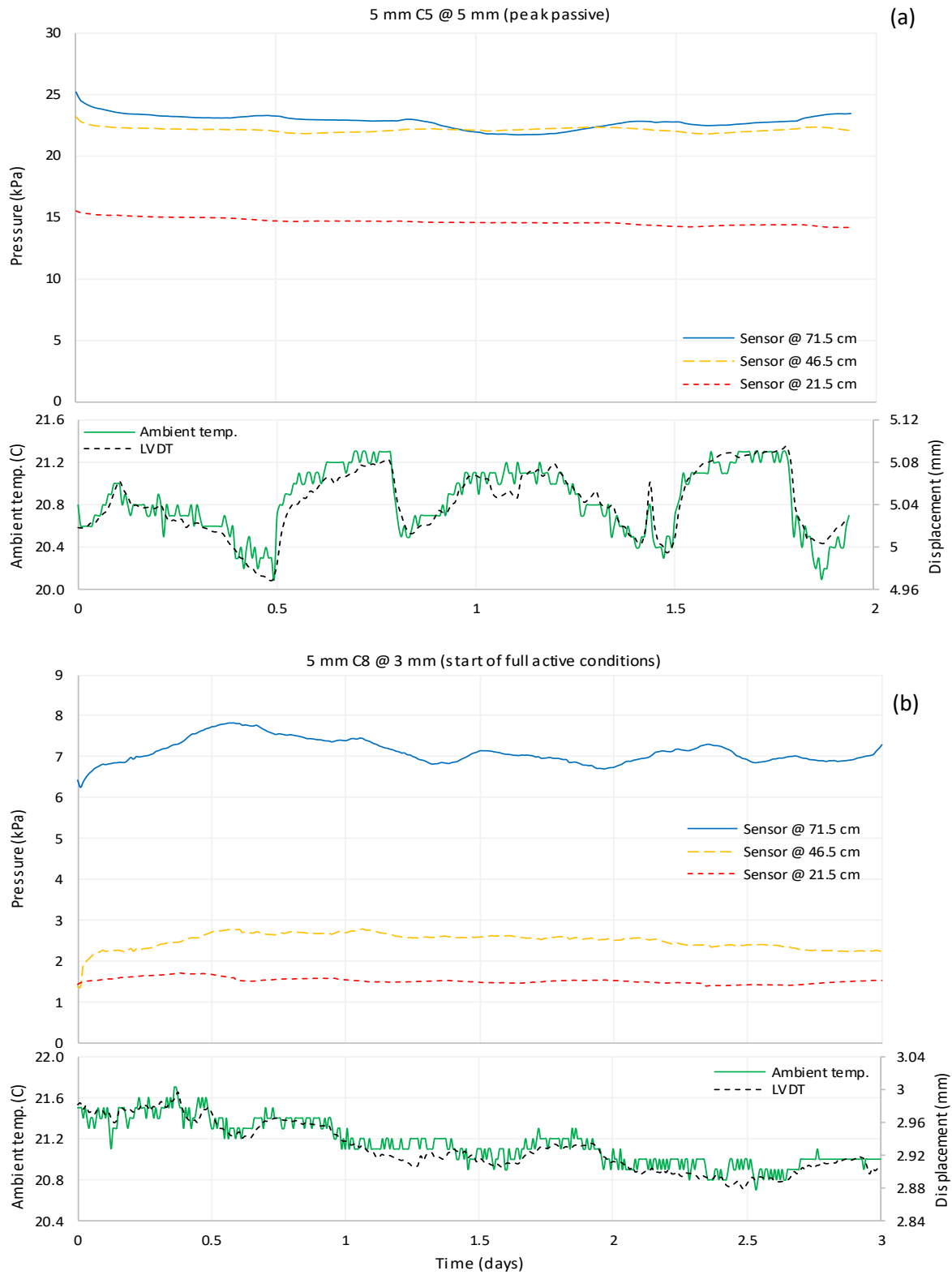


Figure 58. Pressure change during the enforced time for ± 5 mm cycles

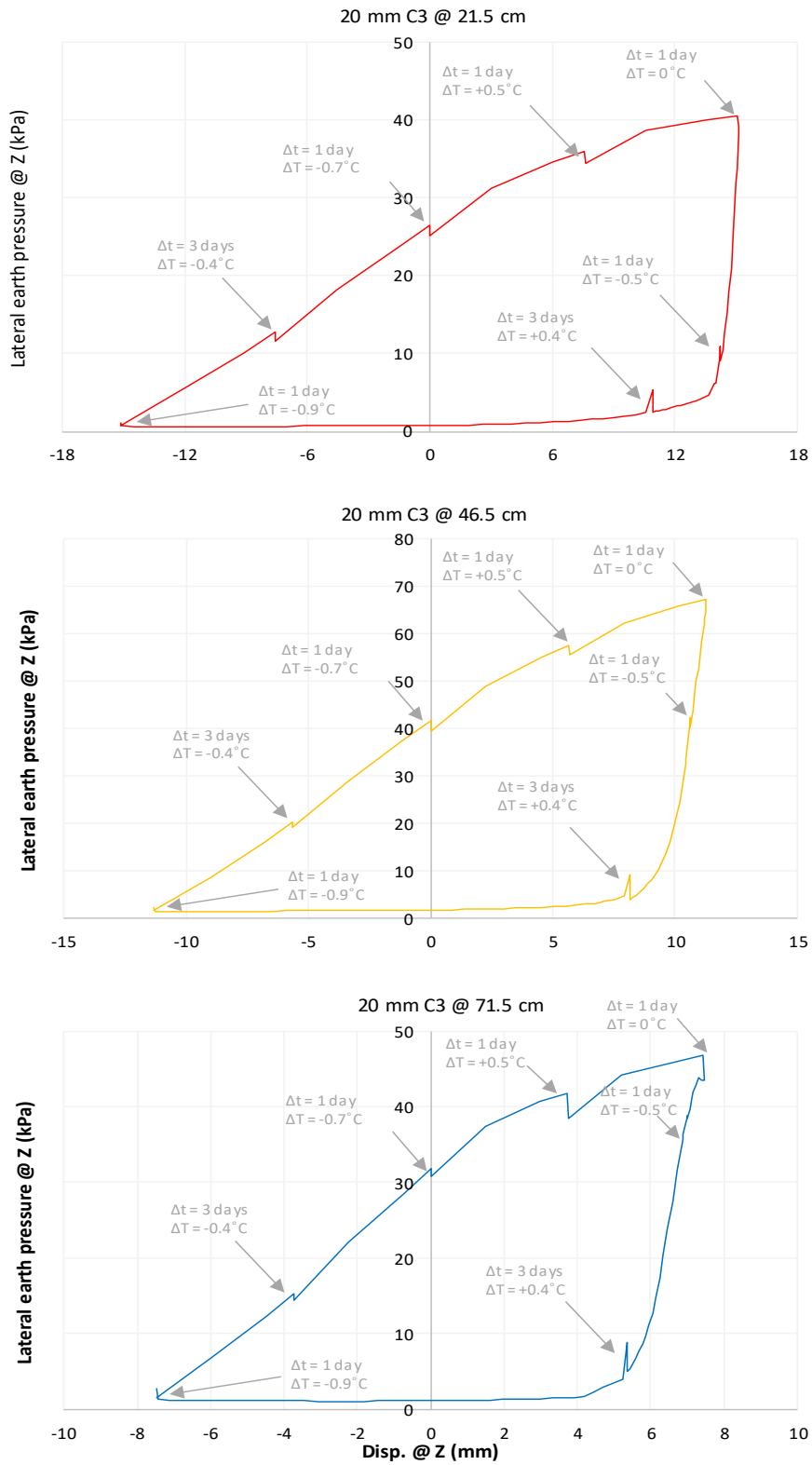


Figure 59. Pressure change during the enforced time for ± 5 mm cycles

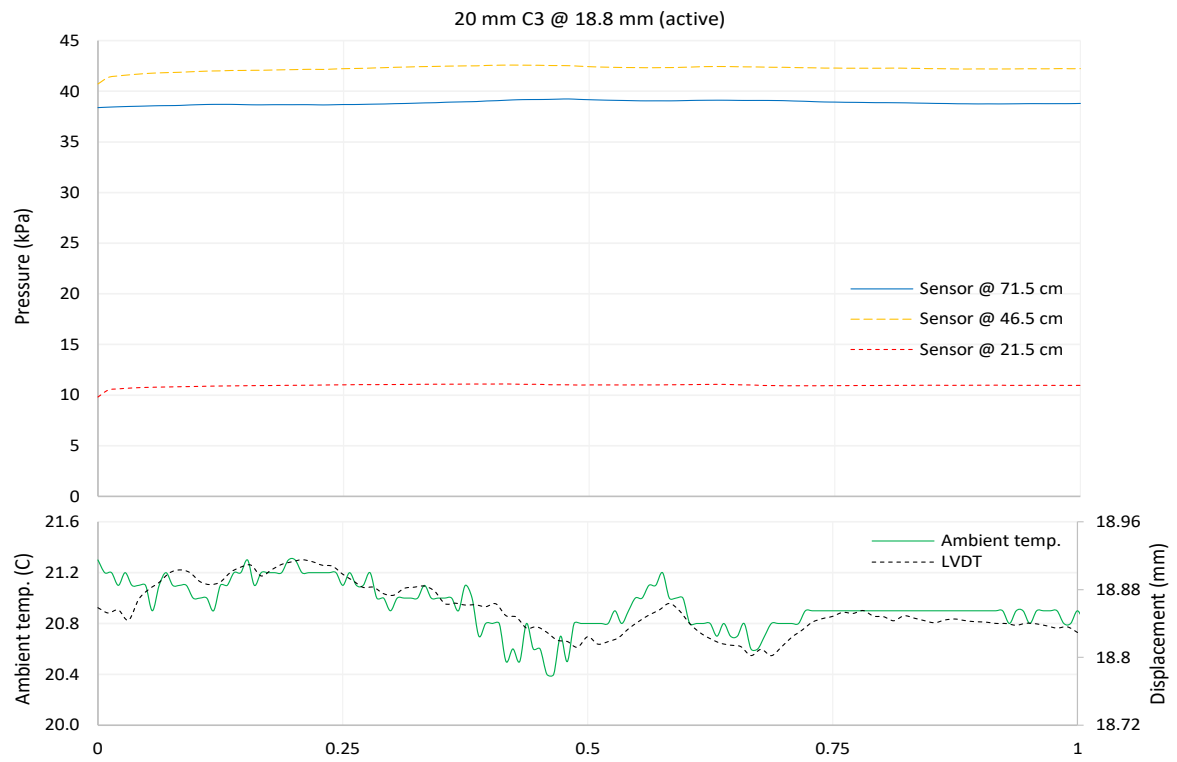
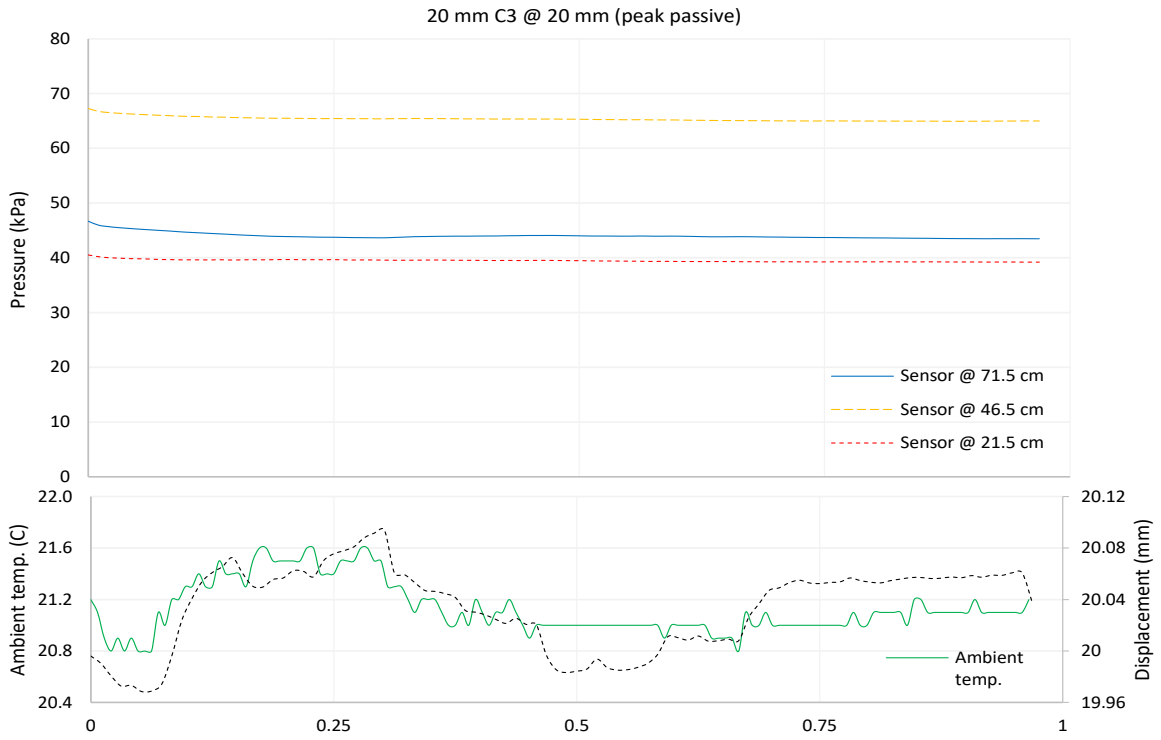


Figure 60. Pressure change during the enforced time for ± 20 mm cycles

CHAPTER V

CONCLUSIONS

Based on the results from four cyclic laboratory scale tests that were conducted on a 1.2m high wall that is supporting sands of different relative densities, the following conclusions can be drawn:

- The passive p-y response during limited cyclic wall movements (less than 20mm wall displacements) from active side to passive side can be approximated by a bi-linear curve consisting of two slopes that are dependent on confinement and density. Slope 1 is highly dependent on density and cycle amplitude while slope 2 is clearly correlated to density. More, importantly, Slope 1 shows a systematic increase with number of cycles while Slope 2 is relatively unaffected by the number of cycles.
- The active p-y response as the wall moves in the opposite path can be approximated by a hyperbolic trend having two distinctive sections, a sharp decrease and a constant value.
- Repetitive cycles gradually increase the passive earth pressures with every passive push indicating densification. This is mostly present during the ± 2 mm cycles where densification is dominant. However, cyclic loading has minimal effect on the active pressures that agree with Lancellota's theory.
- Lateral pressures are directly related to backfill density. The denser the soil the stiffer is the p-y response.

- 10 cycles were not enough to reach a stable p-y response. In fact, increasing the number of cycles to 22 did not also yield a stable response, although the rate of increase in the stiffness and maximum passive pressures reduced with number of cycles.
- Measurements of the interface friction angle on the side walls indicated that it is inversely proportional to backfill density and wall displacement. Moreover, a sidewall interface made of PLEXI-glass and coated with grease and plastic wraps allowed for low angles of friction that did not exceed 6° and 3° for loose and dense backfill, respectively.
- The absence of intermediate cycles with smaller amplitudes before any given cycle has a negative impact on the p-y response of the higher amplitude cycle. Also, the first cycle of each amplitude is affected by the preceding smaller displacement cycles. It starts with the stiffness achieved from previous cycles and shifts to a linear horizontal path indicating a reduction in stiffness as virgin sand (undensified) in the passive zone is mobilized.
- Pressure readings can be affected by ambient temperature and waiting intervals. The first can affect the piston and induce active or passive movements, while the second factor allows for dissipation of accumulated friction stresses at the sidewalls due to the viscous nature of the wax/oil that is used.
- Enforcing long waiting intervals to ensure a stable response did not generate a significantly different p-y response. As a result, conducting relatively fast tests with waiting times that are in the order of minutes should not have any dramatic impact on the measured p-y curves, provided that changes in ambient temperature in the laboratory are restricted to less than 1 degree.

REFERENCES

- Allotey, N. (2007). Nonlinear Soil-Structure Interaction in Performance-Based Design (Doctoral dissertation). University of Western Ontario, London, Ontario, Canada.
- Allotey, N., & El Naggar, M. H. (2007). Generalized dynamic non-linear winkler model of soil-structure interaction analysis. *Canadian Geotechnical Journal*(45), 560-573.
- Allotey N, El Naggar MH. A numerical study into lateral cyclic nonlinear soil– pile response. *Can Geotech J* 2008;45(9):1268–81.
- Badoni D, Makris N. Nonlinear response of single piles under lateral inertial and seismic loads. *Soil Dyn Earthq Eng* 1996;15:29–43.
- Boulanger, R. W., Curras, C. J., Kutter, B. L., Wilson, D. W., & Abghari, A. (1999). Seismic soil-pile-structure interaction experiments and analyses. *Journal of Geotechnical and Geoenvironmental Engineering*, 125(9), 750-759.
- Briaud, J.-L. K.-K. (1998). Beam-Column Method for Tieback Walls. *Journal of Geotechnical and Geoenvironmental Engineering*, 124(1), 67-79.
- Brown, D. A., Morrison, C., & Reese, L. C. (1988). Lateral load behavior of pile group in sand. *Journal of Geotechnical Engineering*, 114(11), 1261-1276.
- Dave, T. N. (2012). Assessment of portable traveling pluviator to prepare reconstituted sand specimens. *Geomechanics and Engineering*, 4(2), 79-90.
- Dunnivant, T. W., & O'Neill, M. W. (1989). Experimental p-y Model for submerged, stiff clay. *Journal of Geotechnical Engineering*, 115(1), 95-114.
- Dutta, S., & Roy, R. (2002). A critical review on idealization and modeling for interaction among soil-foundation-structure system. *Computers and Structures*, 80, 1579-1594.

Elchiti, I., Saad, G., Najjar, S. & Nasreddine, N. 2017. Investigation of Active Soil Pressures on Retaining Walls Using Finite Element Analyses. *Geotechnical Frontiers*: 159–169.

Elchiti, I., Saad, G., Najjar, S. & Alzoer, S. 2018. Numerically derived P-Y curves for rigid walls under active conditions. 9th European Conference on Numerical Methods in Geotechnical Engineering, Porto, Portugal, 25–27 June 2018.

Elchiti, I., Najjar, S.S., Saad, G., and Sadek, S. (2019). “Experimentally-derived cyclic p-y curves for rigid walls supporting granular backfill”, Proceedings of the seventh International Conference on Earthquake Geotechnical Engineering, June 17 - 20, Rome, Italy.

El Ganainy, H. & El Naggar, M.H. 2009. Seismic performance of three-dimensional frame structures with underground stories. *Soil Dynamics and Earthquake Engineering* 29(9): 1249–1261.

El Naggar MH, Bentley KJ. Dynamic analysis of laterally loaded piles and dynamic p–y curves. *Can Geotech J* 2000;37:1166–83.

El Naggar MH, Novak M. Nonlinear analysis for dynamic lateral pile response. *Soil Dyn Earthq Eng* 1996;15:233–44.

Gade, V. K. (2016). Development of a Mechanized Traveling Pluviator to Prepare Reconstituted Uniform Sand Specimens. *Journal of Materials in Civil Engineering*, 28(2).

G. Saad, f. Saddik & s. Najjar(2012) “Impact of soil structure interaction on the seismic design of reinforced concrete buildings with underground stories” american university of beirut, lebanon lisbo(2012).

Iannelli, M. (2016). Determination of Seismic Earth Pressures on Retaining Walls through Finite Element Analysis. doi: 10.15368/theses.2016.147

Kerr, A. (1984). On the formal development of elastic foundation models. *Ingenieur-Archive*. 54. 455-464.

Kim, N.-K. B.-L. (1994). A beam column method for tieback walls. *Res. Rep. to Schnabel Found. and the Fed. Hwy. Admin.* College Station: Texas A&M University.

Kramer, S. L. (1996). *Geotechnical earthquake engineering*, Prentice Hall, Upper Saddle River, NJ.

Liam Finn, W. D. (2005). A Study of Piles during Earthquakes: Issues of Design and Analysis. *Bullet of Earthquake Engineering*, 3, 141-234.

Maleki, S., & Mahjoubi, S. (2010). A New Approach for Estimating the Seismic Soil Pressure on Retaining Walls. *Scientia Iranica*, 17(4), 273-284.

Matlock, H. (1970) Correlations for Design of Laterally Loaded Piles in Soft Clay. *Proceedings of the 2nd Offshore Technology Conference*, Houston, 22-24 April 1970, 577-594. <http://dx.doi.org/10.4043/1204-ms>

Matlock, H., & Ripperger, E. A. (1956). Procedures and instrumentation for tests on a laterally loaded pile. *Proceedings, Eighth Texas Conference on Soil Mechanics. Special Publication No. 29*. Texas: Bureau of Engineering Research.

Nadim F., W. R. (1983). Seismically Induced Movements of Retaining Walls. *Journal of Geotechnical Engineering*, 109(7), 915-931.

Randolph. (1981). Response of flexible piles to lateral loading. *Geotechnique*, 31(2), 247-259.

Reese, L. C., Cox, W. R., & Koop, F. D. (1974). Analysis of laterally loaded pile in sand. *Offshore Technology Conference*, (pp. 473-483). Dallas.

Richard, R. J. (1999). Seismic Earth Pressure on Retaining Structures. *Journal of Geotechnical and Geoenvironmental Engineering*, 125, 771-778.

Sanchez, S. I. (1982). *Static and dynamic stiffnesses of single piles*. University of Texas at Austin, Department of Civil Engineering, Austin.

Scott, R. F. (1973). Earthquake-induced pressures on retaining walls. *Fifth World Conference on Earthquake Engineering* (pp. 45-54). Rome: California Institute of Technology.

Tabaroei, A. A. (2017). Comparison between Two Different Pluviation Setups of Sand Specimens. *Journal of Materials in Civil Engineering*, 29(10).

Wang, S., Kutter, B. L., Chacko, M. J., Wilson, D. W., Boulanger, R. W., & Abghari, A. (1998). Nonlinear seismic soil-pile structure interaction. *Earthquake Spectra*, 14(No. 2), 377-396.

Wilson, D. W. (1998). *Soil-pile-superstructure interaction in liquifying sand and soft clay*. University of California at Davis, Civil and Environmental Engineering. Davis: University of California at Davis.

Winkler, E. O. (1967). *Theory of Elasticity and Strength*. Prague: H. Dominicus.
Wood, John Holm (1973) Earthquake-Induced Soil Pressures on Structures. Dissertation (Ph.D.), California Institute of Technology. doi:10.7907/MZWQ-BA46

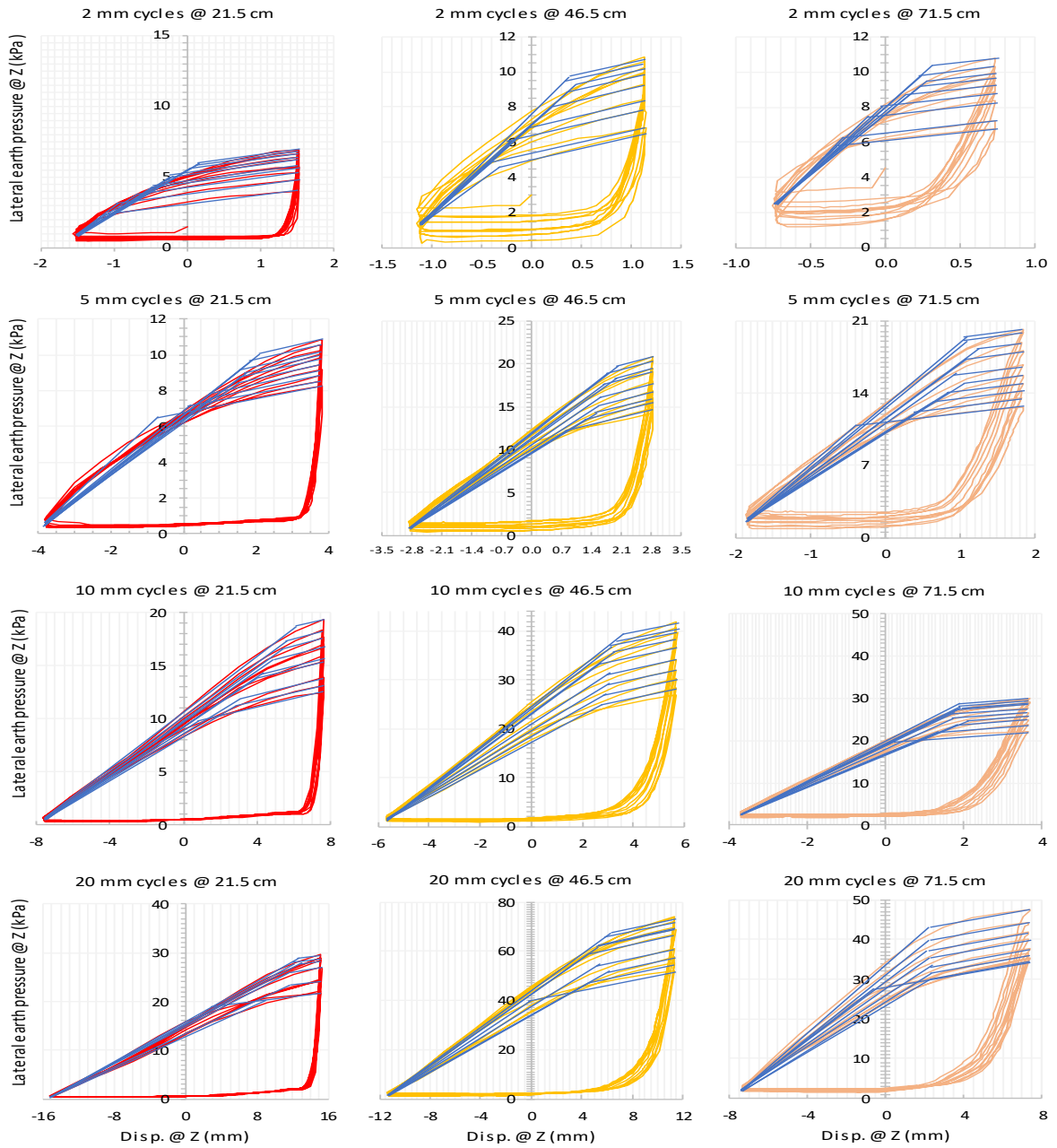
Wood, John Holm (1973) Earthquake-Induced Soil Pressures on Structures. Dissertation (Ph.D.), California Institute of Technology. doi:10.7907/MZWQ-BA46

Wood, J. (1975). Earthquake induced pressures on a rigid wall structure. *Bulletin of New Zealand National Society for Earthquake Engineering*, 8(3), 175-186.

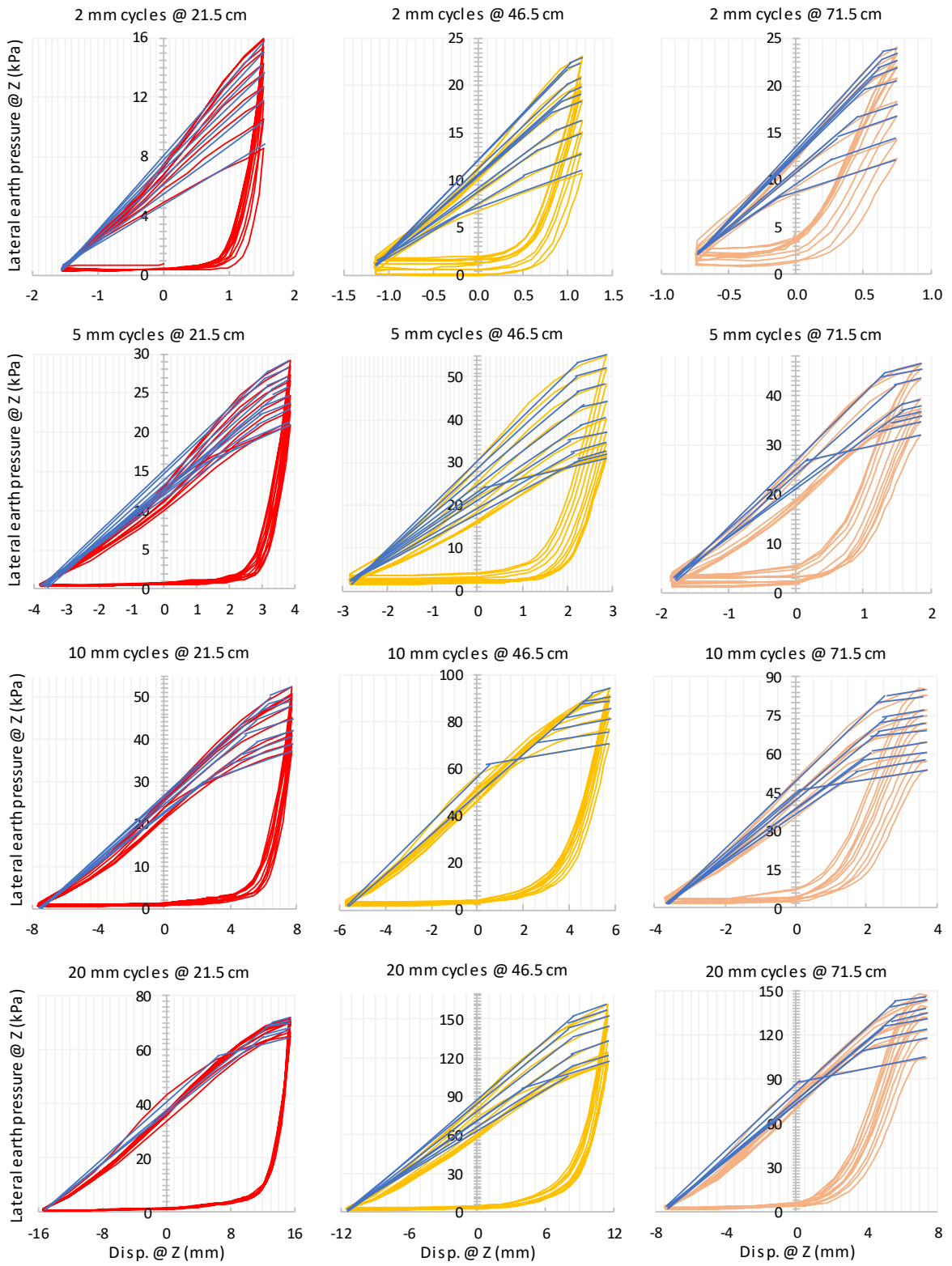
Wu, G., & Finn, W. L. (1999). Seismic lateral pressures for design of rigid walls. *Canadian Geotechnical Journal*, 36(3), 509–522. doi: 10.1139/t99-013

APPENDIX

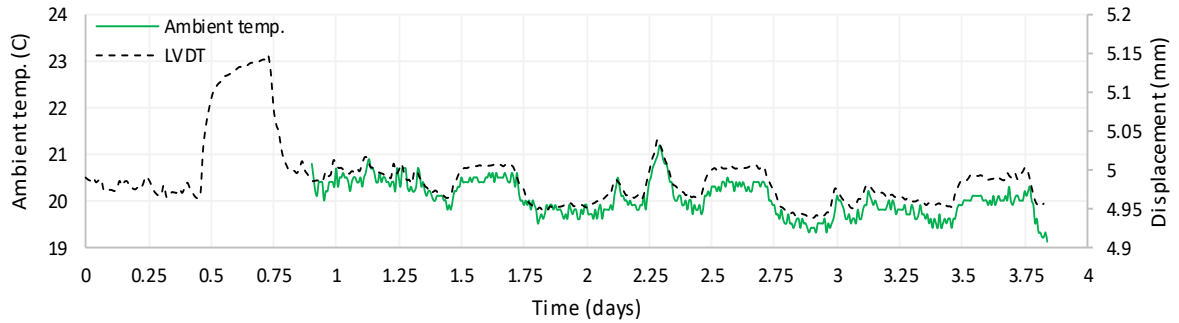
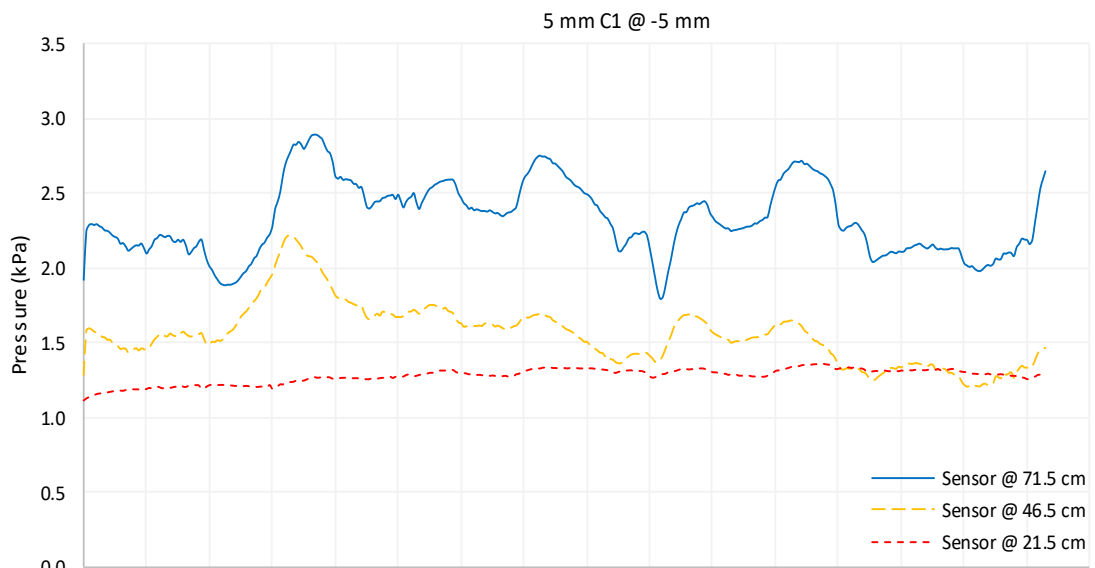
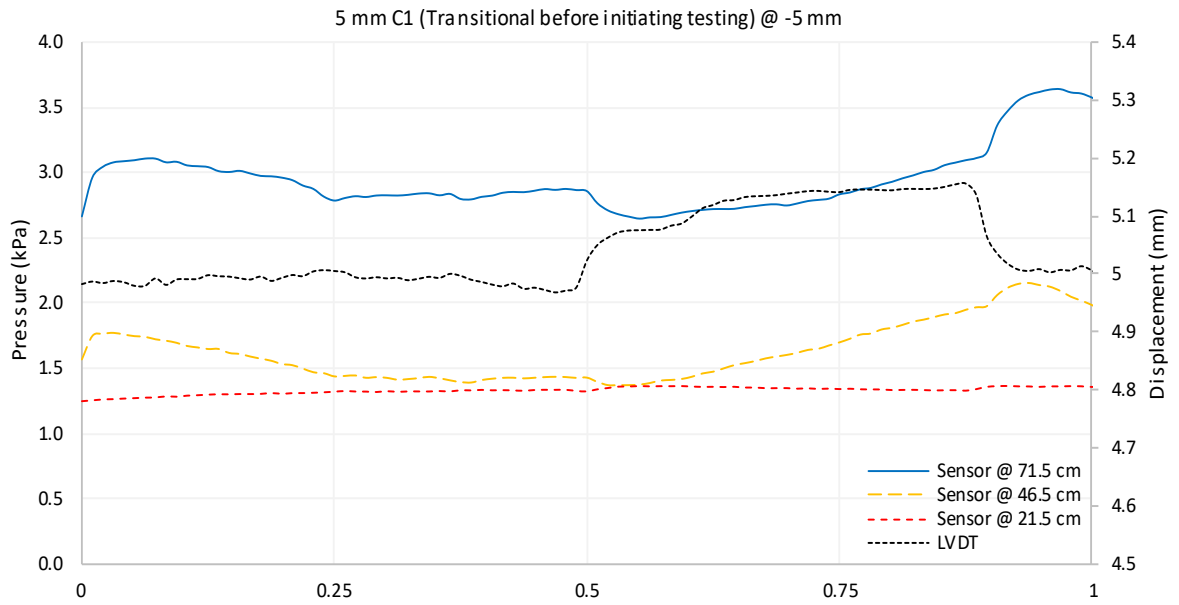
EXPERIMENTAL RESULTS



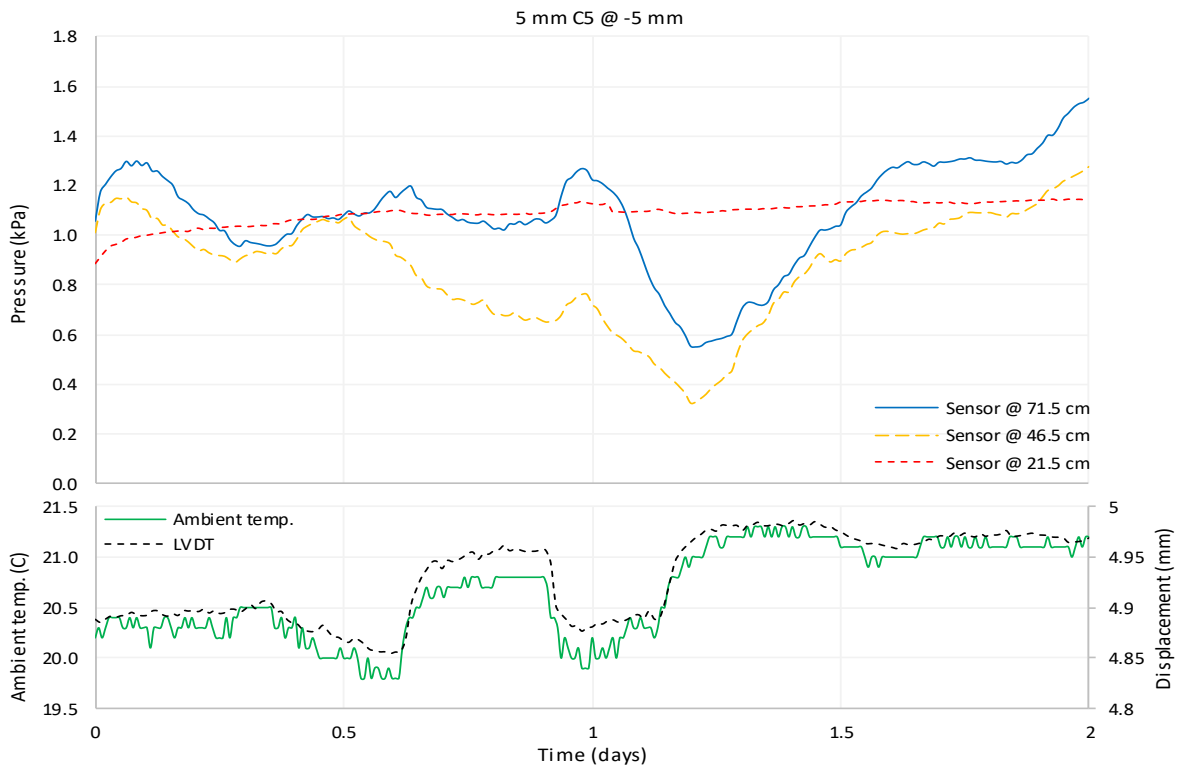
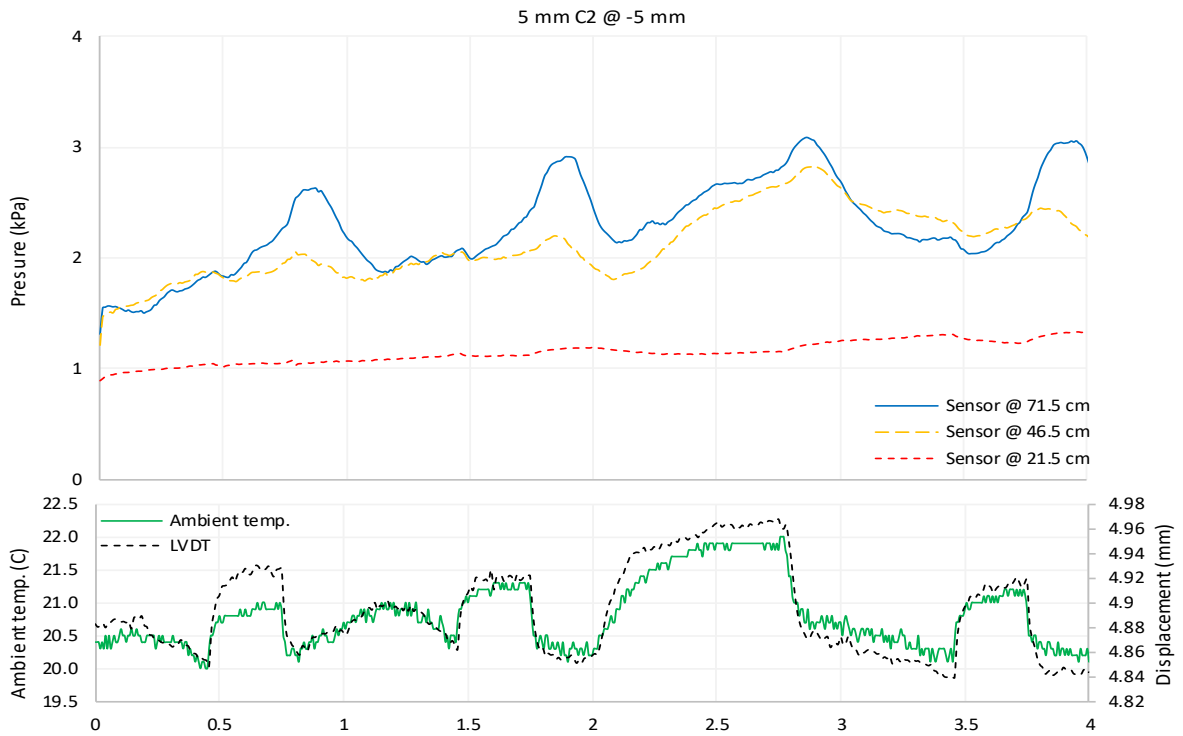
Bi-linear slope approximation for test #1 (Loose Sand)



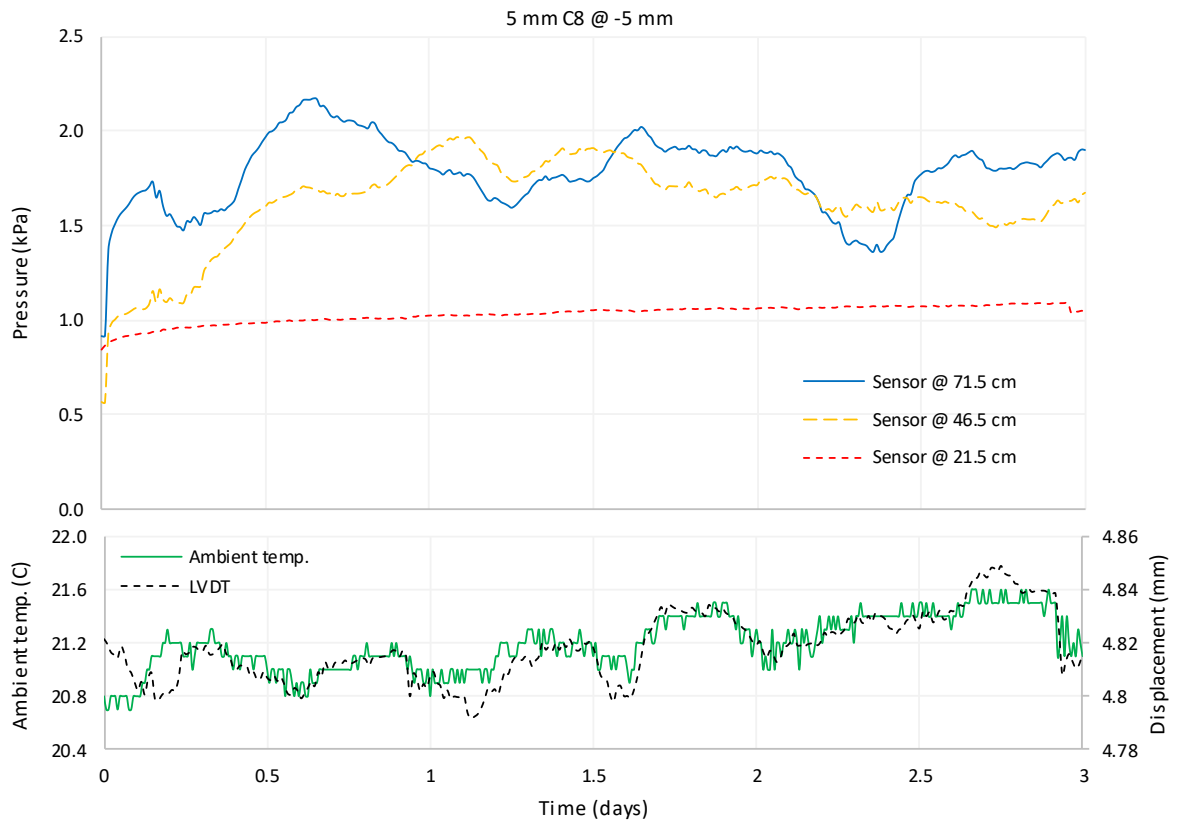
Bi-linear slope approximation for test #2 (Dense Sand)



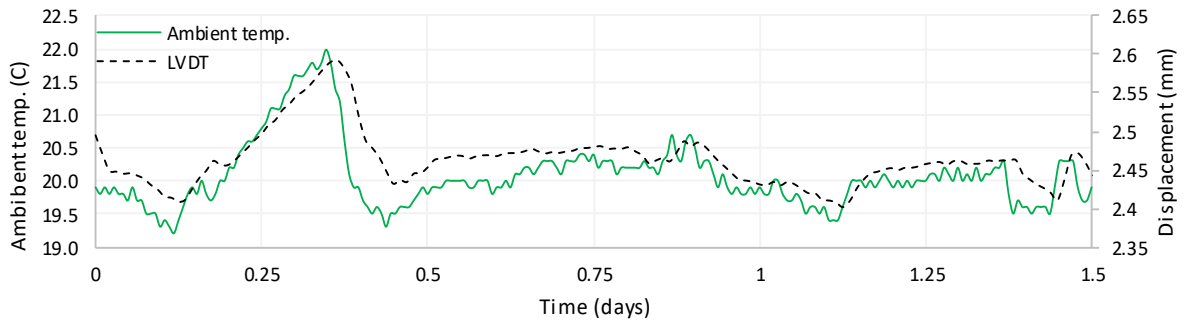
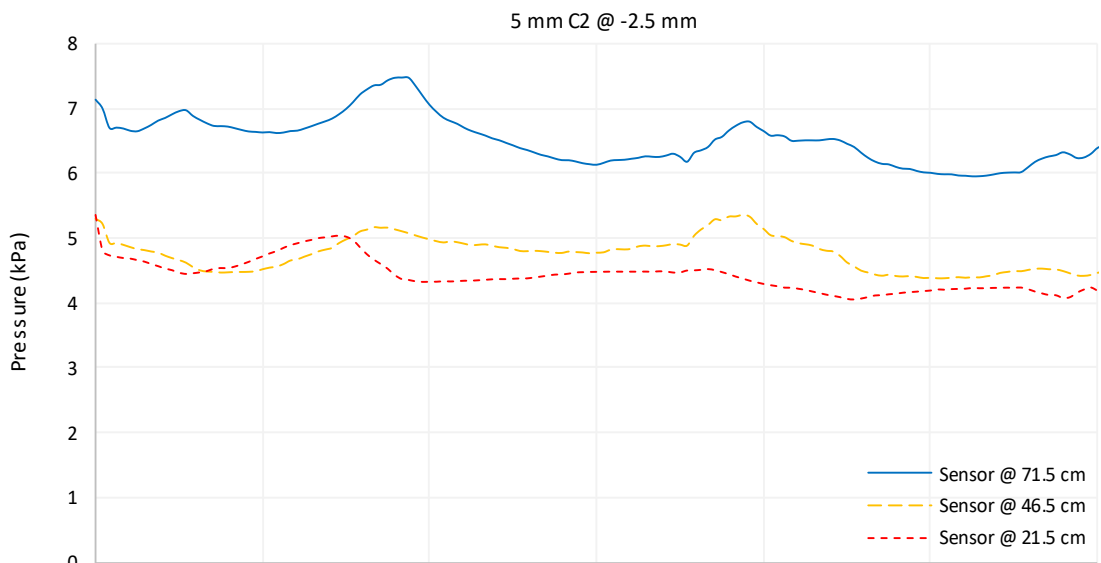
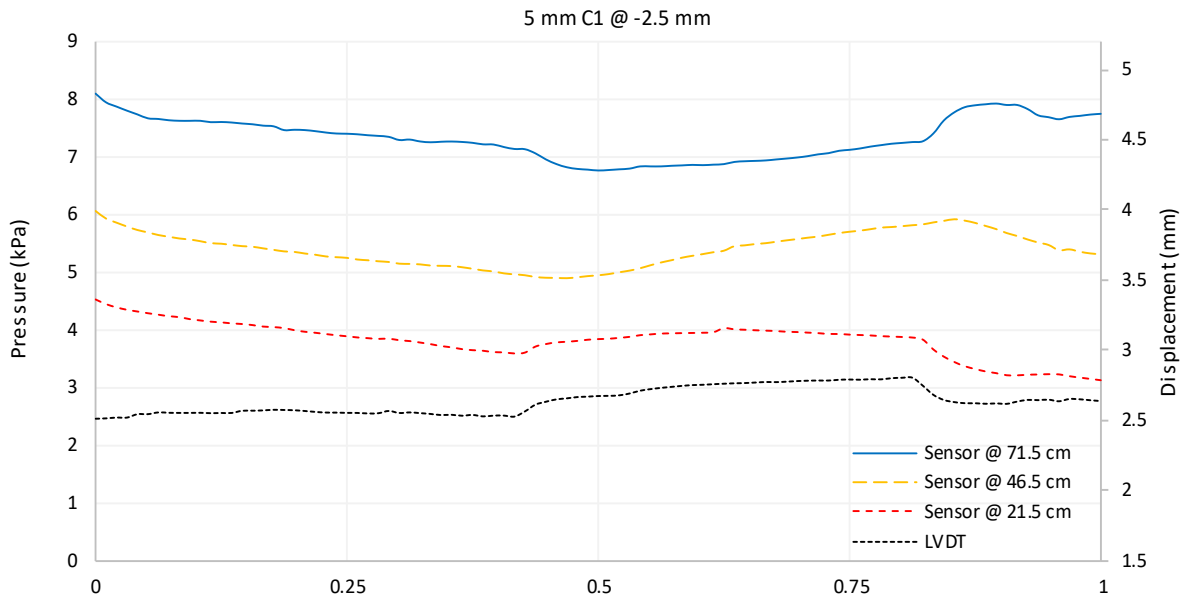
Variation of stresses, wall displacement, and temperature with holding time (-5mm, active, C1)



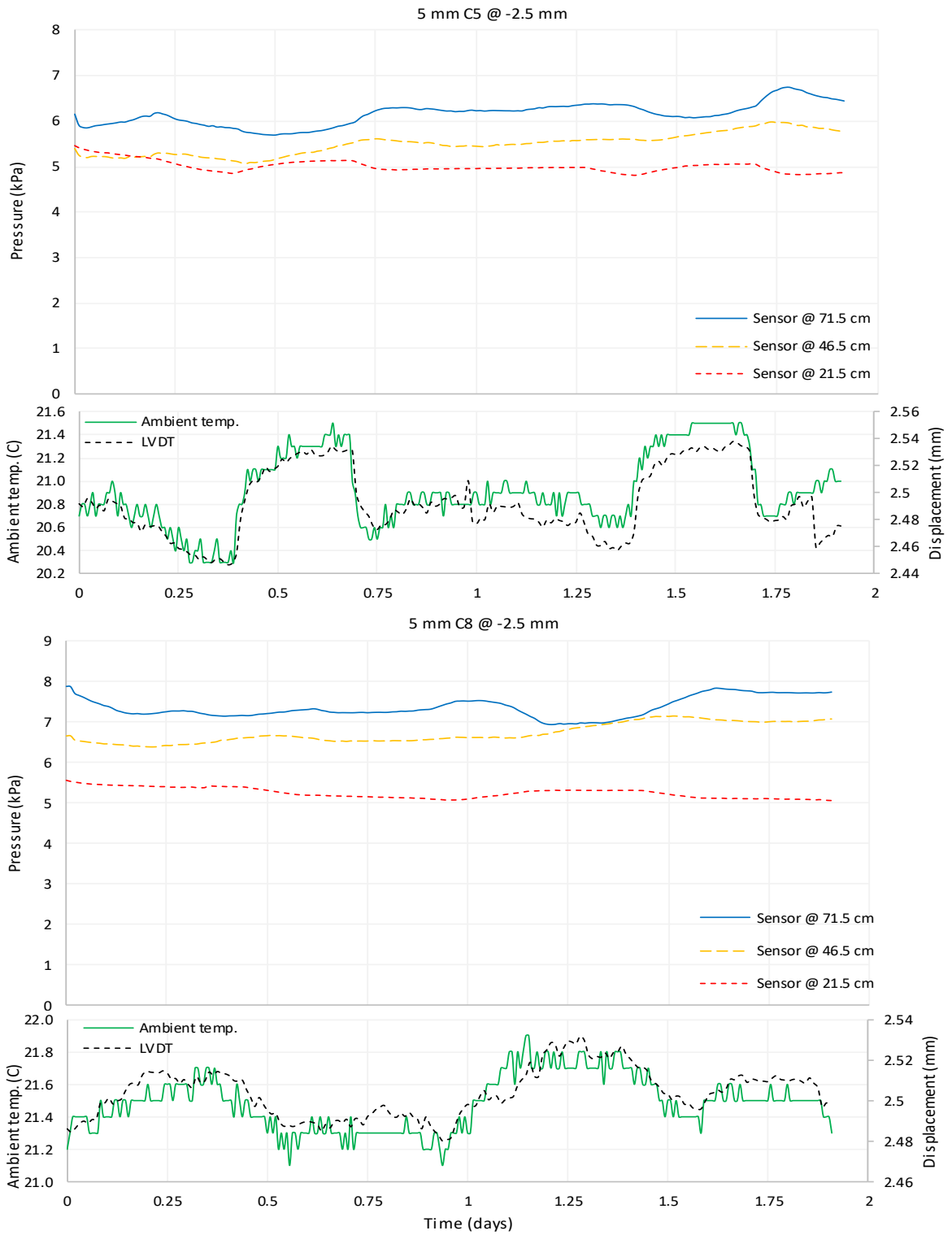
Variation of stresses, wall displacement, and temperature with holding time (-5mm, active, C2, C5)



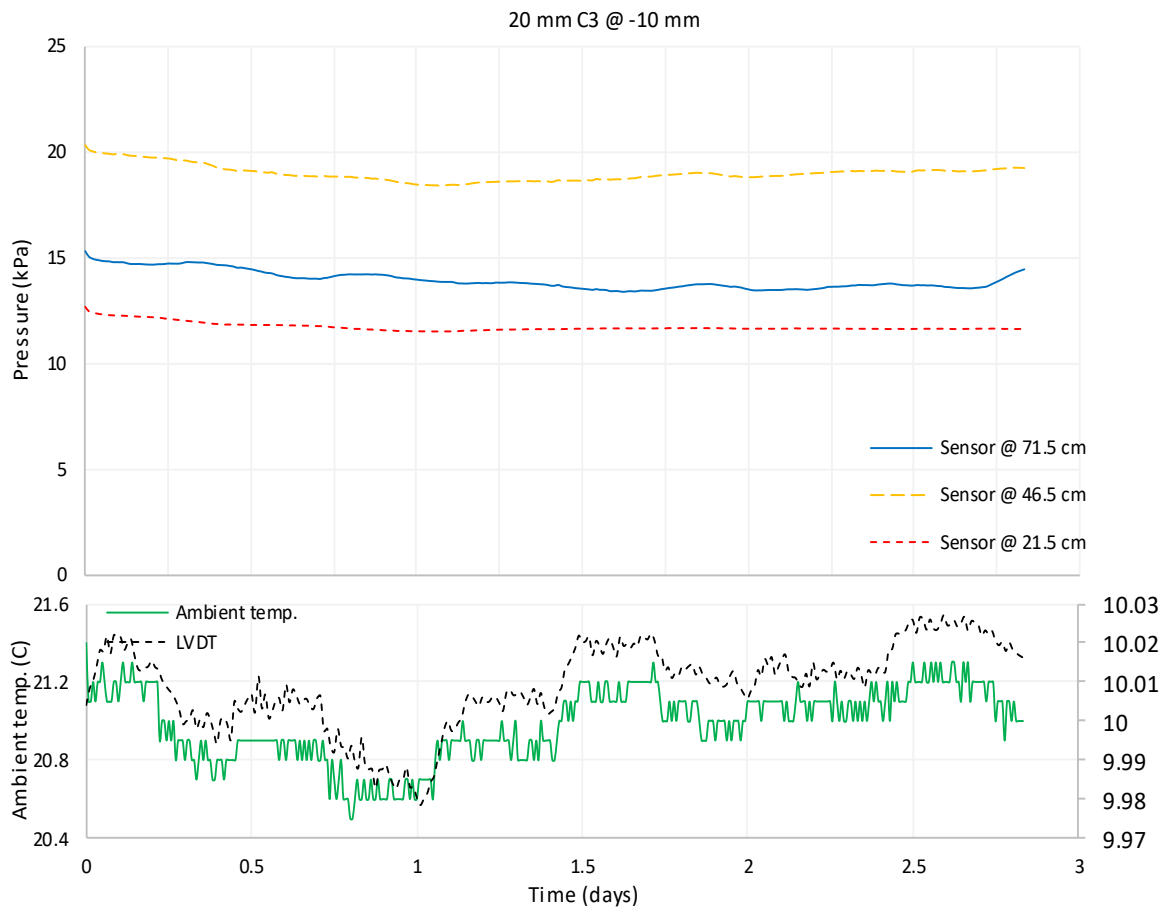
Variation of lateral stresses, wall displacement, and temperature with holding time (-5mm, active, C8)



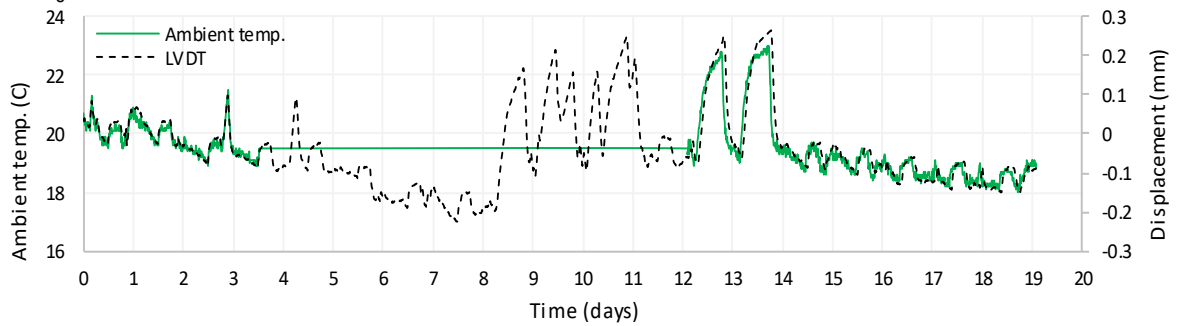
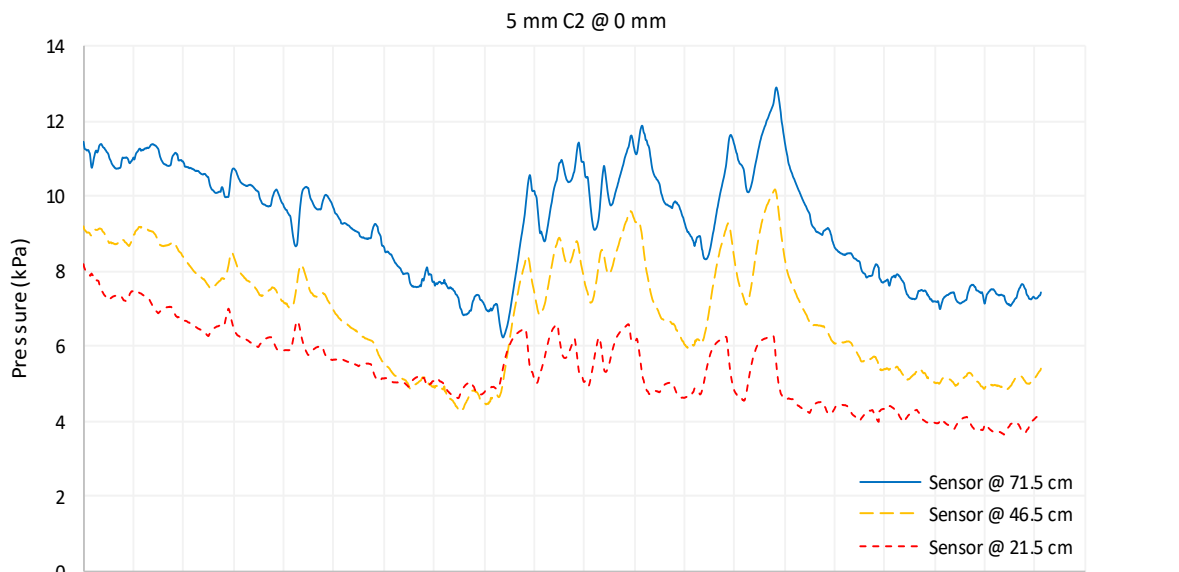
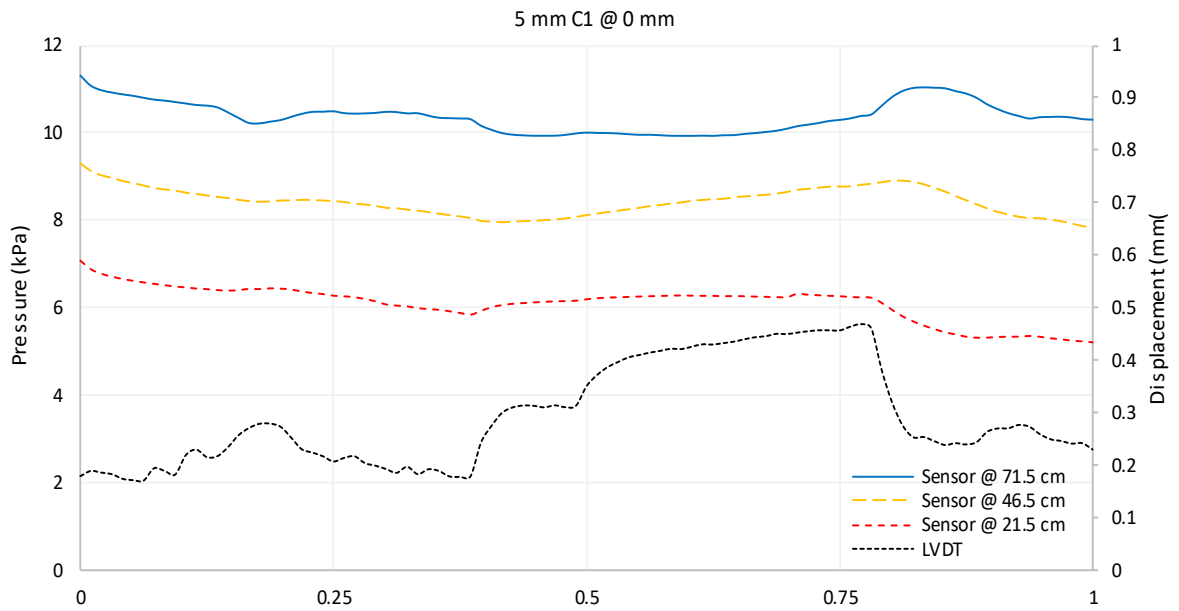
Variation of stresses, wall displacement, and temperature with holding time (-2.5mm, passive, C1, C2)



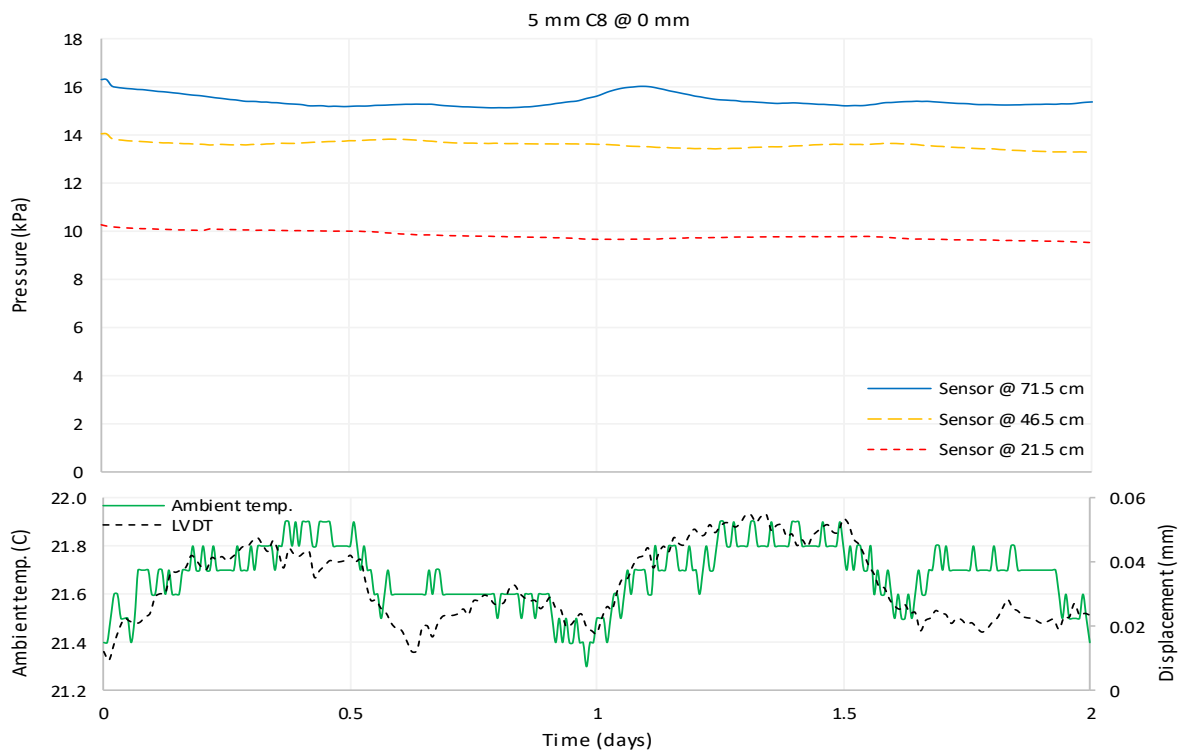
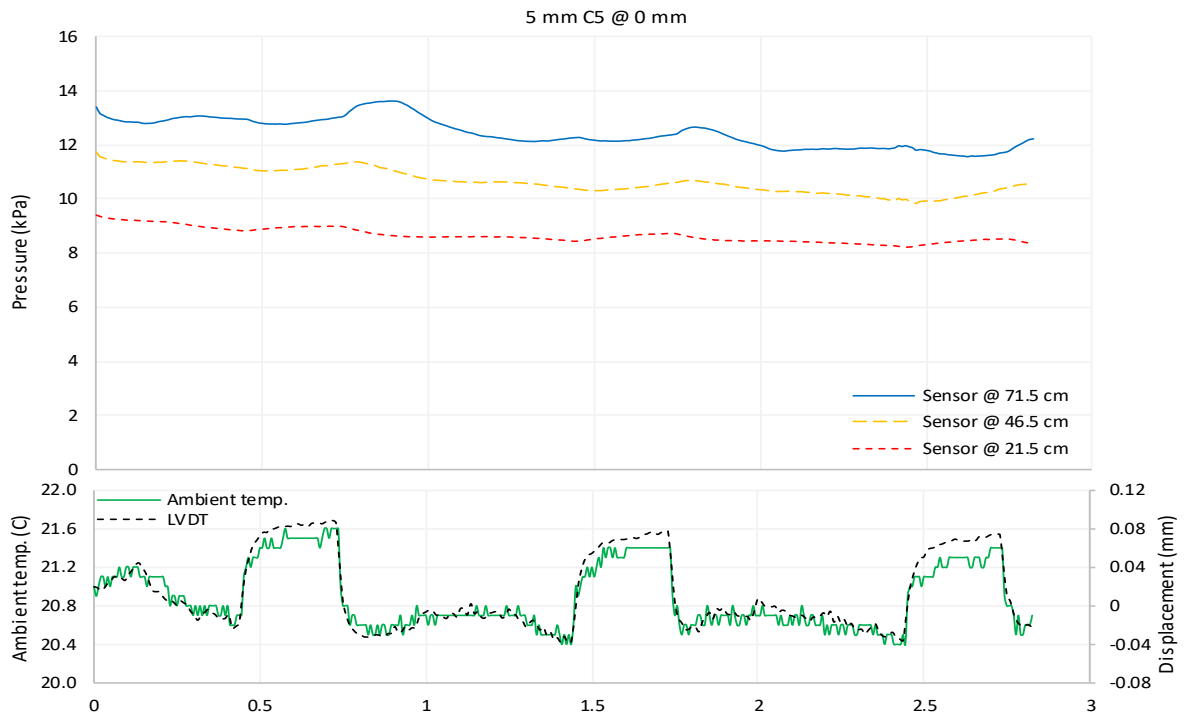
Variation of stresses, wall displacement, and temperature with holding time (-2.5mm, passive, C5, C8)



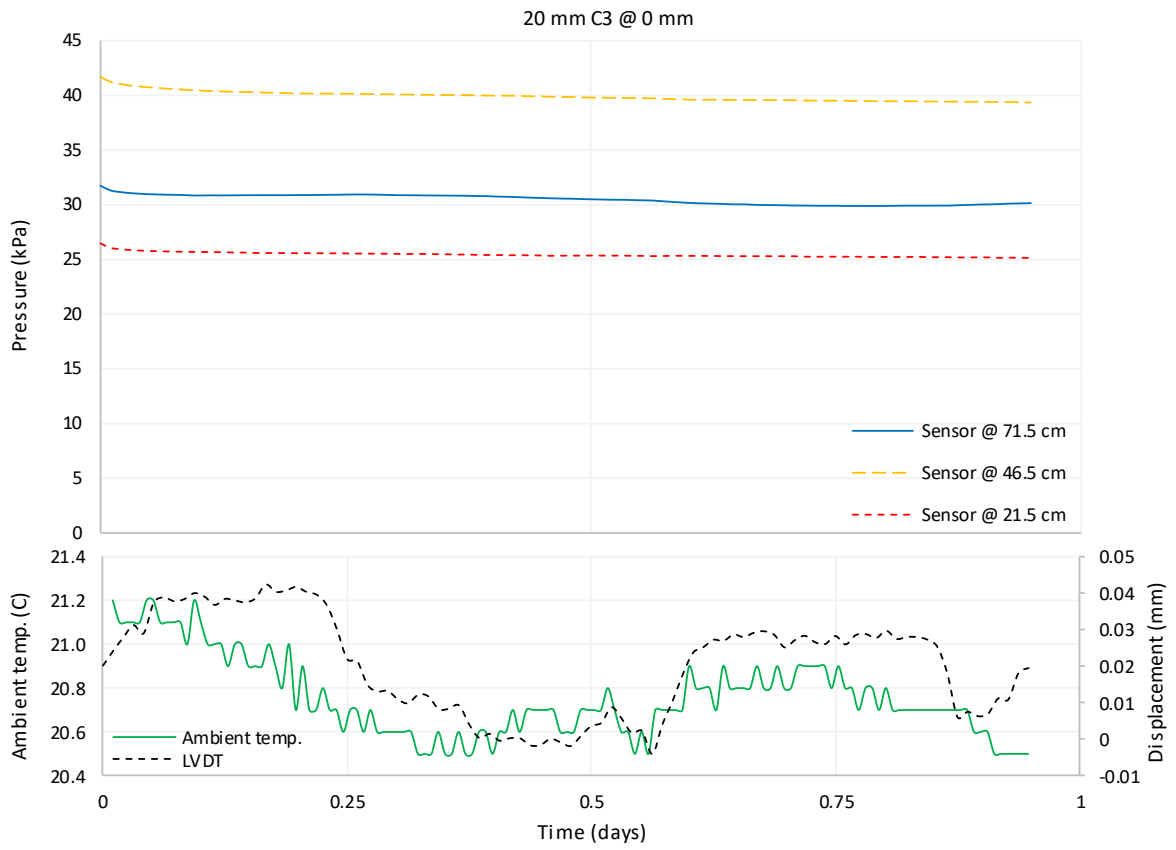
Variation of stresses, wall displacement, and temperature with holding time (-10mm, passive, 20mm cycle, C3)



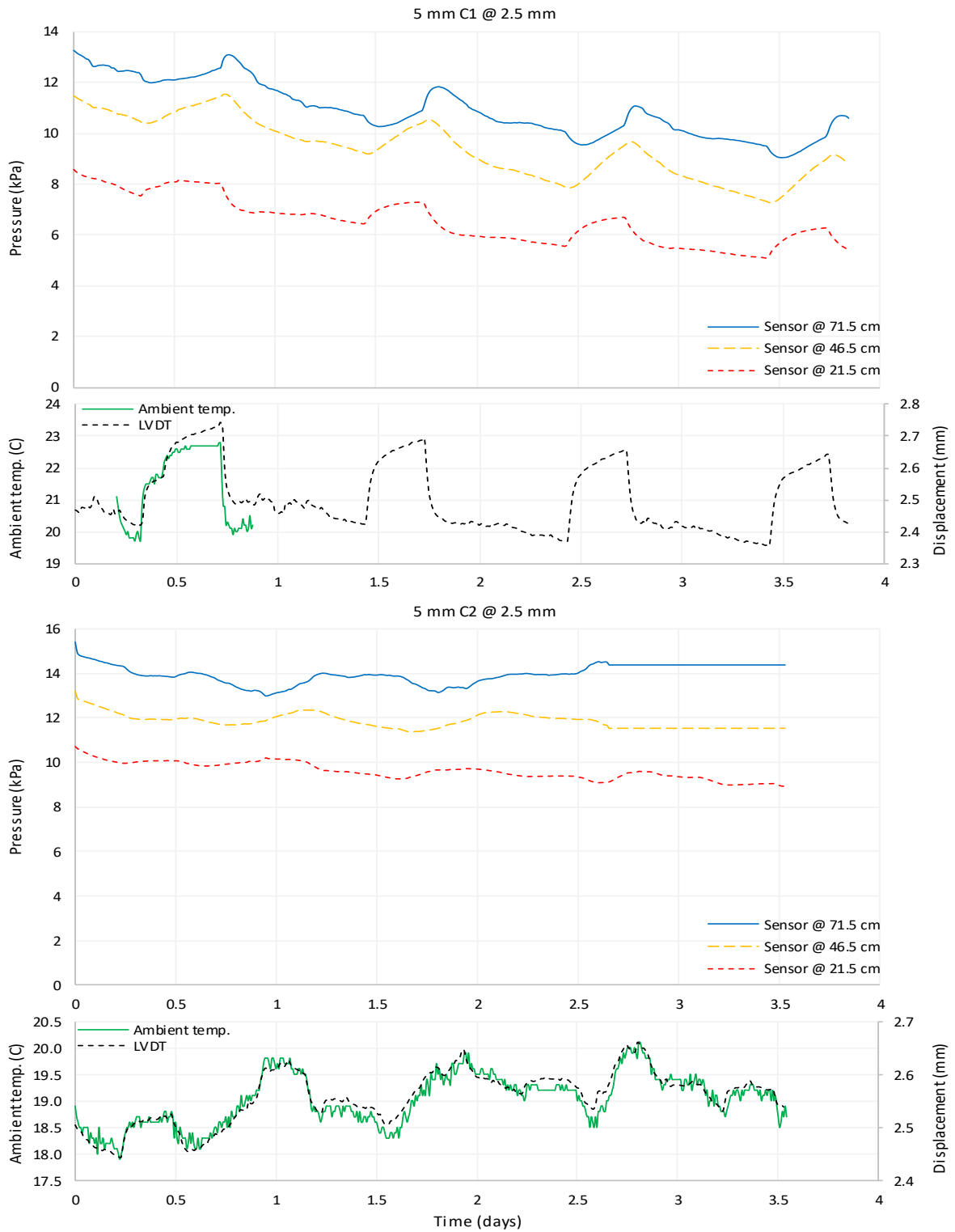
Variation of stresses, wall displacement, and temperature with holding time (0 mm, passive, C1, C2)



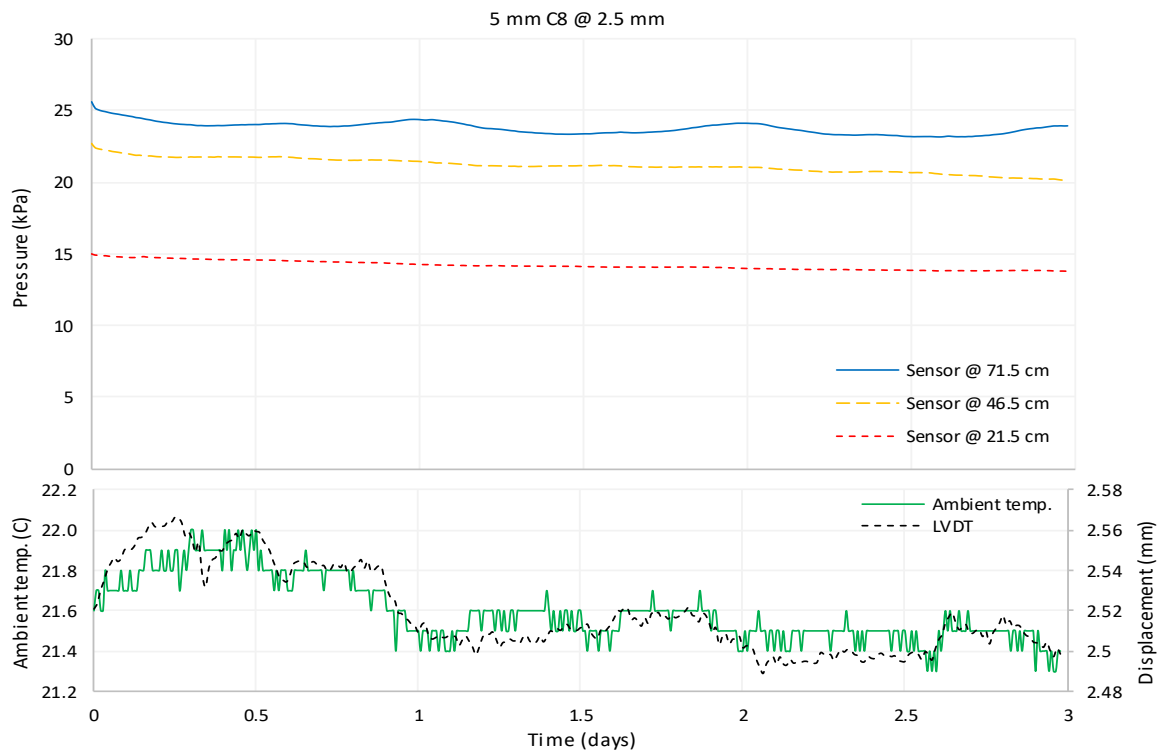
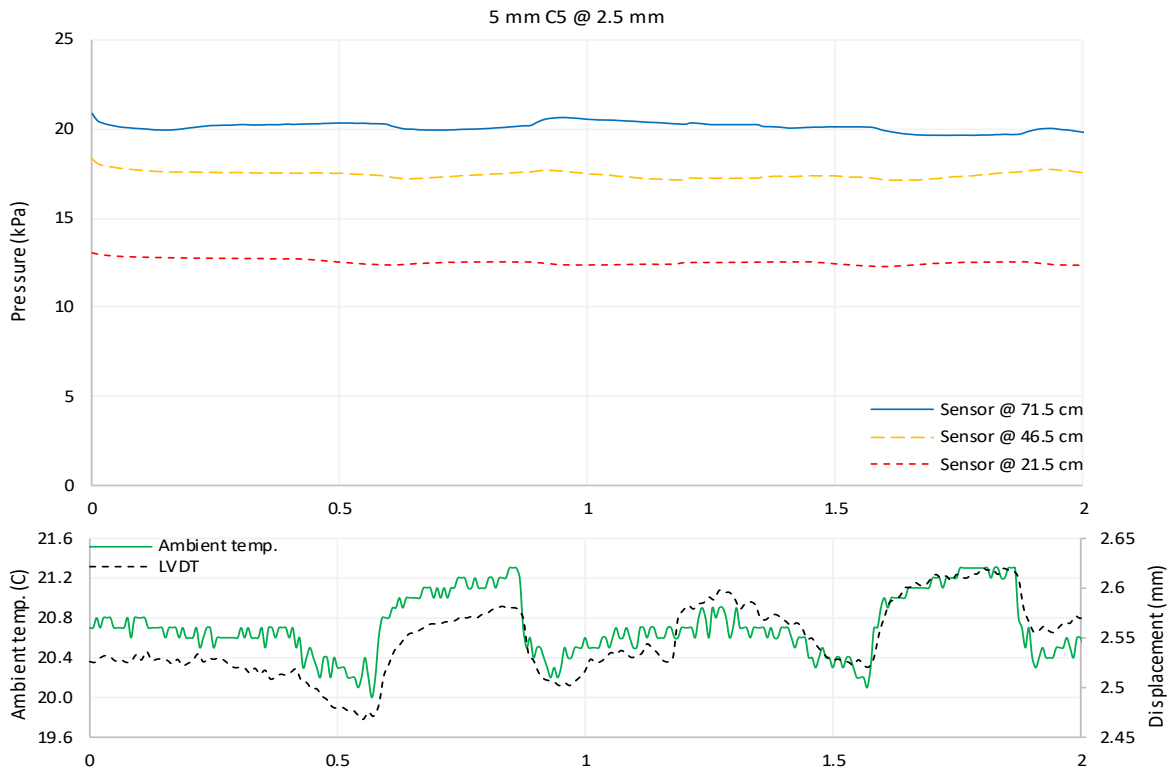
Variation of stresses, wall displacement, and temperature with holding time (0 mm, passive, C5, C8)



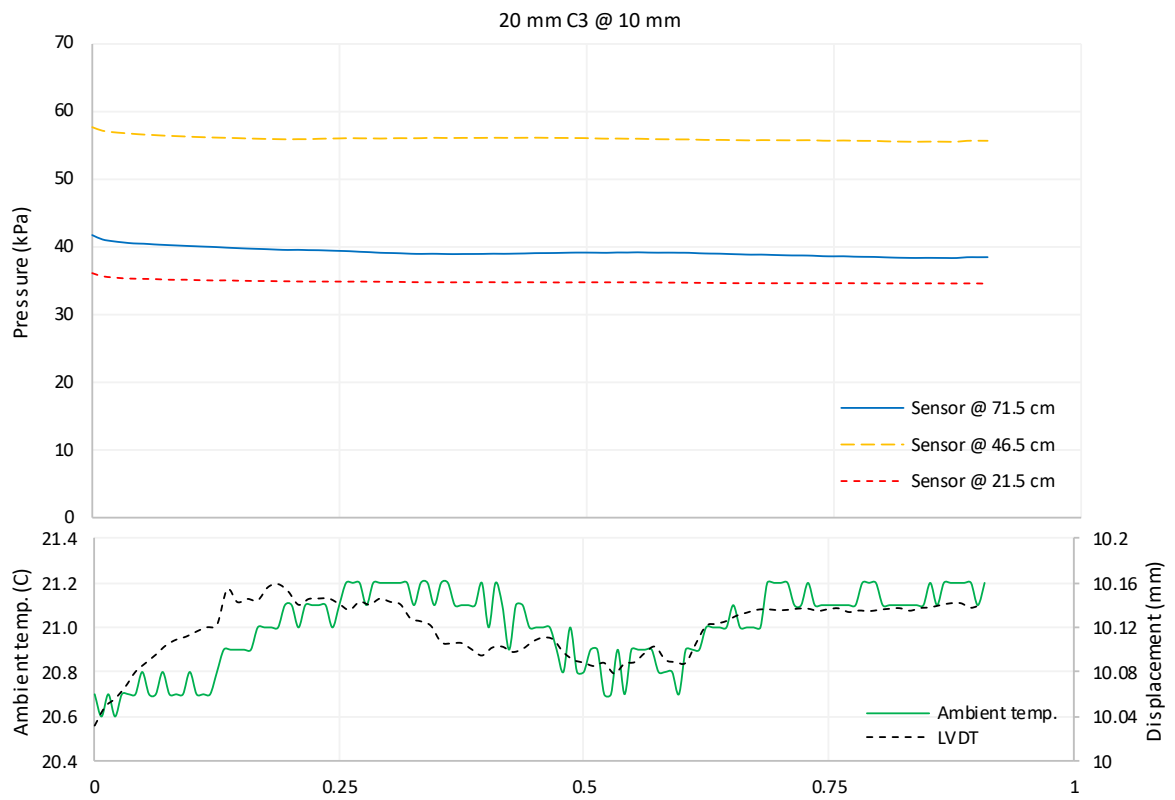
Variation of stresses, wall displacement, and temperature with holding time (0mm, passive, 20mm cycle, C3)



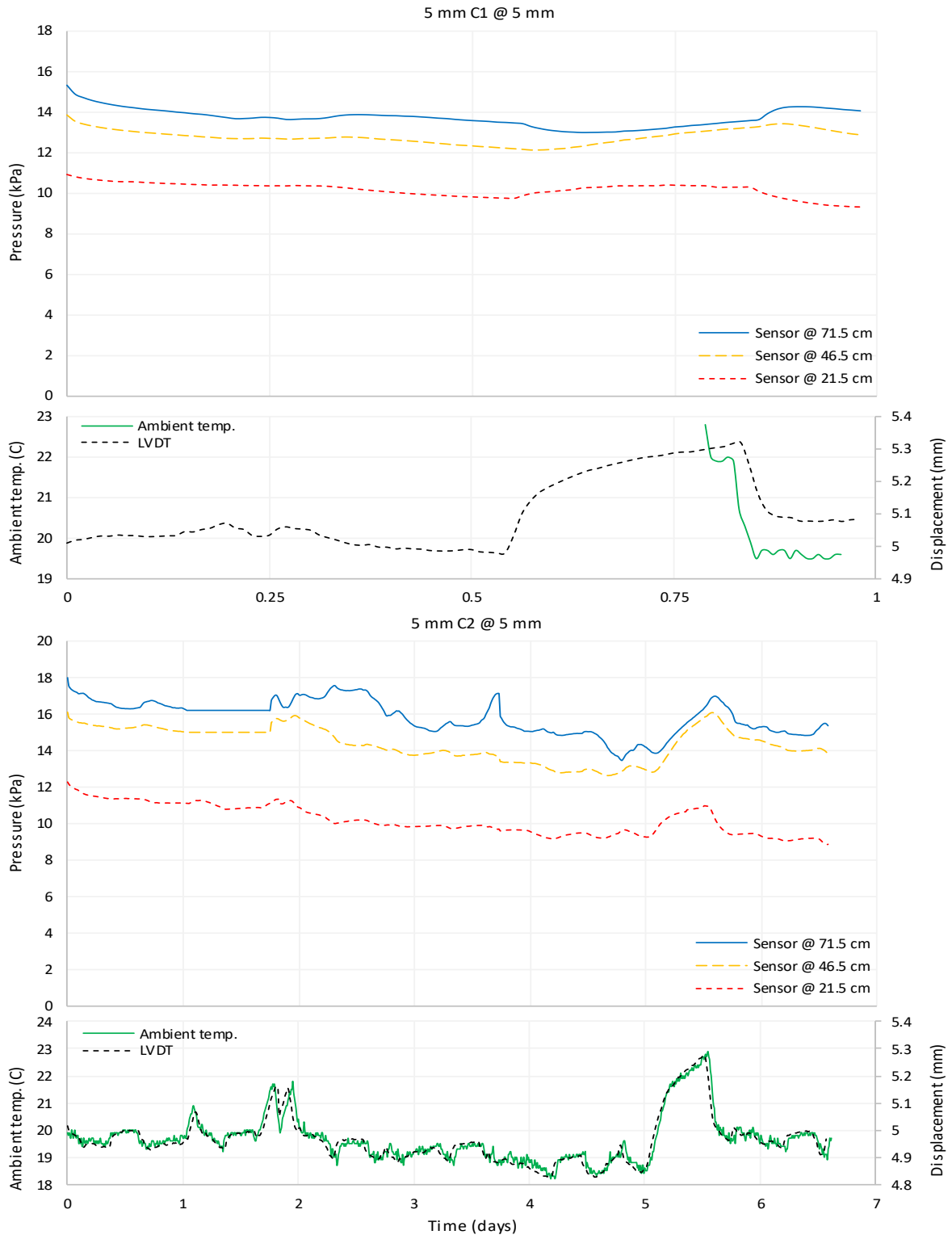
Variation of stresses, wall displacement, and temperature with holding time (2.5 mm, passive, C1, C2)



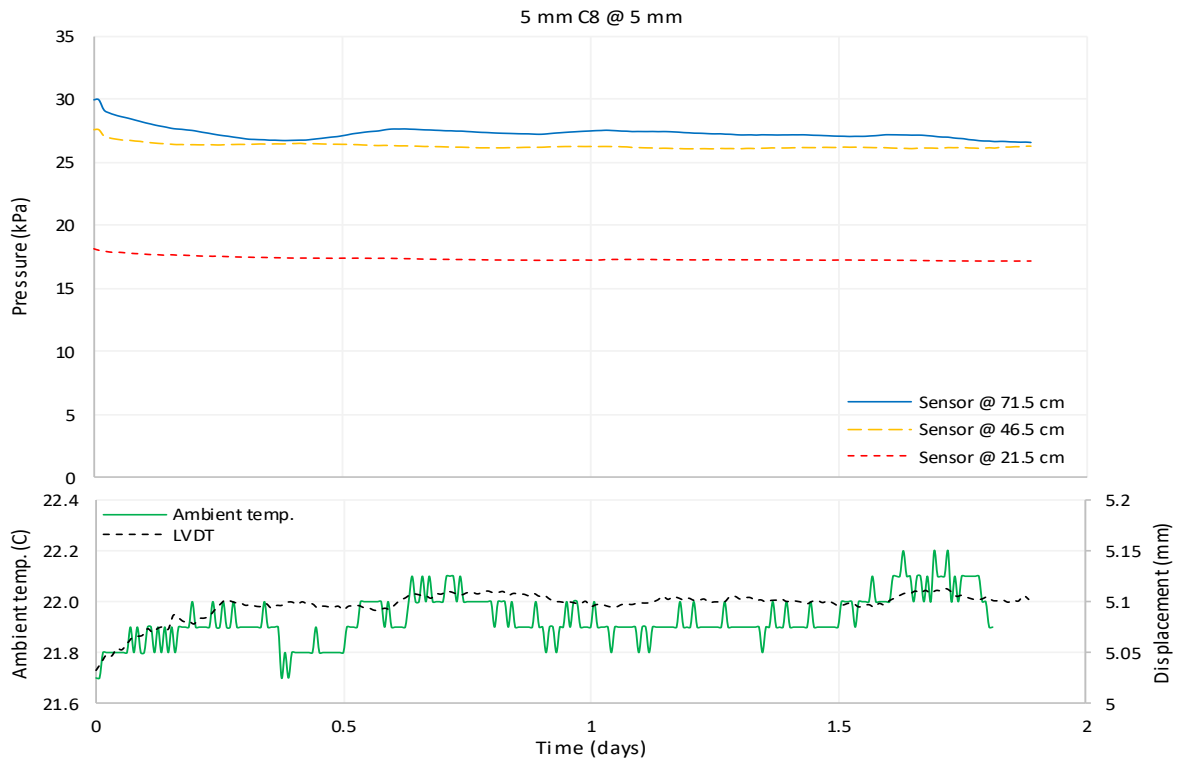
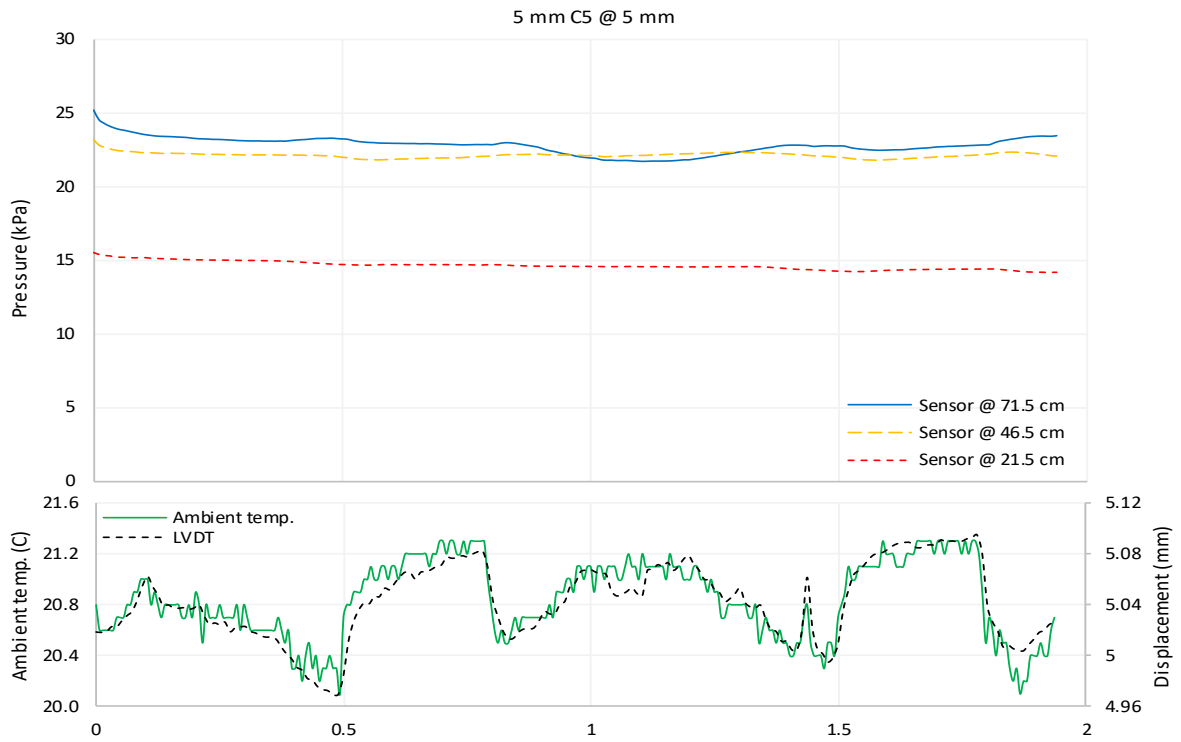
Variation of stresses, wall displacement, and temperature with holding time (2.5 mm, passive, C5, C8)



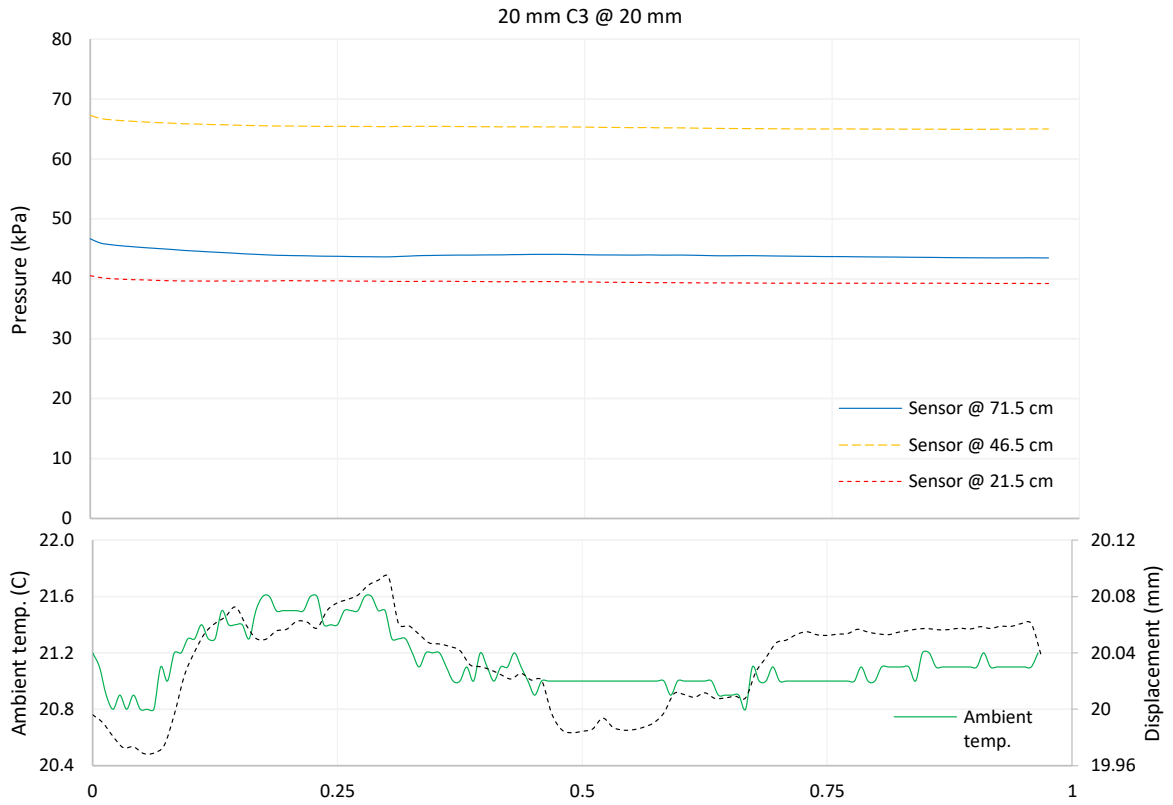
Variation of stresses, wall displacement, and temperature with holding time (10mm, passive, 20mm cycle, C3)



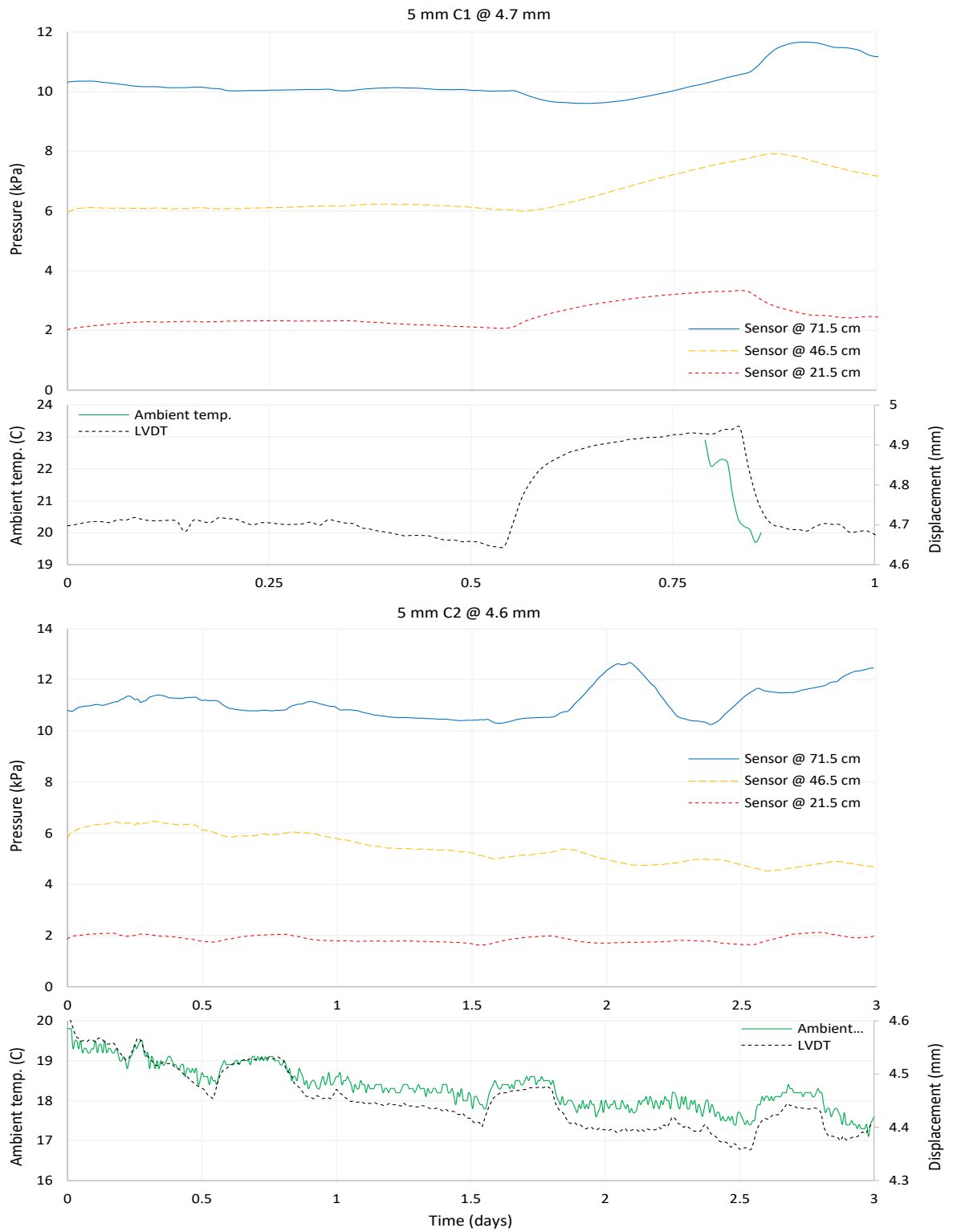
Variation of stresses, wall displacement, and temperature with holding time (5 mm, passive, C1, C2)



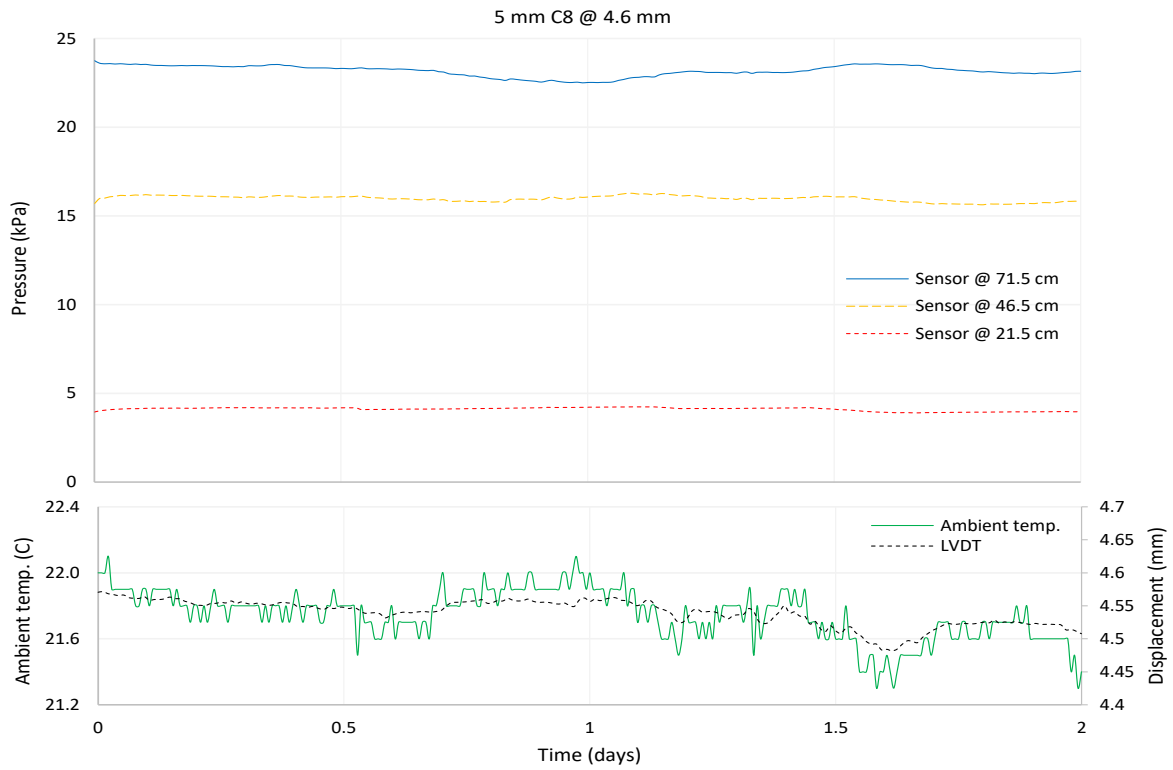
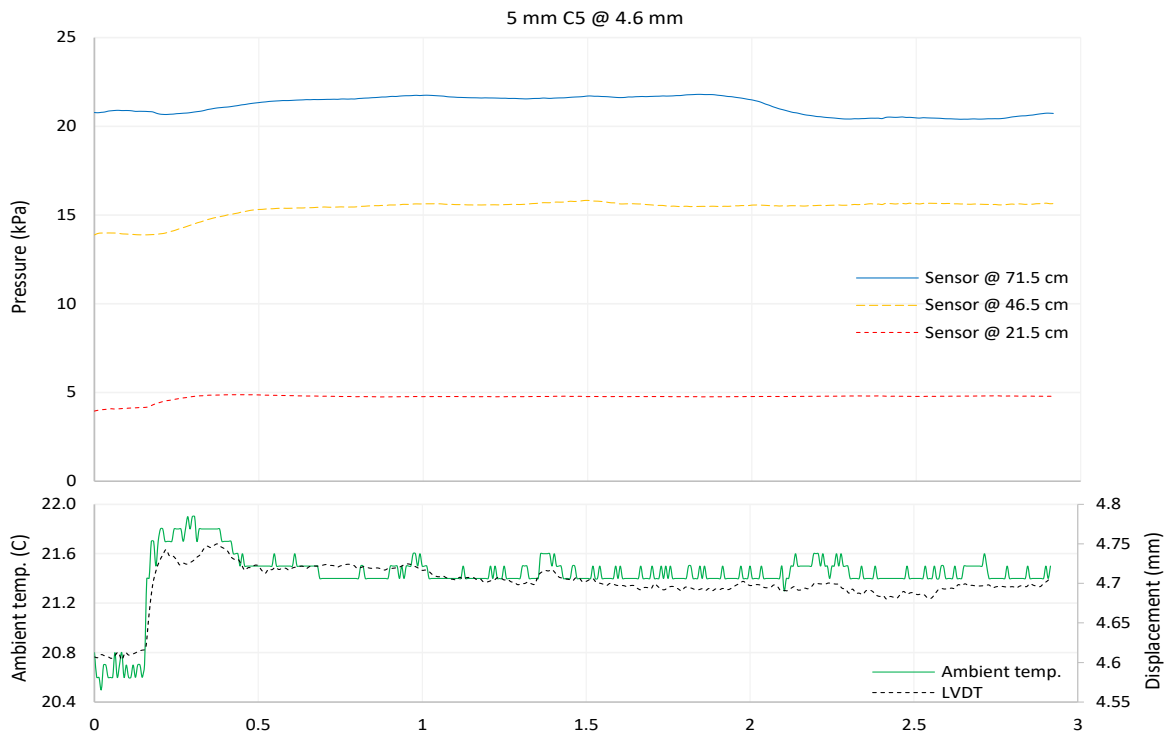
Variation of stresses, wall displacement, and temperature with holding time (5 mm, passive, C5, C8)



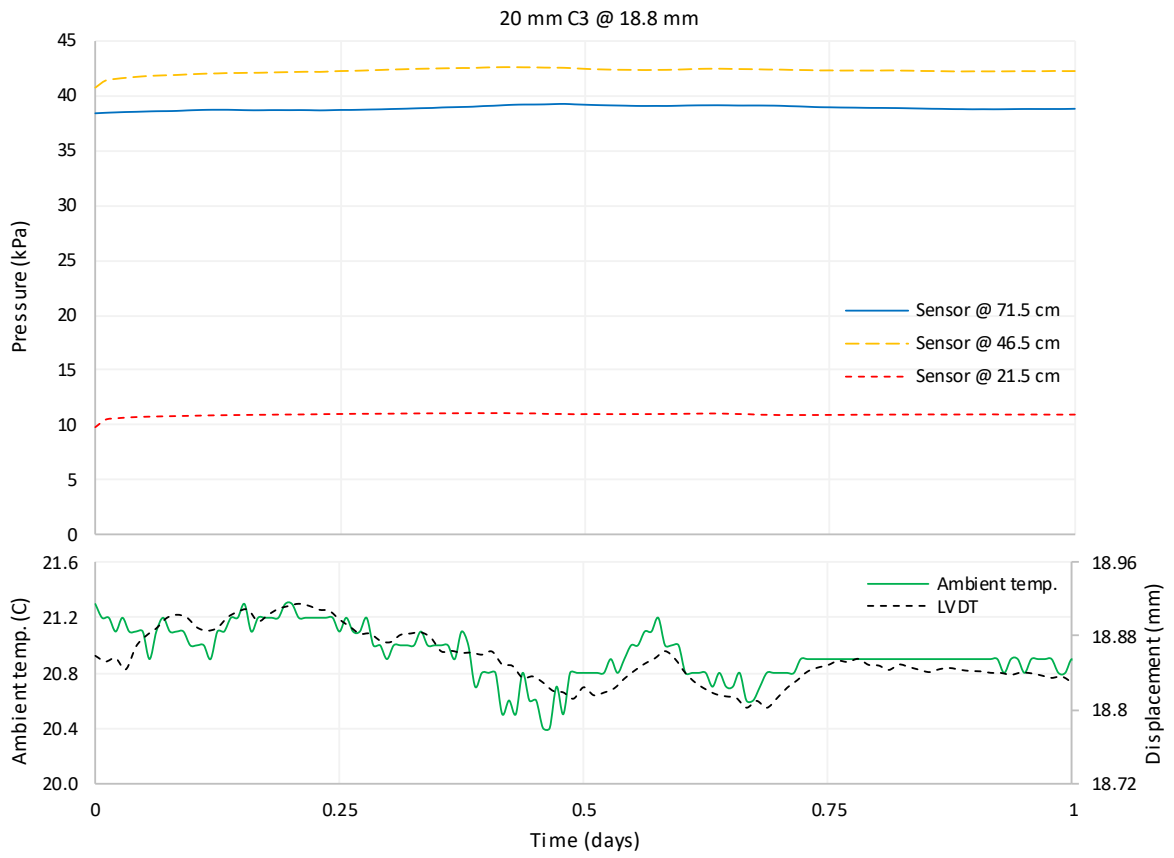
Variation of stresses, wall displacement, and temperature with holding time (20mm, passive, 20mm cycle, C3)



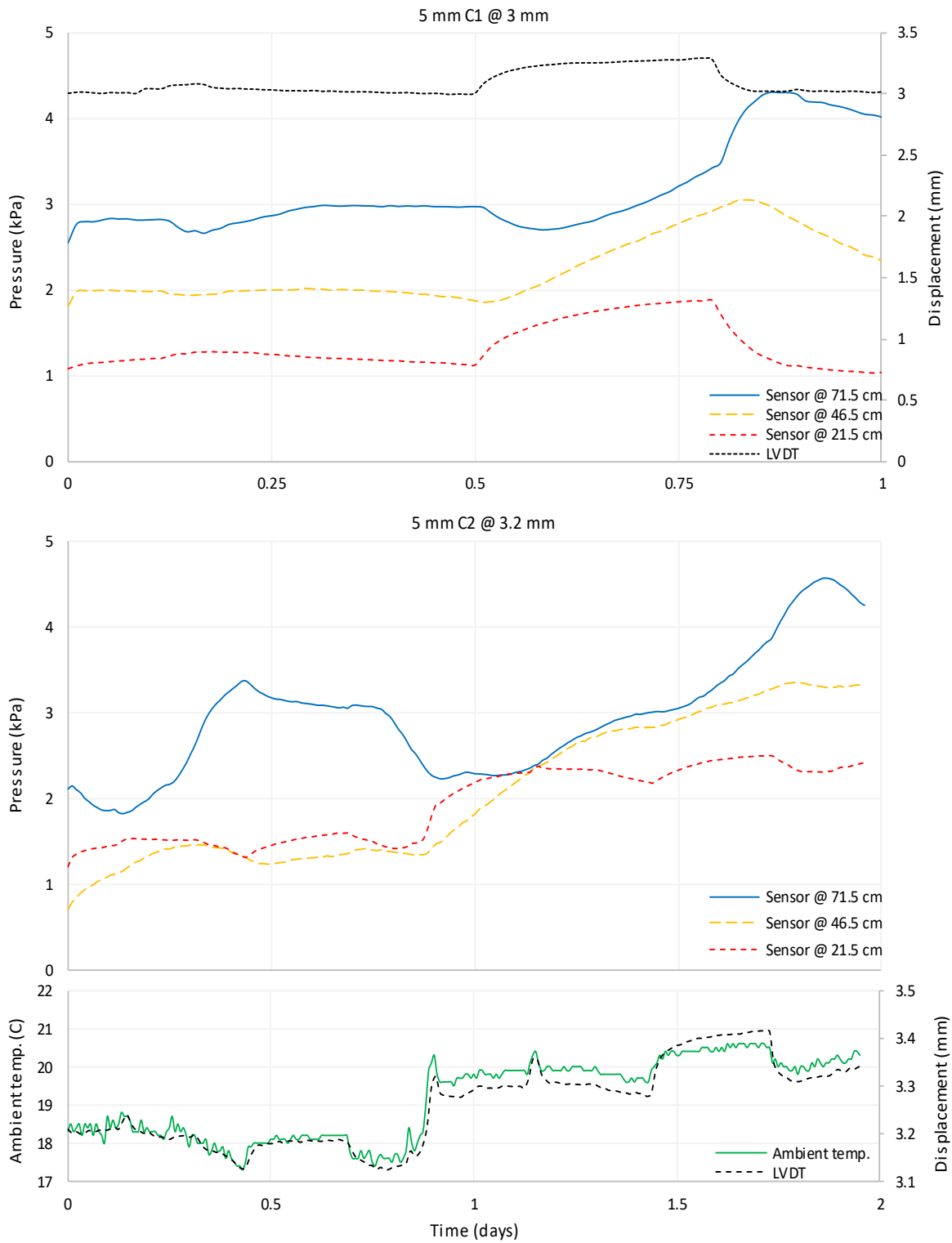
Variation of stresses, wall displacement, and temperature with holding time (4.6 mm, active, C1, C2)



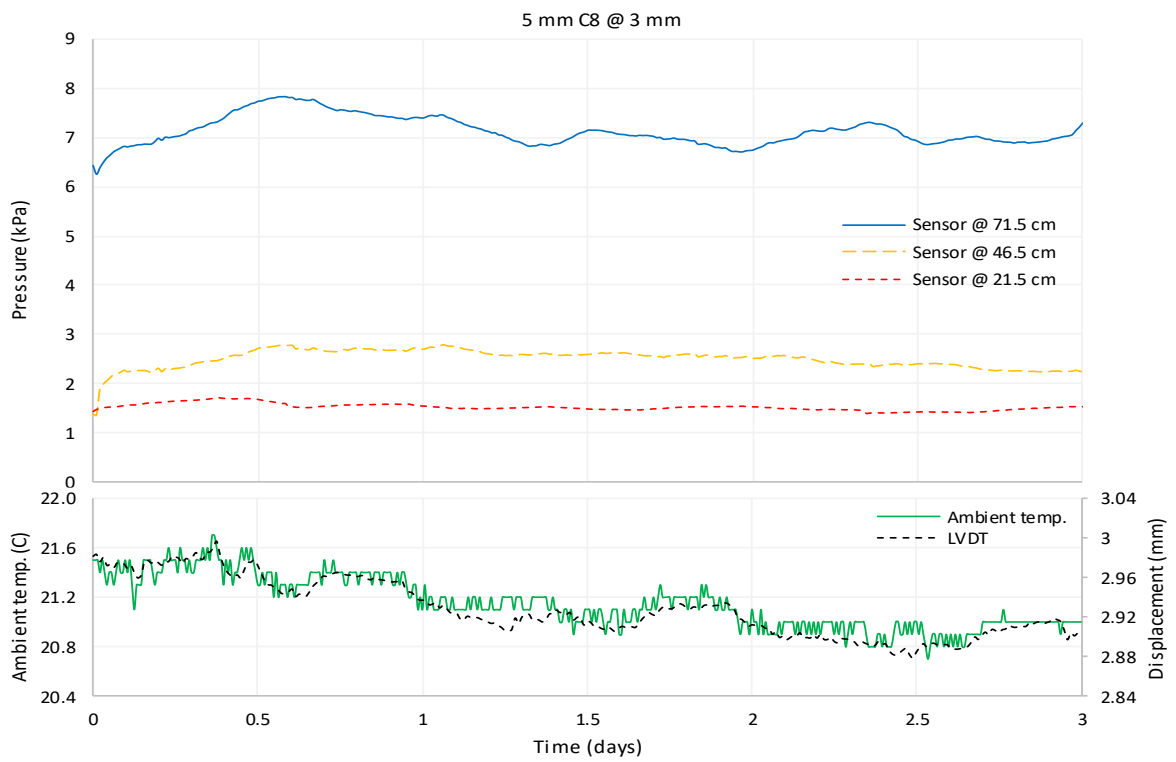
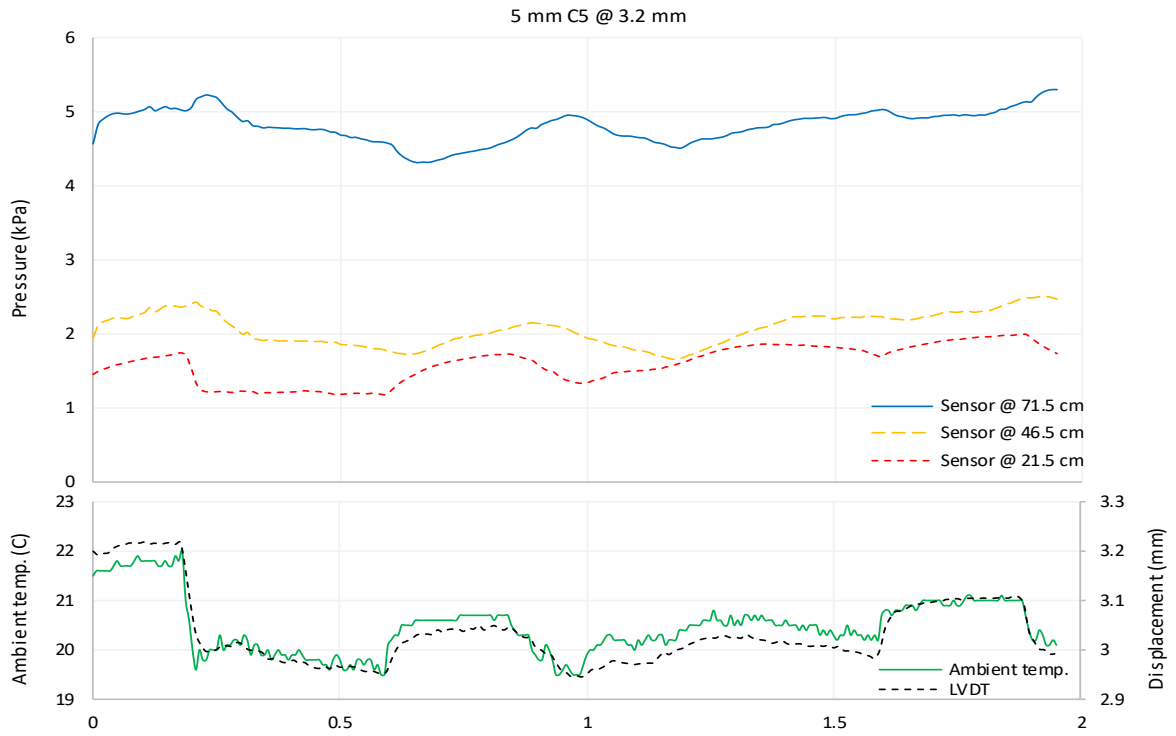
Variation of stresses, wall displacement, and temperature with holding time (4.6 mm, active, C5, C8)



Variation of stresses, wall displacement, and temperature with holding time (18.8mm, active, 20mm cycle, C3)



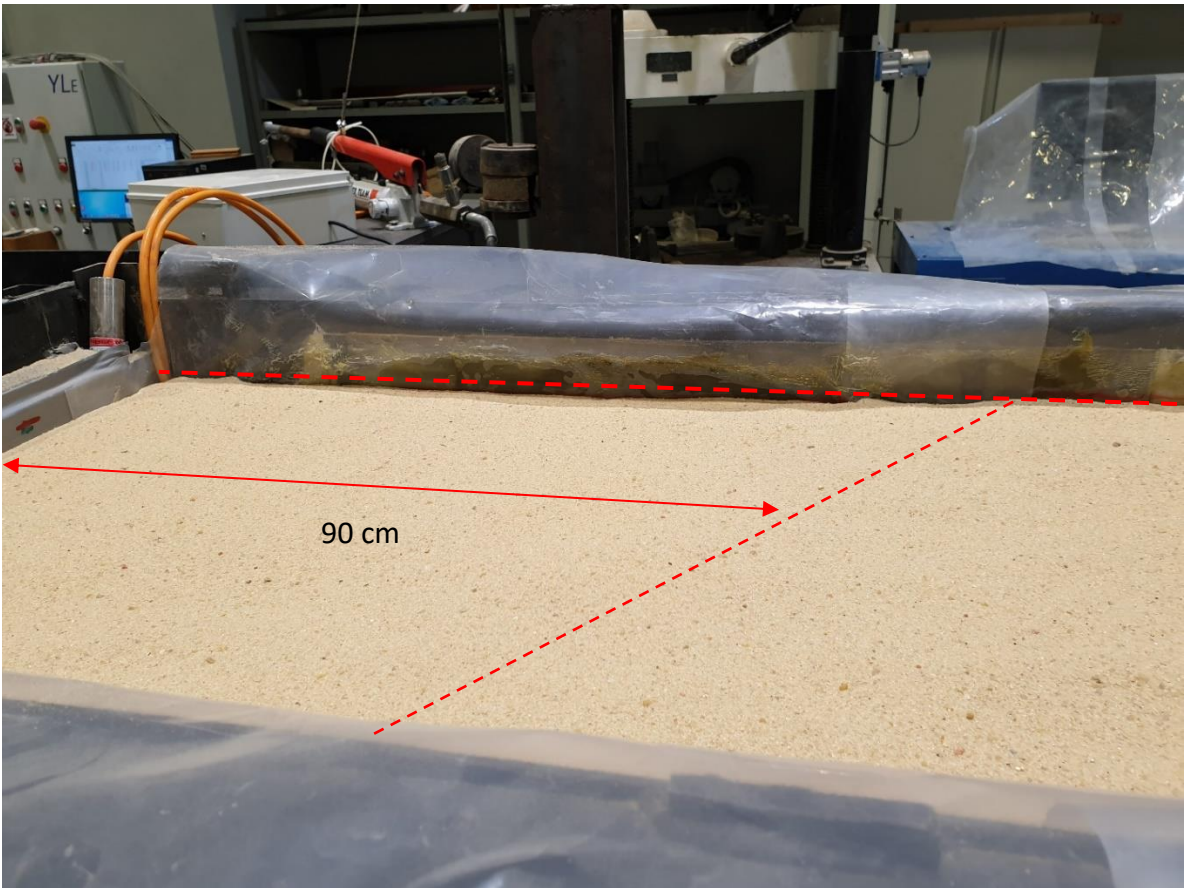
Variation of stresses, wall displacement, and temperature with holding time (3 mm, active, C1, C2)



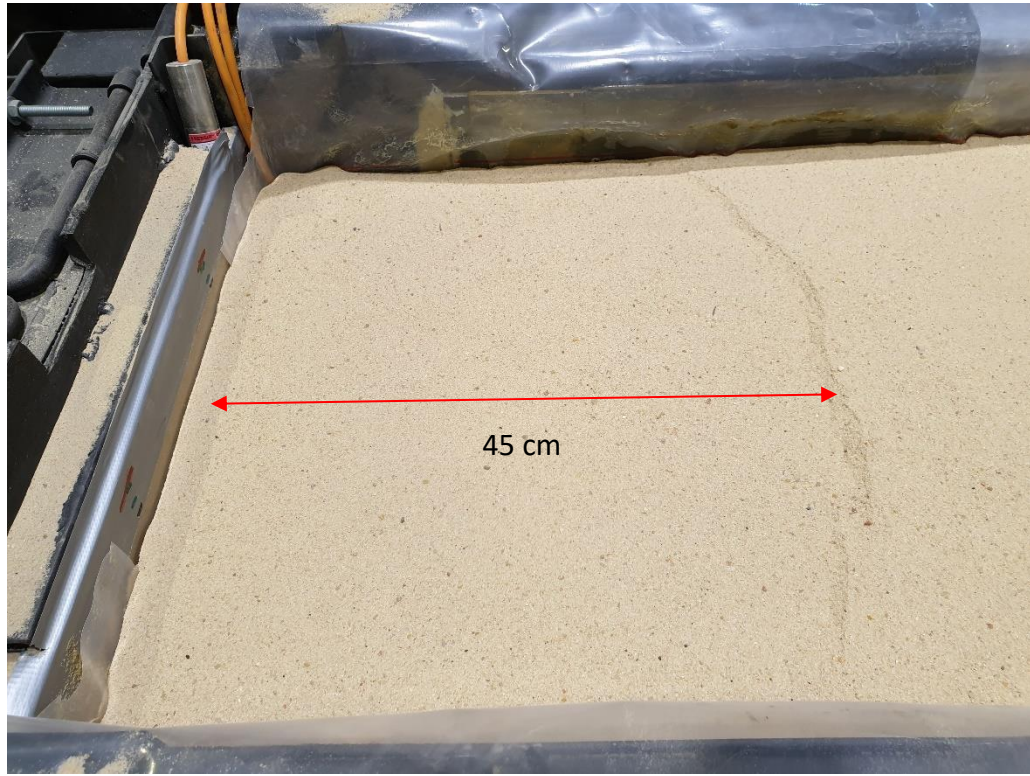
Variation of stresses, wall displacement, and temperature with holding time (3 mm, active, C5, C8)



Surface level at the end of ± 2 mm cycles, red marks the initial bed after filling tank at 1.2 m, and green marks the new level after the 1st cycle ± 2 mm cycle – test #1



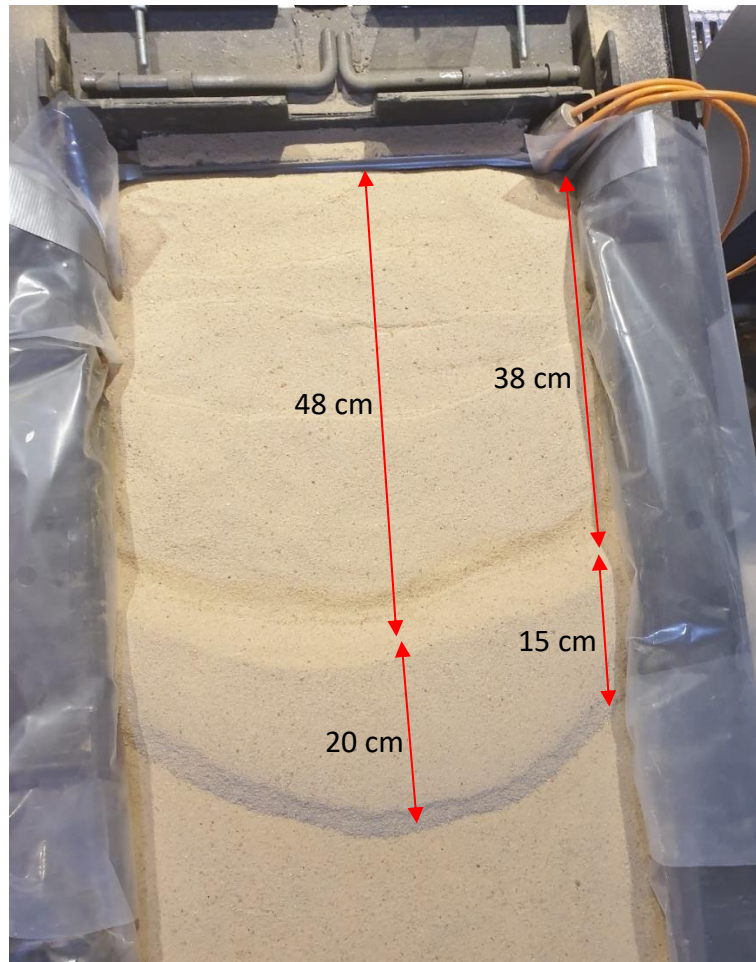
Sand drop 90 cm away from the face of wall at the end of ± 2 mm cycles – test #1



Drop 45 cm away from the face of wall after 1st active ± 10 mm motion – test #1



End of static push (at peak passive) – test #1



End of static push (at peak passive) – test #1



End of static push (at least active) – test #1



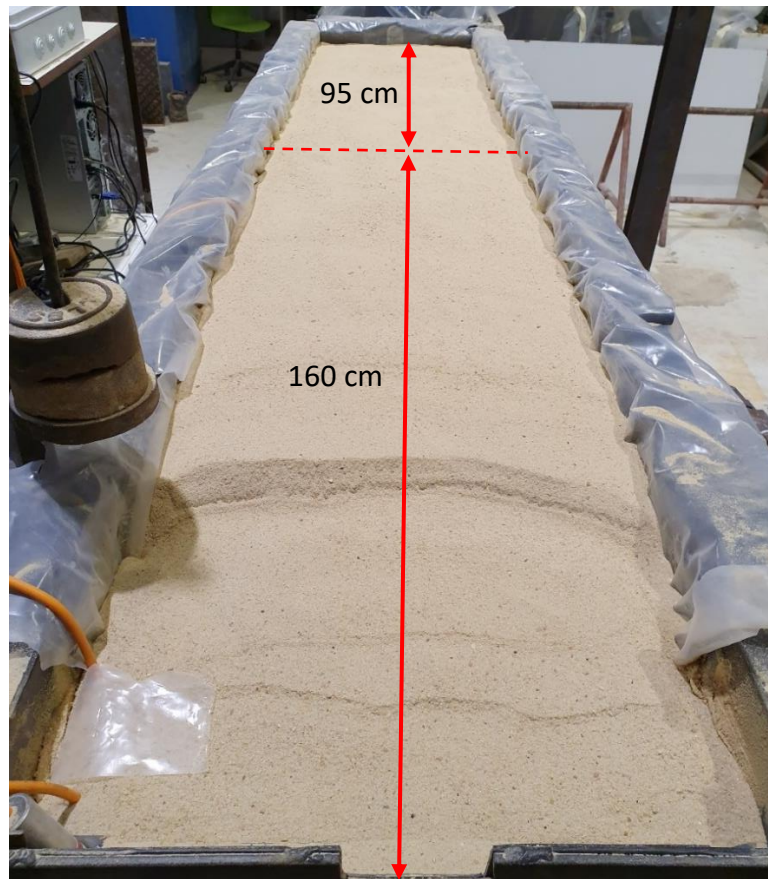
End of static push (at least active) – test #1



Bump at 49 cm away from the face of wall after 10 ± 20 mm cycles – test #3



At -20 mm, after 12 ± 20 mm cycles – test #3



End of static push (at peak passive) where the peak increase in soil surface reached 3 cm at 84 cm away from wall, then decreased till 160 cm – test #3

